Development of Novel Surface Finishing Processes for Additively Manufactured Metal Parts

by

Manyou Sun

A thesis

presented to the University of Waterloo

in fulfillment of the

thesis requirement for the degree of

Doctor of Philosophy

in

Mechanical and Mechatronics Engineering

Waterloo, Ontario, Canada, 2025

© Manyou Sun 2025

Examining Committee Membership

The following served on the Examining Committee for this thesis. The decision of the Examining Committee is by majority vote.

External Examiner:	Ali Nasiri, Ph.D. Associate Professor Department of Mechanical Engineering Dalhousie University
Supervisor:	Ehsan Toyserkani, Ph.D. Professor Department of Mechanical and Mechatronics Engineering University of Waterloo
Internal Member:	Sanjeev Bedi, Ph.D. Professor Department of Mechanical and Mechatronics Engineering University of Waterloo
Internal Member:	Peng Peng, Ph.D. Assistant Professor Department of Mechanical and Mechatronics Engineering University of Waterloo
Internal-External Member:	Michael Pope, Ph.D. Associate Professor Department of Chemical Engineering University of Waterloo

Author's Declaration

This thesis consists of material all of which I authored or co-authored: see Statement of Contributions included in the thesis. This is a true copy of the thesis, including any required final revisions, as accepted by my examiners.

I understand that my thesis may be made electronically available to the public.

Statement of Contributions

Manyou Sun was the sole author for Chapter 1, 2, 3, 6 and 7, all of which are unpublished contents written under the supervision of Professor Ehsan Toyserkani.

The thesis consists in part of two manuscripts written for publication. Details are as follows.

Research work in Chapter 4 was conducted by Manyou Sun solely under the supervision of Professor Ehsan Toyserkani and was published in *Inventions*.

Research work in Chapter 5 was investigated by Manyou Sun under the supervision of Professor Ehsan Toyserkani, with the help from Ali Mohammadnejad in design optimization and improving the visualization of the manuscript. The research work presented in this chapter has been submitted to a peer-reviewed journal.

Citations:

Chapter 4: M. Sun, E. Toyserkani, A novel hybrid ultrasound abrasive-driven electrochemical surface finishing technique for additively manufactured Ti6Al4V parts, *Inventions* 9 (2024) 45. https://doi.org/10.3390/inventions9020045.

Chapter 5: Manuscript entitled “Feasibility of 3D-printed polymeric covers for electrode wires in electropolishing of additively manufactured parts with internal channels” submitted to a peer-reviewed journal.

Abstract

Poor surface quality is one of the drawbacks of metal parts made by various additive manufacturing (AM) processes. They normally possess high surface roughness and different types of surface irregularities. Post-processing operations are needed to reduce the surface roughness to have ready-to-use parts. Among all the surface treatment techniques, electrochemical surface finishing methods have the highest finishing efficiency.

However, there are challenges with electropolishing in terms of reducing surface roughness of metals parts made via AM. Firstly, parts made with AM have both small-scale surface roughness and large-scale surface waviness. Electropolishing is only suitable for the reduction of micro-scale surface roughness while it is difficult to use the method to remove meso- to macro-scale surface waviness. In addition, it is still challenging to use electropolishing to reduce the surface roughness of internal channels of additively manufactured parts, benefiting from the promising feature of AM to produce parts with complex internal geometries. Finally, how to improve process sustainability is another question that needs to be addressed, since hazardous and corrosive chemicals are always used for the technique.

To address the aforementioned problems, novel approaches were developed, incorporating both modeling and experimental investigations. Analytical and numerical models were constructed to explore the mechanisms of electropolishing and to understand the surface evolution during the process. The results offer valuable insights that can guide the design of experiments and foster the development of novel processes.

The first experimental study focuses on using hybrid surface finishing technique to reduce meso-/macro- surface waviness. A novel surface finishing technique combining electrochemical polishing, ultrasonic cavitation and abrasive finishing was designed.

Experiments were conducted on both electropolishing and hybrid finishing and the results were compared. While similar optimal arithmetic mean height values ($Sa \approx 1$ μm) are achieved for both processes, the arithmetic mean waviness values (*Wa*) obtained from hybrid finishing are much less than those from sole electropolishing after the same processing time.

The second experimental investigation aims at electropolishing internal channels. For doing this, a novel cathode tool was invented and fabricated using polymer 3D printing. Electropolishing was conducted on both straight and curved channels with different curvatures. Preliminary experiments demonstrated a maximum surface roughness *Sa* reduction, from 10.86 ± 0.50 μm to 1.44 ± 0.46 μm. Apart from this, electropolishing failure mechanisms were explained and design optimization was conducted through numerical simulation. The investigations show that the method is promising in reducing surface roughness of internal channels.

In addition, experimental trials were also conducted to improve the sustainability of the surface finishing processes, including using greener electrolytes for electropolishing, and developing shear thickening polishing. Both alcohol-salt electrolyte system and deep eutectic solvent electrolyte were investigated, demonstrating effective surface roughness reduction. Shear thickening polishing using the corn starch slurry was also explored. In spite of some promising results, the process was not repeatable due to numerous influencing factors.

Acknowledgements

I would like to extend my deepest gratitude to all the warm people who supported and helped me during my PhD journey.

I would like to express my sincerest gratitude to my supervisor, Professor Ehsan Toyserkani, for giving me the opportunity for doing PhD and providing precious guidance and support on my PhD research.

I would like to acknowledge my committee members, including Prof. Ali Nasiri from Dalhousie University, Prof. Sanjeev Bedi, Prof. Peng Peng, and Prof. Michael Pope from University of Waterloo for their valuable feedback and suggestions.

I would like to acknowledge all the financial support from Natural Sciences and Engineering Research Council of Canada (NSERC).

I would like to thank my colleagues and friends in Multi-Scale Additive Manufacturing Lab (MSAM) for their academic discussions and mental support.

Last but not least, I would like to thank my family for their unconditional support, and for always being here with me.

Dedication

To my family and friends

Table of Contents

Examining Committee Membership ii

Author's Declaration iii

Statement of Contributions iv

Abstract v

Acknowledgements vii

Dedication viii

List of Figures xiv

List of Tables xx

List of Abbreviations xxi

List of Symbols xxii

1. Introduction 1

    1.1. Research Motivation 1

    1.2. Research Objectives 2

    1.3. Thesis Outline 3

2. Literature Review 5

    2.1. Chapter Overview 5

    2.2. Additive Manufacturing and Laser Powder Bed Fusion 6

    2.3. Surface Roughness and Surface Irregularities 7

        2.3.1. Types and Forming Mechanisms 7

        2.3.2. Effects on Material Properties 8

        2.3.3. Surface Roughness Characterization 9

2.4. Surface Finishing Techniques 11
2.4.1. Mechanical Finishing Techniques 11
2.4.2. Chemical Finishing Techniques 15
2.4.3. Hybrid Finishing Techniques 18
2.4.4. Laser-based Finishing Techniques 19
2.5. Surface Finishing of Internal Channels 20
2.6. Modeling Approaches 21
2.7. Summary 23
3. Analytical and Numerical Model on Surface Finishing Processes 24
3.1. Chapter Overview 24
3.2. Process Description 25
3.2.1. Introduction to Electropolishing 25
3.2.2. Introduction to Ultrasonic Cavitation Abrasive Finishing 27
3.3. Analytical Model for Electropolishing 28
3.3.1. Faraday's Law for Material Removal 28
3.3.2. Effect of Initial Surface Roughness 30
3.4. Numerical Model for Electropolishing 33
3.4.1. Model Description 33
3.4.2. Effect of Influencing Parameters 34
3.4.3. Surface Roughness Evolution 35
3.5. Analytical Model for Ultrasonic Cavitation Abrasive Finishing 36
3.5.1. Model Description 36

3.5.2. Effect of Working Parameters on Material Removal 39

3.6. Summary 41

4. Development of a Novel Hybrid Ultrasound Abrasive-Driven Electropolishing Technique 42

4.1. Chapter Overview 42

4.2. Experiments and Methods 43

4.2.1. Sample Preparation 43

4.2.2. Measurement of Polarization Curve 43

4.2.3. Optimization of Electropolishing Parameters 44

4.2.4. Experimental Study on Ultrasound and Abrasion 46

4.2.5. Optimization of Hybrid Surface Finishing 46

4.2.6. Surface Roughness Characterization 48

4.2.7. Investigation of Surface Waviness 48

4.3. Results 49

4.3.1. Surface Analysis of As-built Samples 49

4.3.2. Polarization Curve 50

4.3.3. Analysis of Electropolishing 51

4.3.4. Effect of Ultrasound and Abrasion on Surface Finishing 54

4.3.5. Analysis of Hybrid Finishing Technique 55

4.3.6. Comparison between Electropolished Surface and Hybrid Finished Surface 57

4.4. Discussions 58

4.5. Summary 63

5. Feasibility of 3D-Printed Polymeric Covers for Electrode Wires in Electropolishing Internal Channels 65

5.1. Chapter Overview 65

5.2. Experiments and Methods 66

5.2.1. Introduction of Polishing Concept 66

5.2.2. Fabrication of Samples with Internal Channels 67

5.2.3. Fabrication of Tool Electrode 68

5.2.4. Electropolishing Tests 69

5.2.5. Surface Characterization 71

5.3. Results and Discussion 72

5.3.1. As-built Surface Analysis 72

5.3.2. Compatibility between the Wire Cover and the Electrolyte 74

5.3.3. Effect of Voltage 75

5.3.4. Surface Roughness Analysis 76

5.3.5. Failure Mechanism and Defect Formation 78

5.3.6. Effect of Channel Curvatures 82

5.3.7. Effect of Ultrasonic Vibration 85

5.4. Numerical Simulation for Design Optimization 86

5.4.1. Design Optimization and Model Description 86

5.4.2. Governing Equations 88

5.4.3. Boundary Conditions and Mesh Independence Analysis 88

5.4.4. Modeling and Optimization Results 90

5.5. Summary 94

6. Methods on Improving Sustainability for Surface Finishing of Additively Manufactured Metal Parts 95

6.1. Chapter Overview 95

6.2. Electropolishing Using Green Electrolytes 96

6.2.1. Introduction and Working Principle 96

6.2.2. Experiments 97

6.2.3. Results and Discussions 97

6.3. Shear Thickening Polishing 100

6.3.1. Introduction and Working Principle 100

6.3.2. Experiments 101

6.3.3. Results and Discussions 103

6.4. Summary 105

7. Conclusions and Future Work 106

7.1. Conclusions 106

7.2. Recommendations and Future Work 107

Letter of Copyright Permission 108

References 115

List of Figures

Figure 1.1 Thesis graphical overview and its concept interconnectivity 4
Figure 2.1 Graphical overview of chapter 2 5
Figure 2.2 Schematics of the LPBF process (reused with permission of Taylor & Francis from [7]) 6
Figure 2.3 Surface roughness due to (a) surface adhered particles, (b-c) staircase effect (reused under the Creative Commons CC-BY license from [10]), (d) large hatching distance (reused under the Creative Commons CC-BY license from [11]), and (e-g) balling effect (reused with permission of Elsevier from [13]) 8
Figure 2.4 Schematics of working principles for (a) contact-based stylus profilometer (reused with permission of Elsevier from [18]) and (b) non-contact based optical profilometer (reused under the Creative Commons CC-BY license from [19]) 10
Figure 2.5 Abrasive flow machining (a) schematics (reused with permission of Elsevier from [22]), (b-e) AFM treated closed pump impeller (reused under the Creative Commons CC-BY license from [24]), (f, g) SEM images of AFM treated waveguide channels (reused with permission of Taylor & Francis from [25]) 12
Figure 2.6 Magnetic abrasive machining (a) schematics (reused under the Creative Commons CC-BY license from [26]), (b) 3D profiles, (c) mirror effect (reused with permission of Springer Nature from [27]) 13
Figure 2.7 Schematics of (a) ultrasonic cavitation abrasive finishing (reused with permission of Elsevier from [30]) and (b) hydrodynamic cavitation abrasive finishing (reused with permission of Elsevier from [31]) 14
Figure 2.8 Examples of chemical polishing (a) Ti6Al7Nb scaffolds (reused with permission of Springer Nature from [32]), (b) Ti6Al4V specimen(reused with permission of Elsevier from [33]), (c) SS316 hidden area (reused with permission of Springer Nature from [34]) 17
Figure 2.9 Examples of hybrid finishing techniques (a) 3D profile of chemical-

abrasive flow polishing (reused with permission of Elsevier from [50]); (b) schematics of novel cathode tool (reused with permission of Elsevier from [51]); (c) electrochemical-mechanical polishing of complex structures (reused with permission of Elsevier from [52]) 19
Figure 2.10 Schematic illustration of laser polishing technique (reused with permission of John Wiley and Sons from [54]) 20
Figure 3.1 Graphical overview of Chapter 3 24
Figure 3.2 Schematic of electropolishing setup 25
Figure 3.3 Polarization curve in electropolishing (redrawn and adapted from [73]) ... 27
Figure 3.4 Schematics of ultrasonic cavitation, redrawn and adapted from [75] 27
Figure 3.5 Mechanisms for ultrasonic cavitation on material removal, redrawn and adapted from [30] 28
Figure 3.6 Influence of (a) electrode gap and (b) electropolishing voltage on volumetric material removal for electropolishing 30
Figure 3.7 Parametric surface expressed by sine wave functions 31
Figure 3.8 Effect of initial surface roughness on material removal (a) surface displacement on amplitude reduction; (b) effect of initial amplitude; (c) effect of wavelength 32
Figure 3.9 Experimental results for average surface plane displacement when decreasing the amplitude from 20 μm to ~1.5 μm 33
Figure 3.10 2D geometry of adhered particles for COMSOL modeling 34
Figure 3.11 Particle evolution under different electropolishing conditions 35
Figure 3.12 Surface roughness evolution for surfaces with different initial roughness 36
Figure 3.13 (a) Frequency and (b) amplitude effect on bubble dynamics 40
Figure 3.14 Particle (a) velocity and (b) impact pressure due to ultrasonic cavitation 40
Figure 3.15 Effect of particle size on volumetric material removal 41

Figure 4.1 Graphical overview of Chapter 4 42
Figure 4.2 Schematic of experiment setup for (a) electropolishing, (b) surface finishing with ultrasound and abrasion, and (c) ultrasound abrasive-driven electrochemical hybrid finishing 45
Figure 4.3 Locations of surface roughness and surface waviness measurements 48
Figure 4.4 Images of as-built coupons: (a) camera image; (b) 3D height profile; (c) laser optical surface image 50
Figure 4.5 SEM images of as-built surface (a) 200×; (b) 1000× 50
Figure 4.6 Polarization curve achieved from electropolishing experiment 51
Figure 4.7 Main effect plots in electropolishing DOE for (a) response means and (b) S/N ratios 52
Figure 4.8 Three-dimensional surface images for samples in electropolishing DOE . 53
Figure 4.9 Comparison between experimental results and calculation results on Faraday's Law 54
Figure 4.10 Surface roughness evolution with time under ultrasound and abrasion ... 55
Figure 4.11 Three-dimensional images of (a) as-built surface; (b) surface after 1 h treatment by ultrasound and abrasion; and (c) surface after 4 h treatment by ultrasound and abrasion 55
Figure 4.12 Main effect plots in hybrid DOE for (a) response means and (b) *S/N* ratios 56
Figure 4.13 Three-dimensional surface images for samples in hybrid DOE 56
Figure 4.14 Surface waviness profile for (a) electropolishing for 30 min; (b) electropolishing for 45 min; (c) hybrid finishing for 30 min; (d) hybrid finishing for 45 min 58
Figure 4.15 Surface roughness and waviness comparison for electropolishing and hybrid finishing 58
Figure 4.16 Surface finishing mechanism for electropolishing and hybrid finishing .. 60

Figure 4.17 Mechanism for roughness removal due to ultrasound and abrasion: (a) cutting due to shallow impact angle; (b) peening due to large impact angle; (c) micro-void formation and material removal due to cavitation bubble collapse 61
Figure 4.18 Hypothesis for waviness removal due to synergistic effect of electropolishing, and application of ultrasound and abrasive particles 62
Figure 4.19 (a) Camera picture of as-built cylinder surface; (b) camera picture of cylinder surface after hybrid finishing.....63
Figure 5.1 Graphical overview of Chapter 5 65
Figure 5.2 Cross-section of internal channels: (a) Non-uniform distance between the wire and the channel wall when inserting the wire directly into the channels; (b) General concept of the tool electrode design.....66
Figure 5.3 Shape of printed straight and curved channels 67
Figure 5.4 Images for tool electrode, including camera picture for wire-cover assembly (blue disk was printed with hard material, and the white bridge was printed with flexible material), CAD design for printed polymeric wire cover, SEM image for wire cover and the SS316 wire.....68
Figure 5.5 Schematics of the experimental setup with electrolyte flow 70
Figure 5.6 Locations for internal channel surface roughness measurements 72
Figure 5.7 (a) 3D profile and (b) SEM image of as-built surface features 73
Figure 5.8 Comparisons of initial roughness for different curvatures 73
Figure 5.9 Percentage mass increase of wire covers at different immersion durations 74
Figure 5.10 Camera pictures of wire covers at different immersion durations.....74
Figure 5.11 3D profile of channel surface after polishing at (a) 25 V and (b) 30 V....75
Figure 5.12 Non-uniform and pitting surface after electropolishing at 30V at (a) lower magnification (200x) and (b) higher magnification (1600x).....76
Figure 5.13 3D surface profile for (a) as-built sample and samples after

electropolishing after (b) 4min, (c) 10 min and (d) 20 min 77
Figure 5.14 Different types of surface roughness evolution with time: (a) arithmetic mean height (*Sa*); (b) maximum height (*Sz*) 78
Figure 5.15 SEM images of polished surface under different magnifications: 78
Figure 5.16 Current density curve for electropolishing internal channels with different curvatures 79
Figure 5.17 Current densities measurements during electropolishing C1 80
Figure 5.18 Current densities measurements during electropolishing C2 81
Figure 5.19 Surface defects due to (a) short circuit; (b) melting due to high localized temperature; (c) pit formation 81
Figure 5.20 Effect of channel curvature on surface roughness after electropolishing for 20 minutes: (a-c) 3D surface profile of channels with different curvatures; (d-e) surface roughness values of electropolished surface 83
Figure 5.21 Microscope images of electropolished (a) C1 and (b) C2 84
Figure 5.22 Microscope picture of the straight channel 84
Figure 5.23 SEM images of non-uniformity of the polished channel surface for (a) C1 and (b) C2, with a Sa value of 1.30 ± 0.24 μm for the more polished areas and 5.11 ± 1.43 μm for the less polished areas 85
Figure 5.24 Comparison of polished and non-polished samples (image taken from C2) 85
Figure 5.25 (a) SEM and (b) 3D profile of pitting formation at the channel wall under ultrasonic cavitation 86
Figure 5.26 Three designs of wire covers 88
Figure 5.27 Geometries and boundary conditions using SC, CC and H for electropolishing internal channels 89
Figure 5.28 Mesh information for numerical modeling 90
Figure 5.29 Normalized current density distributions for reference geometry, and

channels with SC, CC and H 91
Figure 5.30 Normalized current density distribution along the channel length for SC, CC, and H 92
Figure 5.31 Flow velocity distributions for wire cover SC, CC and H (unit: m/s)..... 93
Figure 6.1 Graphical overview for Chapter 6 95
Figure 6.2 Camera picture of the DES at (a) 20 ºC and (b) 30 ºC 98
Figure 6.3 Voltage - current curve for DES electrolyte 98
Figure 6.4 Optical image and surface profile after electropolishing in DES electrolyte 99
Figure 6.5 Voltage - current curve for alcohol - salt electrolyte 99
Figure 6.6 Optical image and surface profile after electropolishing in alcohol - salt electrolyte 100
Figure 6.7 (a) Physical mechanism; (b) process mechanism for STP (reused with permission of Elsevier from [100]) 101
Figure 6.8 (a) Shear stress and (b) effective viscosity at different shear rate for corn starch at different volumetric concentrations (reused under the Creative Commons CC-BY license from [101]) 102
Figure 6.9 Experimental setup for shear thickening polishing 103
Figure 6.10 (a) Surface after laser melting, and (b) surface after STP 103
Figure 6.11 3D profile of the as-built surface for shear thickening polishing 104
Figure 6.12 Surface profile after STP for (a) 30 min, (b) 60 min and (c) side surface 104

List of Tables

Table 2.1 Classifications for Surface Roughness Parameters 10

Table 2.2 A summary of electropolishing research on AM parts 16

Table 4.1 Printing parameters for Ti6Al4V coupons 43

Table 4.2 Taguchi L9 design for electropolishing DOE 45

Table 4.3 Taguchi L9 design and output response for hybrid DOE 47

Table 4.4 Parameter Selection for Surface Waviness Investigation 49

Table 5.1 Printing parameters for cylinders 67

Table 5.2 Test Parameters 70

Table 5.3 Parameters Used for Numerical Simulation 89

List of Abbreviations

AM	Additive Manufacturing
PBF	Powder Bed Fusion
LPBF	Laser Powder Bed Fusion
SEM	Scanning Electron Microscopy
HIP	Hot Isostatic Pressing
AFM	Abrasive Flow Machining
MAF	Magnetic Abrasive Finishing
CAF	Cavitation Abrasive Finishing
HCAF	Hydrodynamic Cavitation Abrasive Finishing
CP	Chemical Polishing
EP	Electrochemical Polishing
LP	Laser Polishing
MDS	Molecular Dynamics Simulation
FEM	Finite Element Method
DEM	Discrete Element Method
CFD	Computational Fluid Dynamics
DES	Deep Eutectic Solvent
IL	Ionic Liquid
STP	Shear Thickening Polishing

List of Symbols

Ra	Arithmetical mean height of a line (μm)
Rz	Maximum height of a line (μm)
Sa	Arithmetical mean height of a surface (μm)
Sz	Maximum height of a surface (μm)
$\dot{m}$	Metal dissolution rate (kg/s)
m	Metal dissolution mass (kg)
t	Processing time (s)
A_w	Atomic weight (kg/mol)
I	Electric current (A)
Z	Valency of the anode material (1)
F	Faraday's constant (C/mol)
S	Processing area of the anode workpiece (m^2)
d	Inter-electrode distance (m)
R_s	Resistance of the electrolyte domain (Ω)
$\sigma_{electrolyte}$	Conductivity of the electrolyte (S/m)
$\sigma_{electrode}$	Conductivity of the electrode (S/m)
$j_{electrolyte}$	Current density of the electrolyte (A/m^2)
$j_{electrode}$	Current density of the electrode (A/m^2)
$\phi_{electrolyte}$	Potential of the electrolyte (V)
$\phi_{electrode}$	Potential of the electrode (V)
$Q_{electrolyte}$	Current source of the electrolyte (A)
$Q_{electrode}$	Current source of the electrode (A)
u	Displacement of the average surface plane (μm)
ΔE	Applied voltage between two electrodes (V)

V	Volumetric material removal (m^3)
n_i	Number of ions in the electrolyte (1)
q_i	The charge of ions (C)
μ_i	The mobility of ionic species ($m^2/(s \cdot V)$)
R	Bubble radius (m)
c	Sound velocity in the liquid slurry (m/s)
ρ_l	Liquid density (kg/m^3)
P	Pressure of the cavitation bubble wall (Pa)
P_0	Static ambient pressure (Pa)
P_v	Vapor pressure (Pa)
σ	Surface tension of the liquid (N/m)
R_0	Initial bubble radius (m)
n	Polytropic exponent of the gas in the bubbles (1)
μ	Liquid viscosity (Pa·s)
P_a	Sound pressure amplitude (Pa)
f	Sound frequency (Hz)
E_l	Bulk modulus of the liquid medium (Pa)
A	Displacement amplitude of the ultrasonic wave (m)
k	Wave number of the sound wave (1/m)
P_∞	Environment pressure (Pa)
u_p	Velocity of shockwave (m/s)
V_j	Microjet velocity (m/s)
P_j	Water hammer pressure (Pa)
H	Distance between the bubble center to the bubble wall (m)
F_r	Resulting force on the abrasive particles (N)

V_p	Abrasive particle velocity (m/s)
r_p	Radius of abrasive particles (m)
m_p	Mass of abrasive particles (kg)
ξ	Resistance coefficient (1)
s	Force area on the abrasive particles (m^2)
P_p	Impact pressure of abrasive particles (Pa)
ρ_p	Density of abrasive particles (kg/m^3)
ν_p	Poisson's ratio for abrasive particles (1)
ν_l	Poisson's ratio for liquid media (1)
E_p	Elastic modulus for the abrasive particle (Pa)
W_D	Deformation wear (m^3)
α	Impact angle of the abrasive particle (º)
V_{el}	Threshold velocity (m/s)
E_w	Elastic modulus for the workpiece material (Pa)
ν_w	Poisson's ratio for the workpiece material (1)
EL	Elastic load limit of the workpiece material (Pa)
j_0	Exchange current density (A/m^2)
α_a	Anodic charge transfer coefficient (1)
α_c	Anodic charge transfer coefficient (1)
η	Overpotential (V)
$\boldsymbol{u}$	Flow velocity field (m/s)
a	Wavelength of the sine wave (μm)
b	Amplitude of the sine wave (μm)
S/N	Signal to noise ratio (1)

1. Introduction

1.1. Research Motivation

Additive manufacturing (AM), also known as 3D printing, is a fabrication technique that builds objects layer-by-layer based on a computer-aided design model. Compared with conventional subtractive manufacturing, AM has the potential to save time and cost while also enabling the production of complex geometries in a simpler way normally without the assistance of any tools or molds. Among all seven categories of AM techniques defined by the ASTM standard [1], powder bed fusion (PBF), particularly laser powder bed fusion (LPBF), is considered one of the most important metal AM techniques. LPBF allows for the creation of nearly fully dense metal parts with excellent mechanical properties without the need for additional heat treatment, making it a superior method for industrial applications.

Despite the aforementioned advantageous characteristics, poor surface quality remains a significant challenge for metal parts manufactured using LPBF, which limits their applications due to reduced fatigue properties and corrosion behaviors. Changing printing parameters may provide some improvement, but for many applications, it is still almost impossible to meet industrial surface quality standards without further surface finishing. Thus, surface finishing must normally be applied after printing to reduce surface roughness and achieve ready-to-use parts with improved surface quality.

Traditional surface finishing techniques such as mechanical grinding [2], abrasive blasting [3] and shot peening [4] have been tested for AM metal parts. However, these methods are time-consuming due to the high initial surface roughness for AM metal parts, and they are not able to access the internal geometries of complex structures. Chemical finishing methods, on the other hand, can reach all surfaces, but the chemicals used in these processes are typically toxic and corrosive, which poses safety hazards to operators and negatively impacts the environment.

To address these issues, novel surface finishing approaches are required to be developed.

To this end, the main goal of this thesis is to develop novel and sustainable surface finishing techniques, which are capable of reducing surface roughness of additively manufactured metal parts, including both external surfaces and conformal internal channels, as well as to explain the scientific phenomena occurred during the process of surface roughness reduction, via both experimental and modeling methods. Once surface roughness is reduced, the fatigue limit [5] and corrosion resistance [6] of metal parts will be improved regardless of its microstructure, making it suitable for various industrial applications.

1.2. Research Objectives

The aim of this research is to develop efficient and safe surface finishing techniques for metal parts fabricated via LPBF. The ultimate objective is to achieve reduced surface roughness and improved surface quality for both external surfaces and internal channels of complicated geometries, to meet the industrial need while maintaining the functional properties and minimizing hazards to both the operators and the environment. The final goal includes the following sub-objectives:

- Design a process which has the capability of efficiently reducing micro- and meso-/macro-scale surface roughness;
- Design a process for achieving surface roughness reduction for internal channels;
- Conduct modeling to gain a deeper understanding of the underlying mechanisms and provide guidance for parameter selections in further experimentation;
- Construct an in-house experiment setup which can fulfill process requirements;
- Study and optimize surface finishing performance on parts with simple geometries;
- Study and optimize surface finishing performance on internal channels;
- Optimize the process to enhance efficiency, minimize hazards and reduce environmental impacts;
- Investigate other possible green approaches that might contribute to surface roughness reduction.

1.3. Thesis Outline

The thesis is organized in the following manner.

Chapter 2 presents a comprehensive literature review on LPBF and surface irregularities of metal parts fabricated via LPBF, as well as recent work dedicated to reducing surface roughness from both an experimental and modeling point of view. **Chapter 3** provides modeling results, including both analytical modeling and numerical modeling, for predicting material removal rate and surface roughness reduction in the electropolishing process. **Chapter 4** proposes a hybrid approach combining electropolishing, ultrasonic vibration and abrasive finishing, and demonstrates its capability on reducing both surface roughness and large-scale surface waviness. In **Chapter 5**, a novel electrode tool consisting of electrode wire and 3D-printed polymeric wire covers is introduced, and experimental and modeling results regarding the usage of the novel tool are reported. **Chapter 6** presents efforts on improving the sustainability of surface finishing techniques, including developing green electrolytes, and introducing shear thickening polishing. Finally, conclusions and future work are offered in **Chapter 7**.

Among seven chapters, contents in Chapter 4 and Chapter 5 have been modified based on two published or to-be-published works, including:

Chapter 4: M. Sun, E. Toyserkani, A novel hybrid ultrasound abrasive-driven electrochemical surface finishing technique for additively manufactured Ti6Al4V parts, *Inventions* 9 (2024) 45. https://doi.org/10.3390/inventions9020045.

Chapter 5: Manuscript entitled “Feasibility of 3D-printed polymeric covers for electrode wires in electropolishing of additively manufactured parts with internal channels” submitted to a peer-reviewed journal.

The graphical overview of the whole thesis is shown in Figure 1.1.

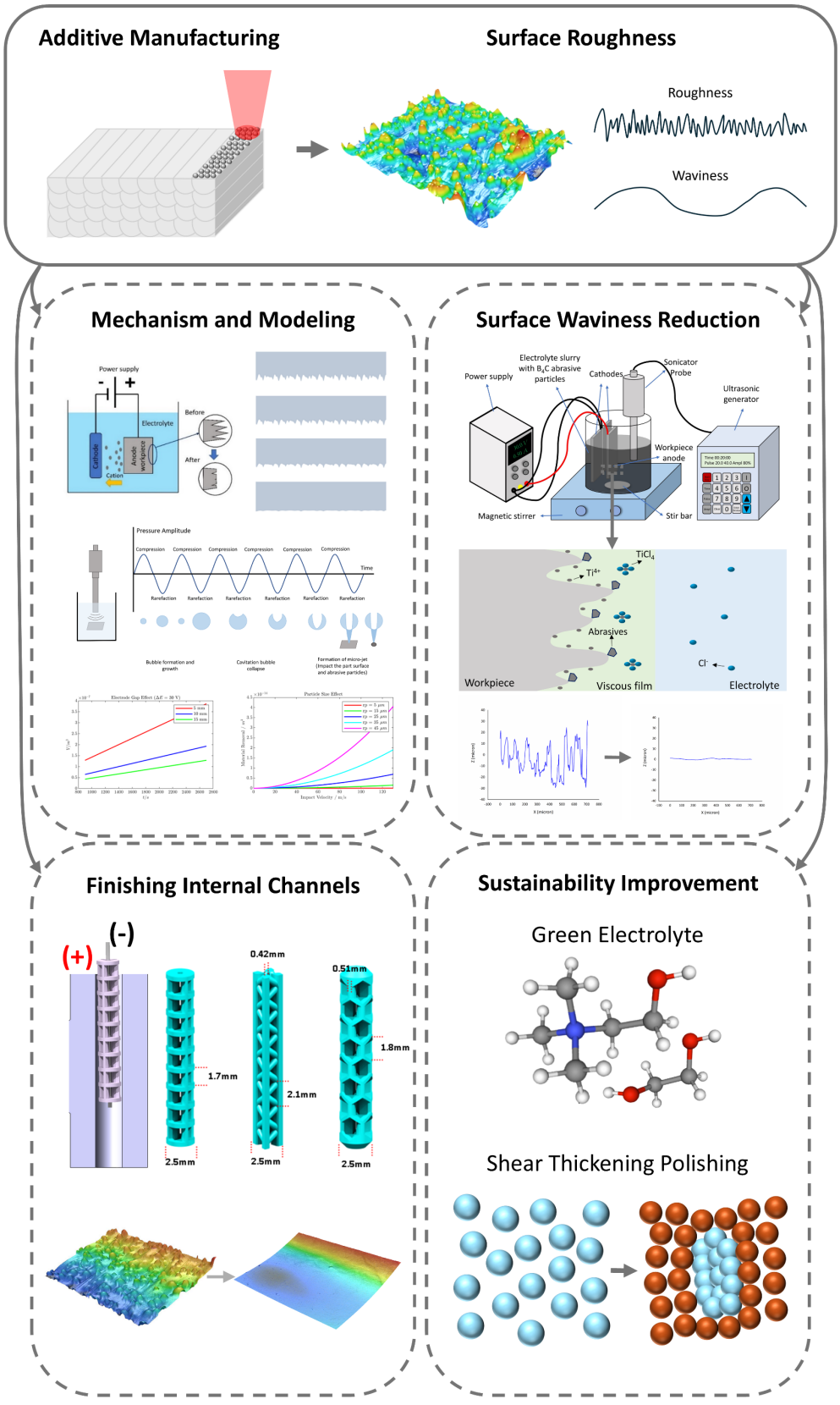


Figure 1.1 Thesis graphical overview and its concept interconnectivity

2. Literature Review

2.1. Chapter Overview

In this chapter, a comprehensive literature review on surface roughness and surface finishing is provided. The LPBF process used for sample fabrication is introduced at first. Then, aspects related to surface roughness including causes of surface roughness, its effect on material properties, as well as its characterization methods are explored. Following that different types of surface finishing techniques are explained and recent studies on development and application of these surface finishing techniques are reviewed. In addition, a brief review on surface roughness reduction for internal channels is presented. Finally, modelling approaches on research focusing on surface finishing are explained and investigated. Figure 2.1 presents the graphical overview of Chapter 2.

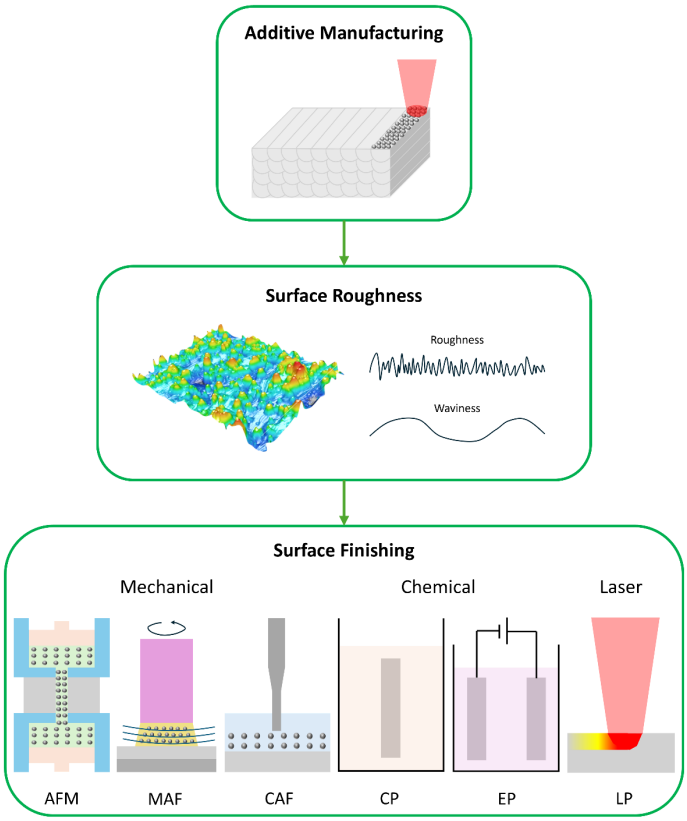


Figure 2.1 Graphical overview of chapter 2

2.2. Additive Manufacturing and Laser Powder Bed Fusion

Additive manufacturing (AM), as defined by the ASTM standard [1], is the process of joining materials to create objects from 3D model data in a layer-upon-layer manner. Based on different techniques involved in AM processes, AM can be divided into seven categories, including vat polymerization, material extrusion, material jetting, binder jetting, powder bed fusion, directed energy deposition and sheet lamination, among which powder bed fusion, especially laser powder bed fusion (LPBF), is the most commonly used for metal additive manufacturing.

LPBF is a highly flexible AM technique for fabricating metal parts with complex geometries that accounts for the highest market share in the metal AM industry. In the LPBF process, a moving laser beam is used to selectively melt the metal powder spread on a building platform, following the cross sections generated by the CAD (computer-aided design) software. After each layer is scanned and melted, the platform is lowered by a predetermined layer thickness and a new layer of powder is recoated on the platform. The process repeats until final parts with desired geometries are achieved. Figure 2.2 [7] shows the schematics of the LPBF process.

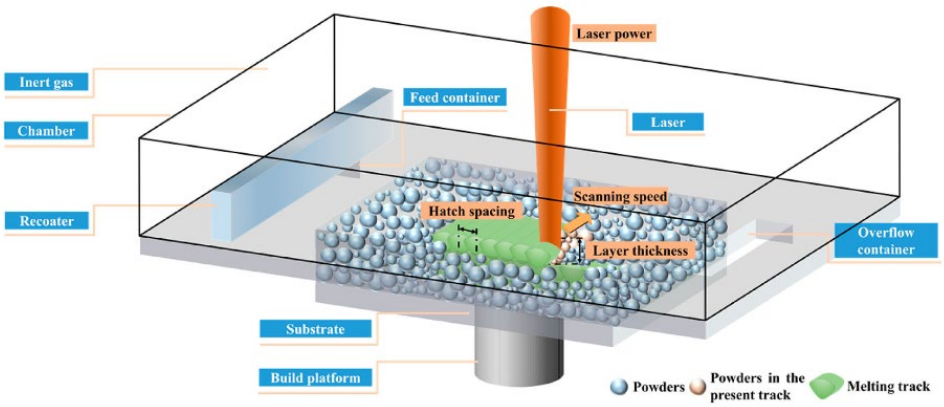


Figure 2.2 Schematics of the LPBF process (reused with permission of Taylor & Francis from [7])

2.3. Surface Roughness and Surface Irregularities

2.3.1. Types and Forming Mechanisms

Due to the layer-by-layer nature of LPBF and the complicated melting and solidification mechanisms involved in the process, metal parts fabricated via this method always possess high surface roughness (with *Ra* being 10-20 μm [8]), which limits their fatigue life and corrosion resistance. Physical mechanisms for surface defect formations will be discussed below.

Partially melted particles are the primary cause of high surface roughness, as unmelted metal powders adhere to the surface at extremely high temperatures, as shown in Figure 2.3 (a). Carter et al. [9] investigated the influence of contour scan parameters and laser energy density on the distribution of surface adhered particles with various printing directions and found that finer particles have a larger tendency to be attached to the surface.

The staircase effect is another major source of increased surface roughness, particularly on tilted and curved surfaces. It is created due to the layer-by-layer nature of the process, where larger layer thickness may result in visible surface discontinuities on inclined edges, as shown in Figure 2.3 (b) and (c) [10]. Similarly, since LPBF uses highly focused laser beams to melt metal powders, hatching distance in the scanning pattern also significantly affects the surface roughness. An extreme case of high surface roughness that resulted from a large hatching distance was illustrated by Yadroitsev and Smurov [11], who obtained their results by setting a much larger hatching distance than the laser spot diameter, as shown in Figure 2.3 (d).

Unusual behavior of the melt pool, such as balling effect, can also cause high surface roughness. Under ideal circumstances, when a focused laser beam passes through the metal surface, the metal underneath the laser spot would melt and form an elongated liquid track. However, the tendency of the melt pool track to minimize its surface energy due to liquid surface tension results in the neck formation of an elongated melt

pool and even the formation of separate spherical droplets. [12] At a high scanning speed, many micro-droplets spatter and solidify near the sintered surface, increasing surface roughness. Figure 2.3 (e) [13] illustrates the forming mechanism for balling effect. Figure 2.3 (f) and (g) show SEM images of metal surfaces with balling.

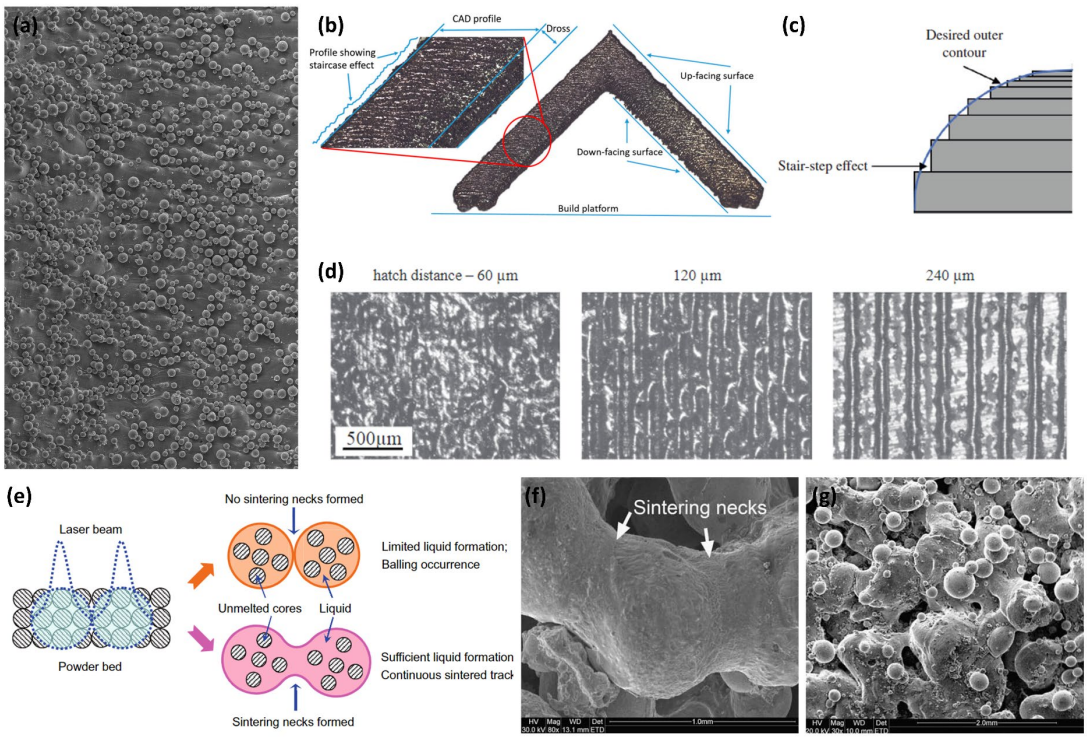


Figure 2.3 Surface roughness due to (a) surface adhered particles, (b-c) staircase effect (reused under the Creative Commons CC-BY license from [10]), (d) large hatching distance (reused under the Creative Commons CC-BY license from [11]), and (e-g) balling effect (reused with permission of Elsevier from [13])

2.3.2. Effects on Material Properties

Surface roughness can significantly affect the fatigue properties of metals, as surface defects and irregularities can act as sites for fatigue crack initiation, resulting in material failure. Balachandramurthi et al. [14] compared the fatigue properties of parts fabricated via both LPBF and electron beam melting (EBM) and concluded that the fatigue performance of LPBF parts is better than EBM parts since EBM parts possess higher surface roughness and a larger lack of fusion defects, which are the primary causes for fatigue crack initiation. Similarly, Natatani et al. [15] studied the impact of

hot isostatic pressing (HIP) on the fatigue properties of LPBF Ti6Al4V parts. Although HIP successfully eliminates internal defects, it does not improve fatigue properties since there is no change with respect to the surface roughness of the material. Therefore, surface defects and roughness have a negative impact on the fatigue strength of metals.

Corrosion behaviors of metals are also greatly influenced by their surface conditions. The presence of surface roughness provides a larger surface area for corrosive substances to interact with the metal and initiate corrosion. Meanwhile, surface defects can also trap corrosive substances and impurities, accelerating the corrosion process. Schaller et al. [16] compared the corrosion behaviors of wrought SS304L and LPBF SS304L before and after polishing. Compared with the wrought part, the as-built LPBF part shows a decreased corrosion resistance with a decreased pitting potential due to its higher surface roughness and porosity. However, the corrosion resistance of the polished LPBF SS304L far exceeds the wrought part in the same testing environment. Miller et al. [17] studied the corrosion behavior of traditionally manufactured (TM) SS316L and LPBF SS316L in sulfuric acid solution. Results show that general corrosion happened on the surface of LPBF SS316L while no major change occurred on the TM SS316L surface.

2.3.3. Surface Roughness Characterization

Methods for surface roughness measurement can be classified into two categories, contact-based method and non-contact-based method. Contact-based measurement techniques use the physical contact between a probe and the metal surface to sense the surface fluctuations and surface defects. On the contrary, non-contact-based methods always use the reflection of light to characterize the surface topology. Figure 2.4 demonstrates the working principle for both contact-based method, with stylus profilometer (Figure 2.4 (a)[18]) as an example, and the schematics of optical profilometer (Figure 2.4 (b)[19]), on behalf of the non-contact-based category. Since additively manufactured metal parts possess large initial surface roughness, the difference between results achieved from contact-based method and non-contact based

method is in the acceptable range.

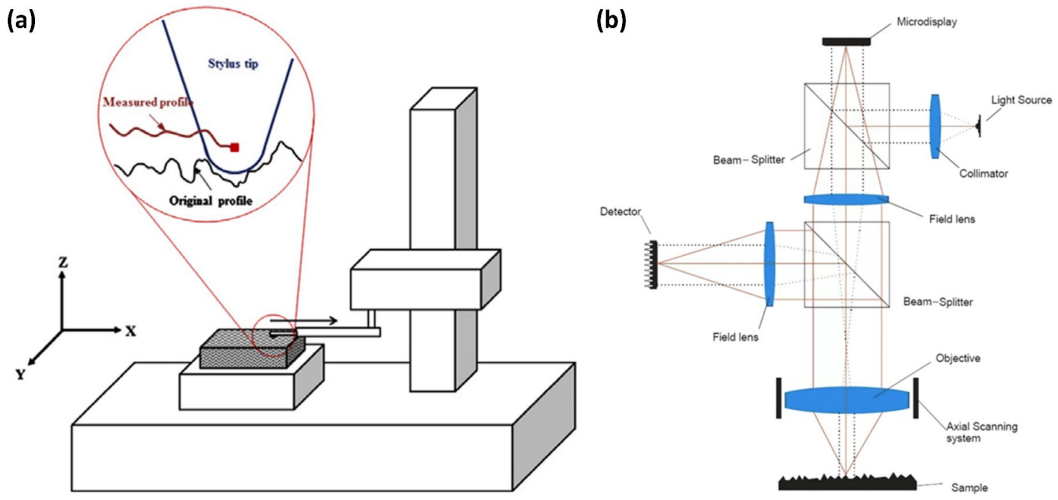


Figure 2.4 Schematics of working principles for (a) contact-based stylus profilometer (reused with permission of Elsevier from [18]) and (b) non-contact based optical profilometer (reused under the Creative Commons CC-BY license from [19])

Different types of surface roughness have been considered for surface roughness characterization. According to ISO 25718, surface roughness parameters that are used for characterizing additively manufactured surfaces are as shown in Table 2.1[20]. Among them, the most commonly used ones for general applications are *Sa* and *Sz*.

Table 2.1 Classifications for Surface Roughness Parameters

Parameter	**Definition**	**Description**
Sa	$Sa = \frac{1}{A}\iint_A \lvert z(x,y)\rvert dxdy$	Arithmetical mean height
Sq	$Sq = \sqrt{\frac{1}{A}\iint_A z^2(x,y)dxdy}$	Root mean square height
Ssk	$Ssk = \frac{1}{Sq^3}\left[\frac{1}{A}\iint_A z^3(x,y)dxdy\right]$	Skewness
Sku	$Sku = \frac{1}{Sq^4}\left[\frac{1}{A}\iint_A z^4(x,y)dxdy\right]$	Kurtosis
Sp	$Sp = \max_A z(x,y)$	Maximum peak height

Sv	$Sv = \left\lvert \min_A z(x,y) \right\rvert$	Maximum pit height
Sz	$Sz = Sv + Sp$	Maximum height

2.4. Surface Finishing Techniques

As explained in the previous sections, high surface roughness, leading to not only poor surface aesthetics but also reduced functional properties, is one of the most significant challenges facing the industrialization of metal AM. Although optimization of printing parameters can help with reducing surface roughness to some extent, it is still impossible to reach some of the industrial requirements of surface roughness, in aerospace, automotive and energy sectors, which are normally $Ra < 1$ μm and $Rz < 20$ μm [21]. Therefore, in order to have ready-to-use metallic AM parts, surface post-treatments should be conducted to reduce surface roughness.

Since metallic AM parts always have complex geometries, only non-conventional surface finishing techniques that can deal with complex geometries are reviewed in this section. Based on the different finishing mechanisms and the energy sources used for the treatment, these finishing techniques can be classified as mechanical, chemical, and laser-based. Mechanical and chemical finishing techniques can also be combined together to form hybrid finishing methods for improving process efficiency. A detailed literature review on these techniques will be given in the subsequent sub-sections.

2.4.1. Mechanical Finishing Techniques

Mechanical energy can be applied to material systems for surface smoothening in the form of abrasive media. In terms of surface finishing of complex geometries and internal channels, abrasive flow machining and magnetic abrasive finishing are promising candidates. Abrasive particles suspended in the liquid media can also be used as the polishing media, with the help of cavitation effect due to pressure drop.

Abrasive flow machining (AFM) is a non-conventional abrasive-based polishing technique which utilizes a viscoelastic fluid with high viscosity loaded with abrasive particles to polish a metal AM part, including both external and internal features, as

shown in Figure 2.5(a) [22]. Typically, high hydraulic pressure is applied through a piston on the abrasive-laden fluid, creating the relative velocity between the workpiece surface and the abrasive fluid; this constitutes the material removal mechanism for AFM. Peng et al. [23] studied the process parameters, including abrasive size, mass fraction of abrasive particles in the fluid, as well as the amount of pressure applied to the abrasive fluid on the surface of AM AlSi10Mg alloy. Their experimental results proved that the AFM process is capable of reducing surface roughness (from initial *Sa* of 13 - 14 µm to 1.8 µm after polishing), while compressive residual stress can be induced in the surface layer.

Compared to other non-traditional surface finishing techniques, AFM is relatively mature and has been used as the surface treatment method for some industrial studies. Adiaconitei et al. [24] manufactured a closed pump impeller for space applications with LPBF and polished the complicated geometry with AFM, as shown in Figure 2.5 (b-e). The surface roughness Ra was reduced from 6.480 - 8.233 µm to 3.85 µm for the shroud (Figure 2.5 (b, c)) and 0.66 µm for the disc (Figure 2.5 (d, e)). François et al. [25] printed Ti6Al4V, and AlSi7Mg0.6 waveguides with LPBF, finished the internal surfaces with AFM, and compared the electromagnetic properties before and after surface finishing. The surface roughness Ra of the waveguide channels decreased from 10 µm to 1 µm after the treatment (the SEM image shown in Figure 2.5 (f, g)), leading to an obvious increase of the surface electrical conductivity and better performance of the waveguides.

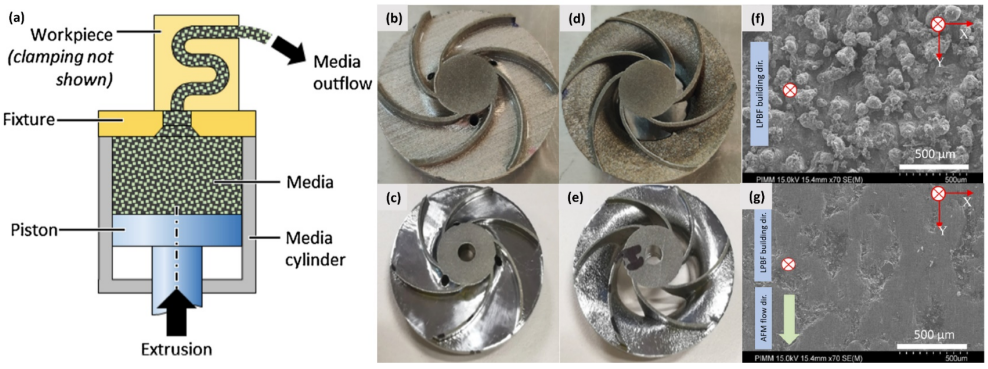


Figure 2.5 Abrasive flow machining (a) schematics (reused with permission of Elsevier from [22]), (b-e) AFM treated closed pump impeller (reused under the

Creative Commons CC-BY license from [24]), (f, g) SEM images of AFM treated waveguide channels (reused with permission of Taylor & Francis from [25])

Magnetic abrasive finishing (MAF) is another novel abrasive-based polishing technique, especially for surface finishing of internal channels. The formation of a flexible magnetic abrasive brush creates the relative motion between abrasive particles and metal surface. As shown in Figure 2.6 (a) [26], the workpiece is placed between the north pole and the south pole of magnets, while the working gap between the workpiece and the magnetic tool is filled with the mixture of magnetic particles and abrasive particles. The interaction between abrasive media and workpiece material is generated by moving or rotating the magnetic tool. Zhu et al. [27] investigated MAF process parameters for LPBF AlSi10Mg coupons printed with different building angles and successfully achieved a surface roughness Sa reduction from 4-10 μm to around 100 nm by removing surface defects within 2 hours. Figure 2.6 (b) and (c) show both 3D morphology of the surface profile and the camera image of the mirror effect when printed vertically. Karakurt et al. [28] modified the concept by adding magnetic particles and abrasive particles into a viscous liquid to form a magnetic slurry instead of simply using dry particles as the abrasive media. Particle movement can be generated by applying an oscillating external magnetic field to obtain some surface smoothening effect. Results show that surface roughness Ra of electron beam melted copper samples can be decreased from 35 μm to about 4 μm after 10000 polishing cycles.

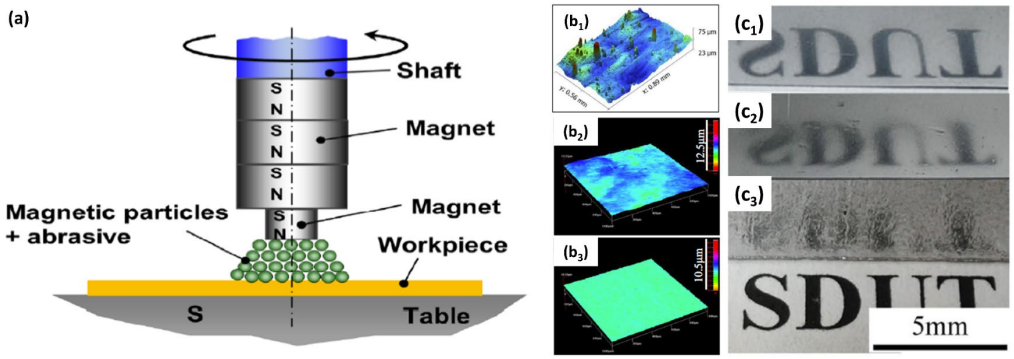


Figure 2.6 Magnetic abrasive machining (a) schematics (reused under the Creative Commons CC-BY license from [26]), (b) 3D profiles, (c) mirror effect (reused with

permission of Springer Nature from [27])

Cavitation abrasive finishing (CAF) is also a promising candidate for finishing complex geometries. Solid-liquid mixtures with abrasive particles are often used as the source of cavitation erosion which acts as the principal material removal mechanism for cavitation abrasive finishing. In the process, vapor bubbles form due to liquid pressure drop due to the ultrasonic vibration (ultrasonic cavitation) or velocity change (hydrodynamic cavitation). The force created by the explosion of vapor bubbles directly removes the material from the part surface or provides initial velocity for abrasive particles to impact the part surface. Tan et al. [29][30] investigated the effect of ultrasonic cavitation abrasive finishing on LPBF IN625 samples with both flat surfaces and curved internal channels, achieving surface roughness Ra improvement of 45% for flat surfaces and 20% for internal channels of 3 mm diameter by removing small-sized partially melted particles from the metal surface. Nagalingam et al. [31] studied the influence of hydrodynamic cavitation erosion on internal surface modification of LPBF AlSi10Mg parts and the resulting surface roughness Sa reduced from 41.3 μm to 6.1 μm with the acceptable thickness loss of under 45 μm. Figure 2.7 (a)[30] and (b)[31] show schematics for ultrasonic cavitation abrasive finishing and hydrodynamic cavitation abrasive finishing.

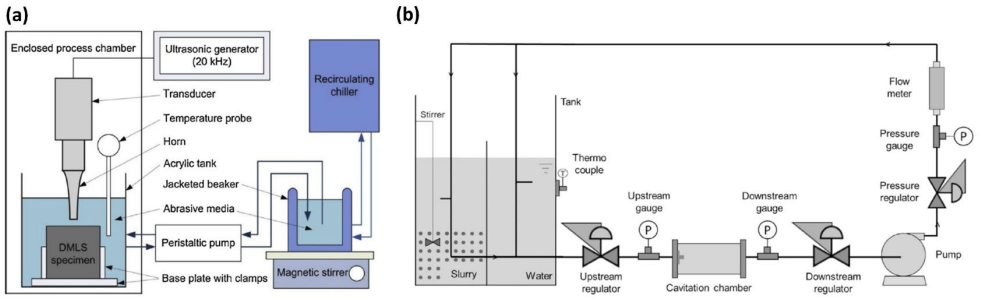


Figure 2.7 Schematics of (a) ultrasonic cavitation abrasive finishing (reused with permission of Elsevier from [30]) and (b) hydrodynamic cavitation abrasive finishing (reused with permission of Elsevier from [31])

Although mechanical finishing techniques are commonly used for surface finishing of

AM parts, its long processing time, its insufficient surface quality, as well as the difficulty of accessing internal geometries limit its industrial use. Compared with mechanical treatments, chemical finishing methods possess some unique advantages (see Section 2.4.2); therefore, the combination of mechanical and chemical finishing techniques (see Section 2.4.3) may be possible to improve process efficiency for meeting industrial needs.

2.4.2. Chemical Finishing Techniques

Metal surfaces can be smoothened via chemical or electrochemical reactions between metals and electrolytes. Based on whether an electric current is applied or not, processes can be divided into chemical polishing (CP) and electrochemical polishing (EP, or electropolishing). Compared with mechanical finishing techniques, chemical finishing techniques, especially chemical polishing as a tool-free method, have the capability of offering access to internal structures which can not be easily accessed by mechanical tools. In addition, chemical post-processing methods also possess higher finishing efficiency, do not need special and expensive equipment, and are easy to operate. Due to the advantages mentioned above, chemical and electrochemical polishing is becoming more and more popular for surface finishing in the AM industry.

For conducting chemical polishing, metal parts are immersed in chemical agents for chemical reactions to occur. Current research always uses strong acids as polishing media to dissolve metal alloys. Titanium alloys are the most commonly studied alloys for chemical polishing research due to their unique mechanical properties, which make them difficult for mechanical machining. At the same time, due to their excellent chemical stability, highly strong acids, including hydrofluoric acid and perchloric acid, need to be used for chemical polishing. Łyczkowska et al. [32] studied the surface quality evolution of LPBF Ti6Al7Nb alloy with complex spatial structures in the mixture of HF and HNO_3 solution and concluded that the reduction of bath concentration together with the extension of the processing time leads to the optimal surface roughness. Figure 2.8 (a) shows the comparison of the titanium scaffold before

and after chemical polishing. HF- HNO_3 mixture is also used in the chemical polishing of other titanium alloys. Bezuidenhout et al. [33] investigated the surface and mechanical properties of LPBF Ti6Al4V specimens after chemical polishing in various concentrations of HF, and results show that when the HF concentration is 4M, a mirror surface without any obvious defects (see Figure 2.8 (b)) could be achieved with an average roughness value Ra of less than 1 μm. Tyagi et al. [34] demonstrated the possibility of chemical polishing to treat the surface in the hidden area by fabricating an AM SS316 sample with an opening of only a few millimeters wide and reducing the surface roughness of the hidden area to ~0.4-μm Ra value, as shown in Figure 2.8 (c).

Although chemical polishing is an effective and simple way of reducing surface roughness, chemical agents involved in the process are highly corrosive and not safe to handle. In order to use less-corrosive chemicals for the same purpose, a potential difference can be applied between the workpiece and an inert electrode to accelerate the reaction, which is called electropolishing. Electropolishing is much more popular than chemical polishing due to the diversity of materials it can work with. Meanwhile, non-hazardous electrolytes can also be used for the electropolishing process. Table 2.2 summarizes electropolishing parameters and surface roughness results for AM research in the last five years. Detailed mechanisms for electropolishing will be elaborated on in the following sections.

Table 2.2 A summary of electropolishing research on AM parts

Ref.	**Material**	**Electrolyte**	**Current Density or Voltage, Temperature**	**Time (min)**	**Initial Roughness (μm)**	**Final Roughness (μm)**
[35]	SS316L	Ethaline (Deep eutectic solvent)	6 V 40 ℃	60	Rz=7±15% (re-melted)	Rz=0.34
[36]	SS316L	85% H_3PO_4 and 15% H_2SO_4	60 A/dm^2 75±2 ℃	30	Sa=13.88±2.66	Sa=2.10±0.75
[37]	SS316L	H_3PO_4, $C_3H_8O_3$, H_2O	12V, 75 ℃	1.5	Ra = 8.45	Ra = 5.96
[38]	SS316L	70% H_3PO_4 and 30% H_2SO_4	~70 A/dm^2 75 ℃	60	Ra = 7.37	Ra = 3.31
[39]	SS316L	S1: NaCl-EG-10%	S1: 1.5 A/cm^2	S1:2.7	Sa = 15~25	Sa = 4.41

		Ethanol S2: commercial A2 electrolyte	S2: 0.25 A/cm^2 Ambient	S2:40		
[40]	Ti6Al4V	60% $HClO_4$ and CH_3COOH (3:7)	240 mA/cm^2 23 ℃	23	Ra=11.74±1.29	Ra=1.26±0.91
[41]	Ti6Al4V	CH_3COOH, 60% $HClO_4$ and ethanol	442 mA/cm^2 4 ℃	20	Ra ~ 24	Ra = 4.5
[42]	Ti6Al4V	Ethylene glycol, 0.4M $MgCl_2$, 0.5% DI water	0.5 A/cm^2 25 ℃	10	Ra ~ 9	Ra = 1.13
[43]	Ti6Al4V	$ZnCl_2$, $AlCl_3$, ethanol, isopropanol	70 V Ambient	6	Sa = 14.02	Sa = 3.29
[44]	Ti6Al4V	NaCl-Ethylene glycol	20 V 30 – 40 ℃	75	Ra ~ 10.5	Ra ~ 5.5
[45]	Ti6Al4V	CH_3COOH, 70% $HClO_4$, oxalic acid	25 V Ambient	20	Sa = 8.47	Sa = 1.09
[46]	IN625	60% $HClO_4$ and CH_3COOH (3:7)	9 V 23 ℃	Till 1000 mA cm^{-2} min	Ra = 16.78	Ra = 1.96
[47]	IN718	20% H_2SO_4, 80% CH_3OH	50 A/dm^2 Ambient	1	Ra = 9.69	Ra = 5.13
[48]	IN718	$HClO_4$ and CH_3COOH (7:3)	50 A/dm^2 10 ℃	80	Sa = 6.702	Sa = 2.395
[49]	IN625	20% H_2SO_4, 80% CH_3OH	30V Ambient	4	Ra = 13	Ra = 0.91

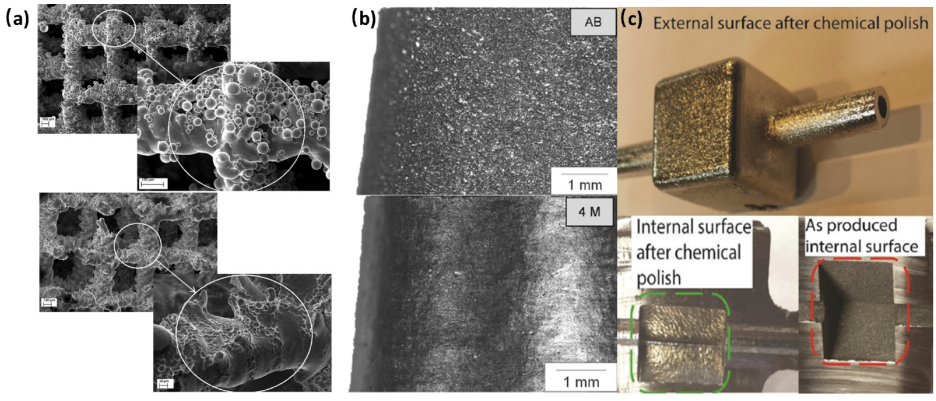


Figure 2.8 Examples of chemical polishing (a) Ti6Al7Nb scaffolds (reused with permission of Springer Nature from [32]), (b) Ti6Al4V specimen(reused with permission of Elsevier from [33]), (c) SS316 hidden area (reused with permission of

Springer Nature from [34])

2.4.3. Hybrid Finishing Techniques

In order to improve the process efficiency and reduce the surface roughness limit that can be reached for complex AM structures with internal channels, hybrid techniques with the combination of mechanical finishing techniques and chemical finishing techniques have appeared in recent years. Mohammadian et al. [50] tested the synergistic effect of chemical finishing and mechanical finishing using acid-based chemicals and abrasive particles when polishing the internal surfaces of tubular IN625 parts. Compared to either chemical flow polishing or abrasive flow polishing conducted individually, the combined chemical-abrasive flow action shows a two-fold increase with respect to the surface roughness reduction, as shown in Figure 2.9(a). Zhao et al. [51] designed a novel finishing method, combining electrochemical and mechanical polishing. They invented a specific cathode tool in which the metallic twisted pair acted as the inert cathode for electropolishing, while the nylon filaments attached to the metal functioned as flexible abrasives to generate some mechanical interactions with internal channels, as shown in Figure 2.9 (b). With the innovative setup, they achieved a Sa reduction from 14.151 μm to 3.880 μm for straight internal channels and from 15.522 μm to 9.095 μm for curved internal holes. Rech et al. [52] invented another hybrid electrochemical-mechanical finishing process by adding abrasive media in the electrolyte flux while rotating the container and the sample at the same time. The process shows promising surface roughness reduction on both simple and complex geometries, as shown in Figure 2.9 (c).

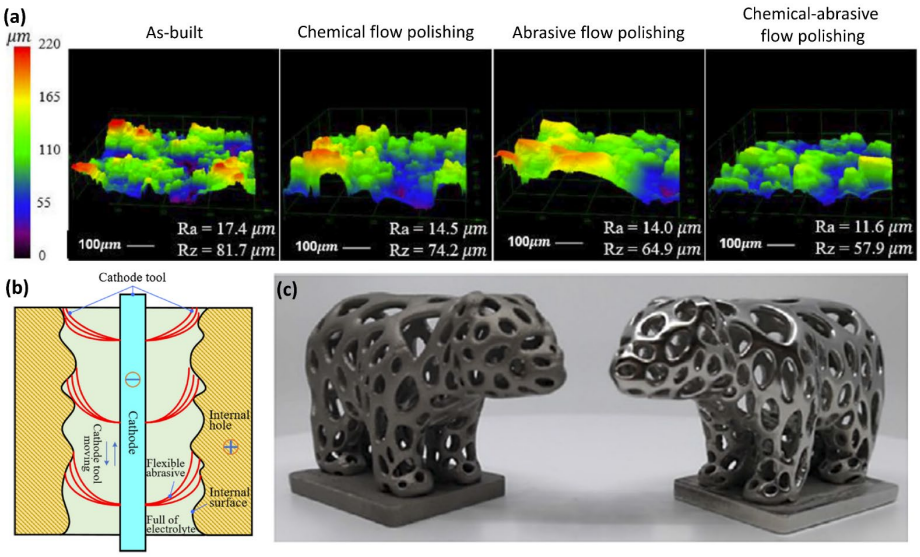


Figure 2.9 Examples of hybrid finishing techniques (a) 3D profile of chemical-abrasive flow polishing (reused with permission of Elsevier from [50]); (b) schematics of novel cathode tool (reused with permission of Elsevier from [51]); (c) electrochemical-mechanical polishing of complex structures (reused with permission of Elsevier from [52])

2.4.4. Laser-based Finishing Techniques

Laser is also a commonly used energy source for polishing metallic materials. In the process of laser polishing, also called laser-remelting, a laser with short pulses irradiates on the metal surface, leading to the formation of a melt pool in the range of a few nanometers on the surface, which levels itself as a result of gravity, surface tension and capillary effect. When the laser beam moves away, the abrupt temperature drop leads to rapid solidification of the leveled melt pool, resulting in a smoothing effect on the metal surface. [53] Figure 2.10 [54] shows the schematic illustration of the laser polishing (LP) process based on the laser remelting process.

Lee et al. [55] conducted laser polishing on Ti6Al4V parts fabricated via LPBF and reduced the surface roughness value by approximately 60-70%. The reduction of surface roughness leads to the improvement of high cycle fatigue resistance, while the introduction of residual stresses due to laser polishing decreases the low cycle fatigue

strength of the part. Besides smoothing the surface, laser polishing also has the capability to create special features on the metallic surface to change some surface properties. Yung et al. [56] studied the laser polishing parameters for additively manufactured CoCr components and reduced the surface roughness (*Sa*) value to less than 1 μm. Meanwhile, the finishing process modified the wettability of the surface to the Wenzel state.

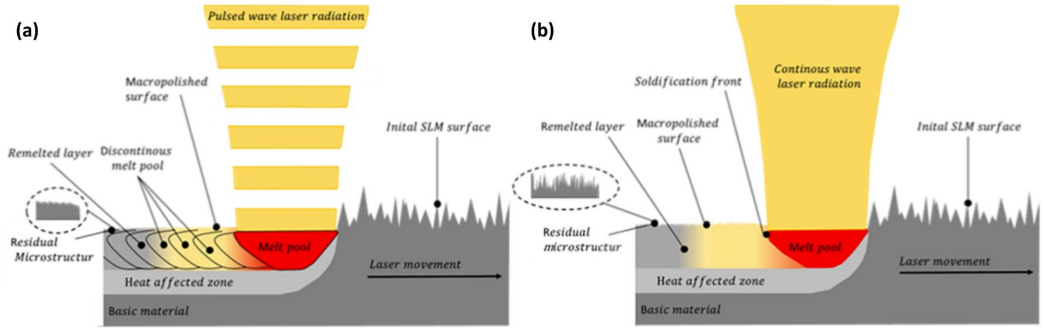


Figure 2.10 Schematic illustration of laser polishing technique (reused with permission of John Wiley and Sons from [54])

2.5. Surface Finishing of Internal Channels

Compared with external surfaces, it is more challenging to achieve a high-quality surface finish for internal structures due to limited access to finishing tools and media in the channels. Recently, more and more attempts have been conducted for smoothening internal surfaces to achieve optimized functional flow[57]. Among them, AFM is the most widely used process for polishing internal channels, where a viscoelastic fluid with abrasive particles is used as the polishing media and the relative motion between the slurry and the channel wall under hydraulic pressure reduces surface roughness [58]. Han et al. [59] tested AFM technique on straight and helical channels printed with maraging steel 300 and obtained a surface roughness reduction from 7.6 μm to 1.3 μm. Guo et al. [60] showed the effective removal of partially melted particles on the Inconel 718 channel walls fabricated via laser powder bed fusion (LPBF) by AFM without causing any subsurface damage. To further control the motion of the polishing slurry more efficiently in the internal channel, a magnetic field has been

applied. For example, Zhang et al. [61] reduced the average line roughness of 316L stainless steel from 11.6 μm to 0.8 μm with the assistance of a magnetic field within minutes. Other than viscose polishing slurry, methods using liquid abrasive flow have also achieved promising performance in terms of finishing internal channels, such as hydrodynamic cavitation abrasive finishing (HCAF). Nagalingam et al. [62] reported the influence of hydrodynamic cavitation erosion on internal surface modification of LPBF AlSi10Mg parts and the resulting surface roughness Sa reduced from 41.3 μm to 6.1 μm with the acceptable thickness loss of under 45 μm.

However, there is a very limited amount of research on using electropolishing for improving the surface quality of internal channels, with most studies focusing on inserting cylindrical cathodes in the straight channels. For instance, Shen et al. [63] used a two-step electropolishing approach to reduce the surface roughness (*Ra*) of 316L stainless steel cylindrical samples with internal channels from 10 μm to 4 μm. Similarly, Ali et al. [49] fabricated cathodes with LPBF according to the shape of internal structures and achieved an average of 80% surface roughness improvement for Inconel 625 parts. Only one research group [64] to date has utilized electropolishing for curved channels by using conductive metal wire electrodes and non-metallic microfilaments arranged between the wire and the channel wall as the inert cathode. Although promising results have been achieved for electropolishing on improving surface quality, the limited accessibility of tool electrodes still remains a challenge for the application.

2.6. Modeling Approaches

The development of computational resources provides the capability for analytically solving complex real-world problems. Conducting simulations or modeling work on surface finishing processes helps researchers predict surface material removal while changing input parameters. It also helps process designers better understand the process mechanisms and select the most suitable experiment parameters for process optimization. Common modeling methods include molecular dynamic simulation (MDS), finite element method (FEM), discrete element method (DEM) and

computational fluid dynamics (CFD).

Molecular dynamic simulation (MDS) is a computer simulation technique used for studying the motions of a set of molecules, or atoms in the case of metals. Equations of motions for atoms and molecules are integrated and calculated in a fixed period of time. Once the positions, the velocities and the accelerations of the particles are known, the state of the system can be predicted. Asadollahi et al. [65] used MDS to study the influencing parameters of abrasive water jet finishing on aluminum alloy 7075 with reinforcements of Al_2O_3, graphite, and SiC, and simulation results of the atomic positions and force-fields matched the experimental data perfectly. Xu et al. [66] created a bi-phasic MDS model including magnetic dipoles and abrasive particles to investigate particle behaviors in magnetorheological polishing slurry under different magnetic field gradients and intensities as well as abrasive particle concentrations.

Discrete element method (DEM) is a numerical technique that simulates the interactions between individual particles and material boundaries to predict bulk material properties, including material removal. Makiuchi et al. [67] proposed a DEM-based material removal model on the basis of Hertz contact theory and Preston's law for vibratory finishing, which offers a useful tool for process optimization. Kopp et al. [68] successfully predicted the roughness reduction of centrifugal disc finishing on additively manufactured metal parts using DEM, with a deviation from experimental results of about 20%.

Finite element method (FEM) solves problems by numerically solving partial differential equations. For doing this, a large system is divided into various smaller parts called finite elements. Jain et al. [69] studied the material removal mechanism of AFM using FEM on a single grain, and the modeling results show the same trend as experimental results achieved on brass. Chaieb et al. [70] investigated the residual stress change in the shot peening process through a new FEM-based approach and saved around 70% of simulation time compared with calculating using DEM.

Computational fluid dynamics (CFD) applies FEM to the calculation of fluid flows.

Different forms of Navier-Stokes equations are selected to calculate fluid properties for different types of fluids. Chai et al. [71] simulated and evaluated the flow velocity field of electrolytes in the interelectrode gap for the electrochemical machining process using CFD analysis. Results show that both the increase of voltage and electrolyte concentration may lead to the increase of the flow velocity. Bouland et al. [72] simulated the velocity and pressure field of a polishing medium using CFD and combined the results from CFD simulation with an analytical model to obtain the material removal rate and surface roughness evolution for abrasive flow machining of LPBF parts.

2.7. Summary

Due to the limitations of current AM techniques in achieving perfect surface finishes, surface modification is recognized as a critical step in the AM holistic workflow to eliminate surface defects arising from the printing step. Although some progresses are made in this field, research gaps and challenges still exist, as listed below.

(1) While extensive research has focused on the modeling of surface finishing techniques, very few have focused on deriving models compatible with AM surfaces with specific surface features/patterns.

(2) Although micro-scale surface roughness can be removed efficiently with current surface finishing techniques, it is still challenging to remove meso-/macro-scale surface waviness caused by stair-stepping effect.

(3) Despite the well-established surface finishing techniques for simple AM parts, effective finishing of complex-shape internal channels remains a significant challenge for researchers and industry.

(4) Corrosive and toxic media are often used in surface finishing processes, highlighting the need for future research in improving the sustainability of the techniques.

Based on the aforementioned challenges, there are four research chapters in the thesis (Chapter 3-6), with each chapter trying to solve one of the challenges above.

3. Analytical and Numerical Model on Surface Finishing Processes

3.1. Chapter Overview

In this chapter, analytical and numerical models on surface finishing techniques tested in this thesis are provided, which serve as the basis for the experimental tests in the following chapters. Firstly, electropolishing and ultrasonic cavitation abrasive finishing are introduced and basic mechanisms involved in the process are explained. Then, analytical equations to calculate material removal rate during electropolishing while considering initial surface roughness are given, with the calculated results in accordance with the experimental results. Following that, a numerical model to analyze the surface roughness evolution under different electropolishing parameters and initial roughness values is developed using COMSOL Multiphysics, further confirming that it is harder to remove large-scale surface waviness than small-scale surface roughness. Finally, an analytical model, along with some calculation results using experimental parameters, to explain material removal during ultrasonic abrasive finishing process is also presented. Graphical overview of this chapter is provided in Figure 3.1.

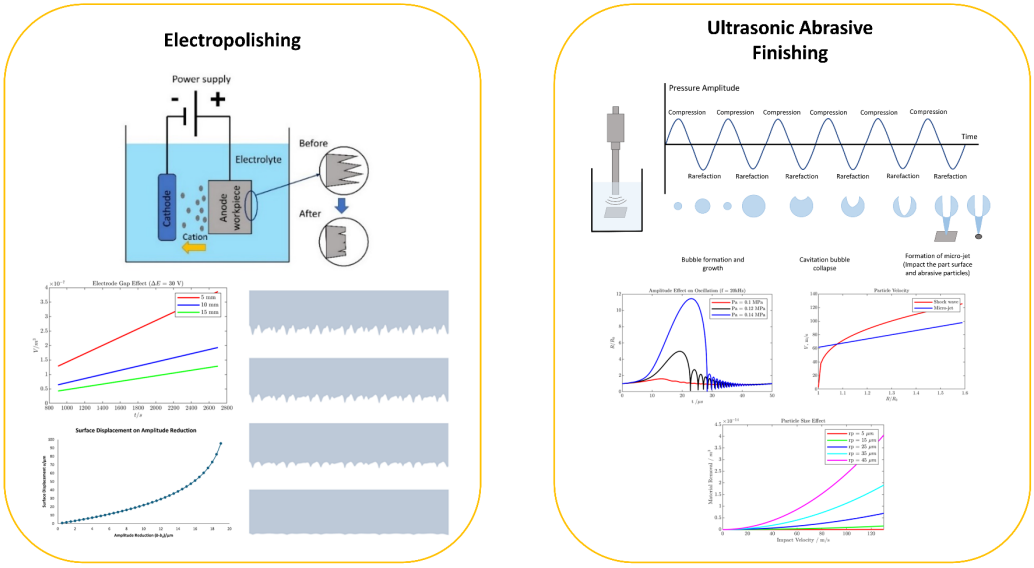


Figure 3.1 Graphical overview of Chapter 3

3.2. Process Description

3.2.1. Introduction to Electropolishing

Electrochemical polishing is a material removal process for conductive metals based on electrochemical reactions. Unlike conventional mechanical machining processes including cutting, milling and grinding, electropolishing is a contactless process that will not cause any damage to the metal surface. As shown in Figure 3.2, the basic component in an electropolishing setup is an electrolytic cell containing a workpiece anode and an inert cathode in the electrolyte bath. Both the cathode and the anode are connected to a power supply. Electrons flow from the anode to the cathode when applying a voltage between two electrodes through the electrical circuit. Meanwhile, due to the oxidation of metal atoms on the workpiece anode, metal cations are formed and dissolved in the electrolyte and move toward the cathode, resulting in the material removal from the metal workpiece.

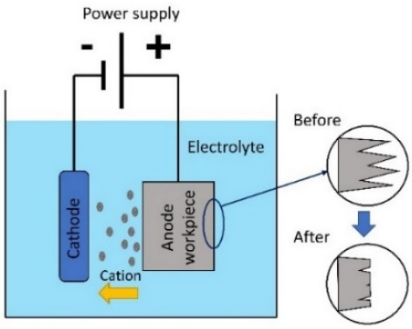


Figure 3.2 Schematic of electropolishing setup

Compared with other novel surface finishing techniques, electropolishing is relatively mature after developing for decades. It is widely accepted that many factors will contribute to the resulting electropolishing performance, including current density, electrolyte temperature, electrolyte composition, inter-electrode distance, initial surface roughness, and electropolishing time.

Several theories have been proposed in order to account for the mechanism of electropolishing, viscous film theory [73] is the simplest and the most popular one

among them. The theory believes that the dissolution product formed at the anode surface creates a viscous layer with high resistance on the surface. Due to the uneven surface, the thickness of the viscous layer at the valley position is high, leading to a high electrical resistance at the valley. Similarly, the thickness of the viscous layer at the protruding position is low, causing a low resistance value at the protrusion. The resistance difference between the valley and the protrusion results in surface leveling and polishing.

Before conducting the electropolishing experiment, a current density–voltage curve was obtained to find the optimal working range of the material system. The concept of the current density–voltage curve was proposed by Jacquet [74], as shown in Figure 3.3 [73]. There are four regions involved in the electropolishing process resulting from voltage differences, including etching, passivating, polishing, and gas evolution. Under a low-voltage regime, the anodic dissolution rate is slower than the rate of mass transfer; etching instead of polishing happens, where the workpiece surface is directly dissolved rather than achieving the smoothening effect. In this region, current density increases with voltage proportionally. The anodic dissolution rate keeps increasing with the increase in voltage, and when the dissolution rate exceeds the mass transfer rate, a passive oxide layer forms on the metal surface, leading to a slight decrease in the current density due to its larger resistivity compared with metal substrates. Since this region happens in a narrow voltage range, it may not easily show on the measured curve. In addition, when the anodic dissolution rate is higher, the reaction enters the mass-limited stage, where the current density remains constant with the voltage increases, and polishing happens in this stage called the limiting current plateau region. After that, increasing the voltage further will cause the breakdown of the passive oxide layer, resulting in the oxygen evolution at the anodic workpiece, leading to the rapid increase in current density and the formation of pitting corrosion on the metal surface.

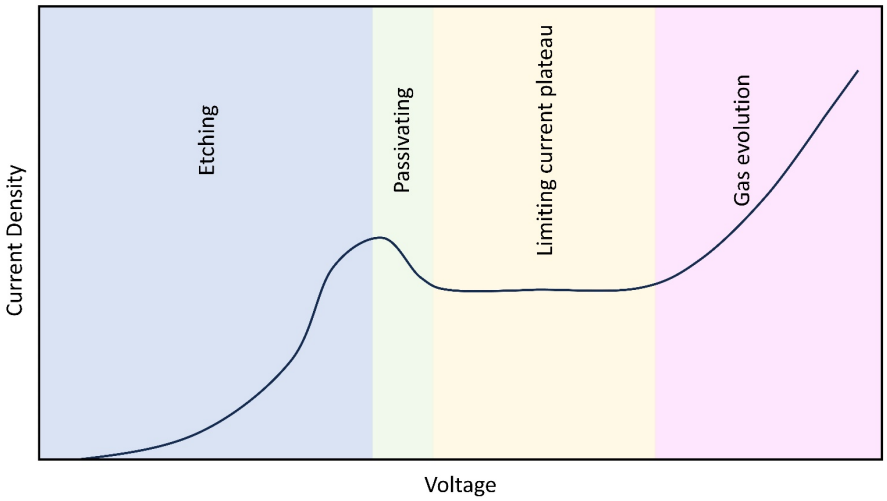


Figure 3.3 Polarization curve in electropolishing (redrawn and adapted from [73])

3.2.2. Introduction to Ultrasonic Cavitation Abrasive Finishing

Initially, the word 'cavitation' refers to a type of erosion where the formation and subsequent collapse of vapor bubbles occur with the change of liquid pressure, causing damage to functional parts. Reduction of liquid's static pressure to below its vapor pressure leads to the formation of cavities or 'gas bubbles', which would collapse when the pressure increases. In ultrasonic cavitation, the driven force of gas bubbles' formation, growth and collapse is the oscillation of ultrasonic pressure amplitude. Figure 3.4 (adapted from [75]) illustrates the mechanism of ultrasonic cavitation.

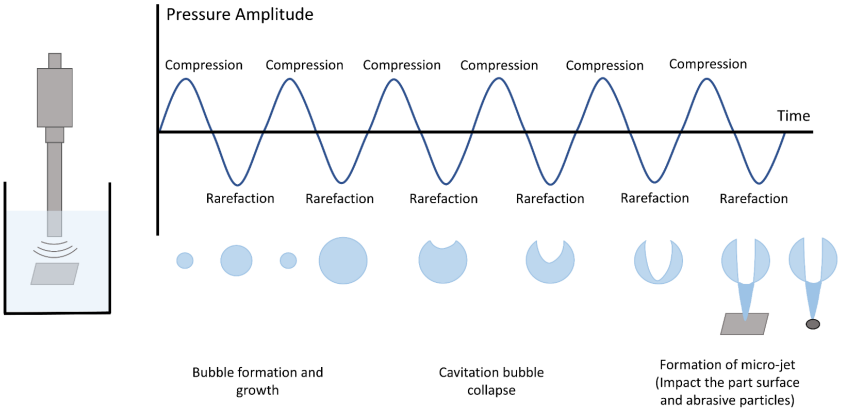


Figure 3.4 Schematics of ultrasonic cavitation, redrawn and adapted from [75]

Ultrasonic cavitation abrasive finishing was first invented by Tan et al. in [29]. An

ultrasonic probe is placed in the abrasive slurry to generate an ultrasonic cavitation effect for material removal. Two basic material removal mechanisms are involved in this novel technique – ultrasonic cavitation and abrasive finishing. According to the authors, vapor cavities near the surface defects and irregularities make the metal surface the preferred site for bubble nucleation and growth. High shear stress was generated due to bubble collapse, leading to crack propagation and eventual removal of surface irregularities such as partially melted powders, which contribute the most to the large surface roughness of AM parts. Figure 3.5 (adapted from [30]) demonstrates the material removal mechanism for the cavitation effect. Another possible mechanism for this technique is the abrasive impact generated by ultrasonic cavitation. Abrasive particles are accelerated by the gas bubble collapse, leading to abrasive erosion on the metal surface. Cavitation erosion has been deeply investigated as structural damage for underwater applications. However, it was recently considered a potential method for surface finishing of parts with large initial surface roughness.

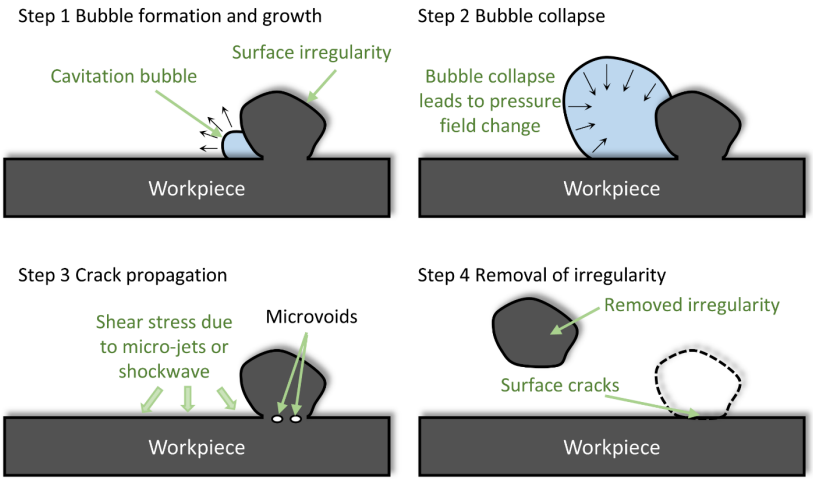


Figure 3.5 Mechanisms for ultrasonic cavitation on material removal, redrawn and adapted from [30]

3.3. Analytical Model for Electropolishing

3.3.1. Faraday's Law for Material Removal

The basis for developing an analytical model for quantifying electrochemical polishing

is Faraday's laws of electrolysis, which states that the number of chemical reactions occurring and the mass of metal dissolving at the anode-electrolyte interface is directly proportional to the quantity of electricity passing by the electrolyte (first law), and the amount of metal dissolution is proportional to the equivalent weight of the metal when the same amount of electricity passes by different electrolytes (second law). According to the law, metal dissolution rate $\dot{m}$ is expressed by the mass of metal dissolution m divided by time t, as stated in Equation (3.1),

$$\dot{m} = \frac{m}{t} = \frac{A_w I}{zF} \tag{3.1}$$

where A_w is the atomic weight, I is the electric current, z is the valency of anode material and F is the Faraday's constant with a value of 96485 C/mol. Assuming that the processing area of the anode workpiece is S and the gap between cathode and anode is d, the resistance of the electrolyte domain R_s can be calculated using Equation (3.2),

$$R_s = \frac{1}{\sigma_{electrolyte}} \frac{d}{S} \tag{3.2}$$

where $\sigma_{electrolyte}$ is the electrical conductivity of the electrolyte. The current I can be calculated according to Ohm's law as shown in Equation (3.3) when the applied voltage between two electrodes is ΔE.

$$I = \frac{\Delta E}{R_s} = \frac{\sigma_{electrolyte} \mathrm{S} \Delta \mathrm{E}}{d} \tag{3.3}$$

Material removal by volume V can be calculated by inserting Equation (3.3) into Equation (3.1) while introducing the workpiece density ρ as shown in Equation (3.4).

$$V = \frac{\mathrm{S A_w}}{zF\rho} \cdot \sigma_{electrolyte} \cdot \frac{\Delta E}{d} \cdot t \tag{3.4}$$

Electrical conductivity of the electrolyte can be expressed as Equation (3.5) [76],

$$\sigma_{electrolyte} = \sum n_i q_i \mu_i \tag{3.5}$$

where n_i is the number of ions which relates closely to the electrolyte concentration, q_i is the charge of ions, and μ_i represents the mobility of ionic species in the electrolyte.

Electrical conductivity is also a function of electrolyte temperature since ion mobility increases with the increase of temperature.

In the electropolishing process, voltage, inter-electrode gap and processing time are the most significant influencing parameters, according to current research studies. Figure 3.6 shows the influence of the inter-electrode gap (Figure 3.6 (a)) and the electropolishing voltage (Figure 3.6 (b)) on the volumetric material removal with the evolution of time. The modeling results accord well with existing studies (see Chapter 4) – Smaller inter-electrode gap, larger voltage, and longer time will cause more material removal from the metal surface. The modeling results presented are also validated with experiments stated in Section 4.3.3.

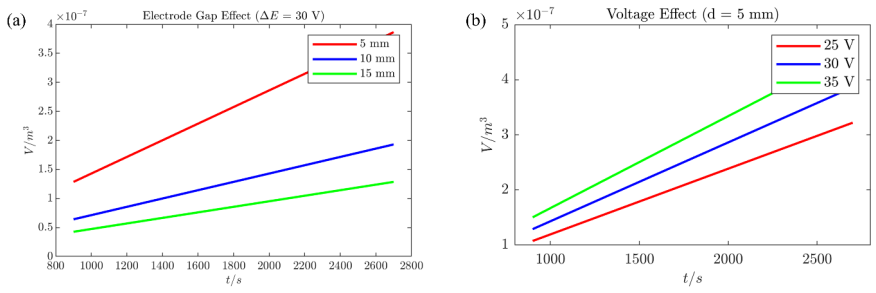


Figure 3.6 Influence of (a) electrode gap and (b) electropolishing voltage on volumetric material removal for electropolishing

3.3.2. Effect of Initial Surface Roughness

Due to the fact that metal parts fabricated via AM possess various surface defects, leading to a wide range of initial surface roughness, initial surface roughness of the work surface needs to be considered when accounting for electropolishing effect. For doing this, initial surface profiles are expressed as a superposition of sine wave functions, with the basic form of $y = bsin(\frac{2\pi x}{a})$, as shown in Figure 3.7, where a stands for the wavelength of the sine wave, while b represents for its amplitude.

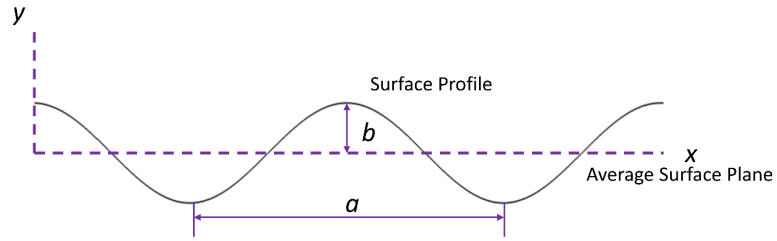


Figure 3.7 Parametric surface expressed by sine wave functions

Equation (3.6) has been derived based on the concentration difference of the acceptor in the electrolyte to account for the effect of initial surface roughness on the electropolishing performance [77]. The equation states that the displacement of the average surface plane (u) is a function of a and b when the amplitude of the surface roughness decreases from b_0 to b, when the amplitude b of the surface roughness is less than the wavelength a, and the wavelength a is much less than the effective thickness of the hydrodynamic boundary layer.

$$u = a\frac{\ln\frac{b_0}{b}}{2\pi} \tag{3.6}$$

Figure 3.8 shows the effect of initial surface roughness on the material removal in terms of the displacement of the average surface plane under different roughness amplitude and wavelength. Figure 3.8 (a) demonstrates the amount of displacement of the average surface plane at different amplitude reductions via electropolishing, starting from the initial amplitude of 20 μm at a wavelength of 200 μm. According to the calculation result, when the amplitude decreases from 20 μm to 1.5 μm, the displacement of the average surface plane reaches 80 μm, corresponding to the experimental result shown in Figure 3.9, conducting in 700 mL/L ethanol, 300 mL/L isopropanol, 60 g/L aluminum chloride, and 250 g/L zinc chloride with an electrical voltage of 30 V, an electrolyte temperature of 40 Celsius and an inter-electrode distance of 5 mm for 45 min.

Figure 3.8 (b) illustrates the surface displacement results for reducing surface roughness from different initial amplitudes to the same final amplitude of 1.5 μm during electropolishing. The plot shows that the increase of the material removal tends to slow

down with the increase of the initial roughness amplitude. However, as shown in Figure 3.8 (c), the average surface plane displacement is proportional to the wavelength of the surface roughness under the same amplitude reduction from 20 μm to 1.5 μm. For removing the roughness with a larger wavelength, more material needs to be removed from the surface, corresponding to longer electropolishing time. The calculation result is in accordance with the experimental observations, where large-scale surface waviness is harder to be removed compared with small-scale surface roughness.

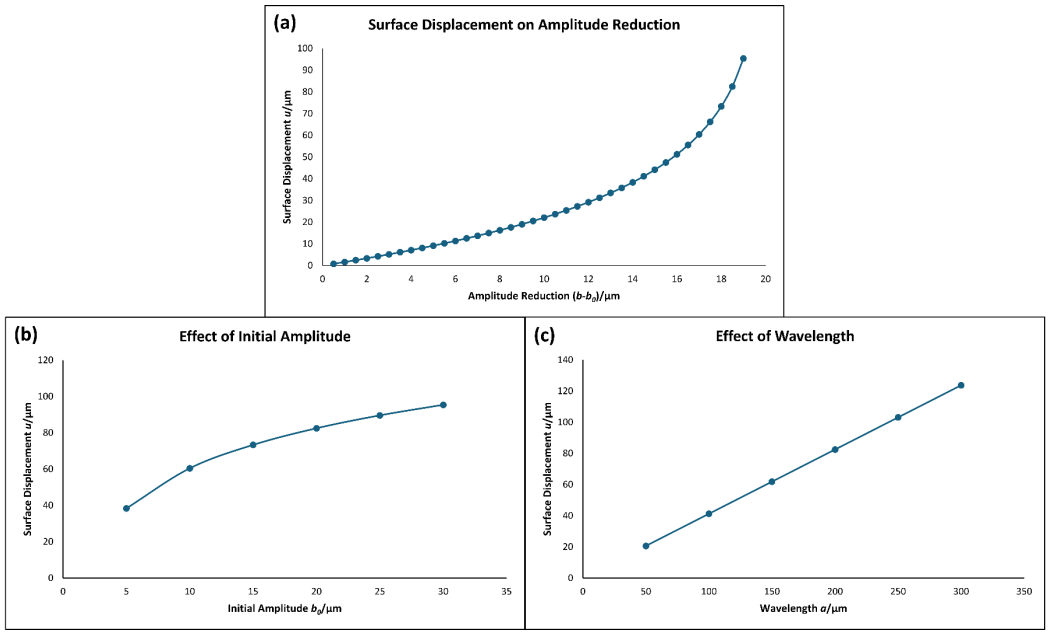


Figure 3.8 Effect of initial surface roughness on material removal (a) surface displacement on amplitude reduction; (b) effect of initial amplitude; (c) effect of wavelength

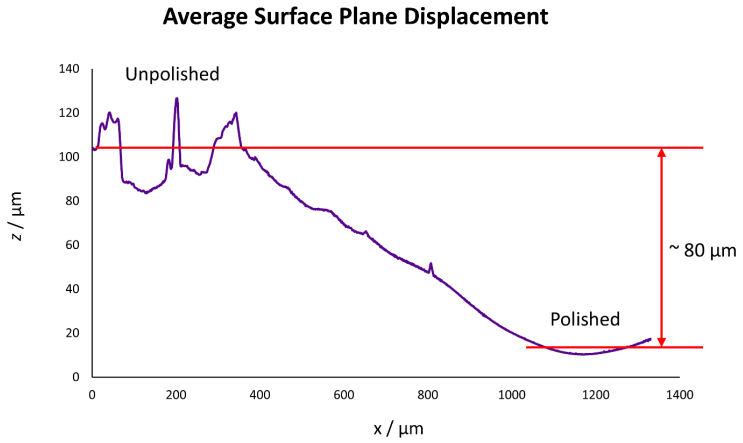


Figure 3.9 Experimental results for average surface plane displacement when decreasing the amplitude from 20 µm to ~1.5 µm

3.4. Numerical Model for Electropolishing

3.4.1. Model Description

Numerical modeling for surface roughness evolution during electropolishing was conducted using primary current distribution and deformed geometry modules in COMSOL Multiphysics 6.2[78]. The main purpose of conducting the modeling is to study the influencing parameters in a more direct way and to provide a guideline on how to select experimental parameters. In addition, due to the unique surface irregularities for metal additively manufactured parts, the results achieved from numerical modeling could also provide some information on the surface roughness evolution over time, as well as reveal the effect of types of surface irregularities on the final polishing performance.

In the primary current distribution, the electrochemical reaction was analyzed by both electrode current density ($j_{electrode}$) and electrolyte ($j_{electrolyte}$) current density, following Ohm's law, as stated in Equation (3.7) and (3.8),

$$j_{electrolyte} = -\sigma_{electrolyte}\nabla\phi_{electrolyte} \tag{3.7}$$

$$j_{electrode} = -\sigma_{electrode}\nabla\phi_{electrode} \tag{3.8}$$

where $\sigma_{electrolyte}$ and $\sigma_{electrode}$ represent for conductivity for electrolyte and

electrode respectively, while $\phi_{electrolyte}$ and $\phi_{electrode}$ stand for electrolyte and electrode potential. Accordingly, the current source of electrode and electrolyte can be calculated using Equation (3.9) and (3.10),

$$\nabla \cdot j_{electrolyte} = Q_{electrolyte} \tag{3.9}$$

$$\nabla \cdot j_{electrode} = Q_{electrode} \tag{3.10}$$

These values were used to calculate the electrochemical reaction rate, and the corresponding material removal was computed using the deformed geometry interface.

3.4.2. Effect of Influencing Parameters

Due to the fact that surface adhered particles contribute the most to the large surface roughness of the as-built surface, a 2D geometry of a surface with adhered particles was created to study the influencing parameters of electropolishing and visualize the surface evolution during the polishing process, as shown in Figure 3.10. Three influencing parameters were investigated based on a time-dependent approach, including electrolyte conductivity, inter-electrode gap and applied voltage.

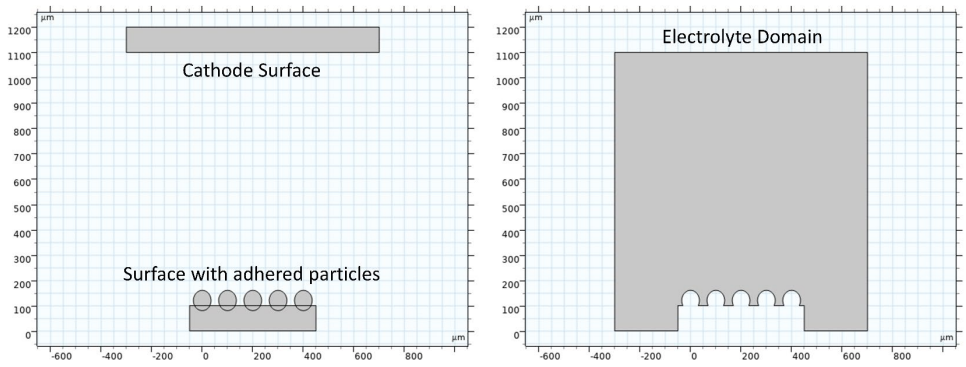


Figure 3.10 2D geometry of adhered particles for COMSOL modeling

Figure 3.11 demonstrates particle evolution achieved from electropolishing modeling after 60 seconds, under different electropolishing conditions. The same trend as analytical modeling results have been observed. With the increase of the voltage and electrolyte conductivity, as well as the decrease of the inter-electrode gap, electropolishing rate increases gradually. It should be noted that the current density at the edge and any sharp locations are larger than the average current density, resulting

in a higher material removal rate, leading to non-uniform surface finishing accordingly.

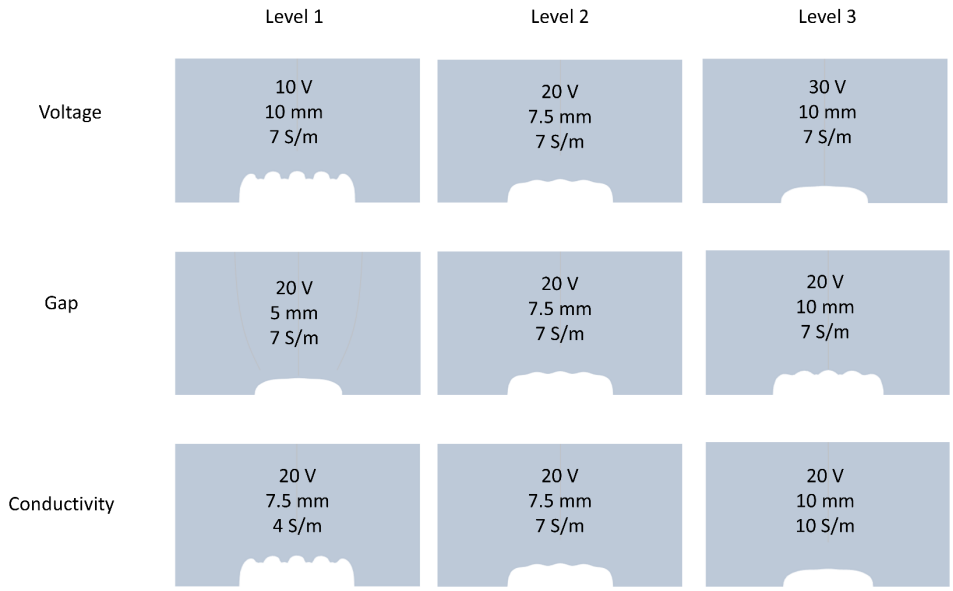


Figure 3.11 Particle evolution under different electropolishing conditions

3.4.3. Surface Roughness Evolution

To simulate the real surface roughness evolution with the current model, the initial surface roughness profile can be obtained experimentally by a laser profilometer. However, for simplifying the process, parametric surfaces were created for modeling the surfaces with different surface roughness and surface waviness. Figure 3.12 displays the results of surface roughness evolution for 3 different surfaces with different levels of surface roughness and surface waviness. The modeling results were obtained with a constant voltage of 20 V, an inter-electrode gap of 7.5 mm and an electrolyte conductivity of 7 S/m. As shown in Figure 3.12, for surfaces with a relatively low roughness, it is faster to achieve a smooth finish compared to surfaces with larger initial roughness. Compared with removing small-scale surface roughness, it is harder to remove the large-scale surface waviness via the electropolishing process.

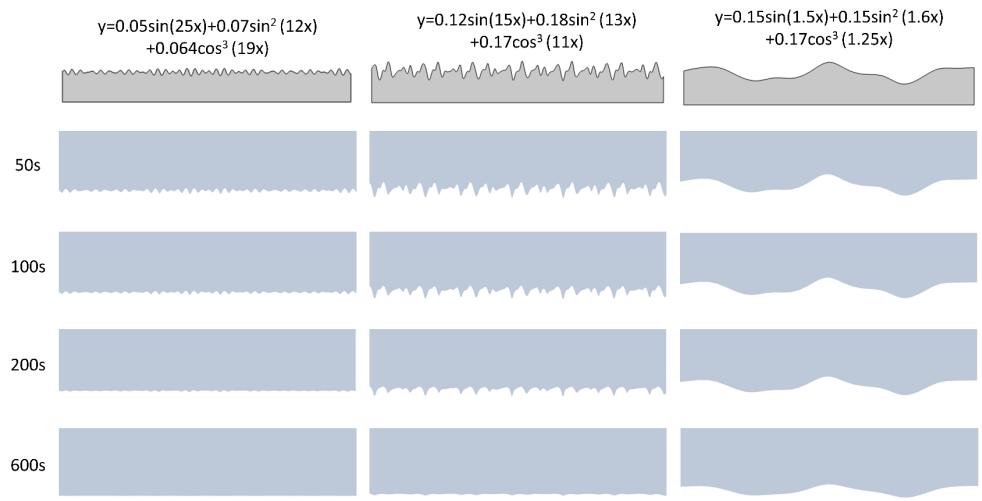


Figure 3.12 Surface roughness evolution for surfaces with different initial roughness

3.5. Analytical Model for Ultrasonic Cavitation Abrasive Finishing

3.5.1. Model Description

The pressure difference between compression and rarefaction of the ultrasonic wave generates cavitation bubbles in the liquid slurry, and the bubble collapse is believed to be the main reason for accelerating the abrasive particles in the slurry. Bubbles form and grow at the rarefaction stage and explode when the pressure exceeds its critical pressure, resulting in the emission of shock wave and the formation of microjets, which provides a large initial velocity for abrasive particles. Fu et al. [79] developed a model to describe the combination of ultrasonic cavitation and abrasive particles and to calculate the particle velocity resulting from the process, which acts as the basis for the model construction and calculation in this work.

To simulate the bubble dynamics generated under ultrasonic waves, a modified Keller-Miksis (K-M) model [80] in Equation (3.11) was used due to its good agreements with a large range of sound amplitudes,

$$\left(1-\frac{\dot{R}}{c}\right)R\ddot{R}+\frac{3}{2}\dot{R}^2\left(1-\frac{\dot{R}}{3c}\right)=\left(\frac{P}{\rho_l}\right)+\frac{1}{\rho_l c}\frac{d}{dt}(RP)$$
$$=\left(1+\frac{\dot{R}}{c}\right)\frac{P}{\rho_l}+\frac{R}{\rho_l c}\frac{dP}{dt} \tag{3.11}$$

$$P(R,\dot{R},t)=\left(P_0-P_v+\frac{2\sigma}{R_0}\right)\left(\frac{R_0}{R}\right)^{3n}-\frac{2\sigma}{R}-4\mu\frac{\dot{R}}{R}-P_0+P_v$$
$$-P_a sin(2\pi ft) \tag{3.12}$$

where R is the bubble radius, $\dot{R}$ and $\ddot{R}$ are the first and second derivatives with respect to time t, c is the sound velocity in the liquid slurry, ρ_l is the liquid density, P is the pressure of the cavitation bubble wall calculated as in Equation (3.12), P_0 is the static ambient pressure, P_v is the vapor pressure, σ is the surface tension of the liquid, R_0 is the initial bubble radius, n is the polytropic exponent of the gas in the bubble, μ is the liquid viscosity, and P_a and f are sound pressure amplitude and sound frequency, respectively.

Equation (3.11) can be integrated to achieve Equation (3.13) to calculate the cavitation wall velocity.

$$\dot{R}=\left\{\frac{2P_\infty}{3\rho}\left[\left(\frac{R_0}{R}\right)^3-1\right]+\frac{2\sigma}{\rho R_0}\left[\left(\frac{R_0}{R}\right)^3-\frac{R_0}{R}\right]\right.$$
$$\left.-\frac{2P_0}{3(1-n)}\left[\left(\frac{R_0}{R}\right)^{3(1-n)}-1\right]\right\}^{\frac{1}{2}} \tag{3.13}$$

In the experiments, the amplitude of the ultrasonic generator is adjusted in the form of displacement amplitude. Therefore, the displacement amplitude needs to be converted into pressure amplitude for being used in the Keller-Miksis model, following Equation (3.14) [81],

$$P_a=E_l Ak \tag{3.14}$$

where E_l is the bulk modulus of the liquid medium, A is the displacement amplitude of the ultrasonic wave, which can be adjusted in the experiment, and k is the wave

number of the sound wave and is affected by the ultrasonic frequency.

Vogel et al. [82] proposed a model for calculating shock wave pressure P_s as shown in Equation (3.15),

$$P_s = c_1 \rho_l u_s \left(10^{\frac{u_s - c}{c_2}} - 1\right) + P_\infty \tag{3.15}$$

where P_∞ is the environment pressure which equals to $P_0 + P_a sin(2\pi ft)$, $c_1 = 5190\ m/s$ and $c_2 = 25306\ m/s$.

Equation (3.16) was used for calculating the velocity of the shockwave front u_p proposed by Rice and Walsh [83],

$$u_p = \dot{R} = c_1 \left(10^{\frac{u_s - c}{c_2}} - 1\right) \tag{3.16}$$

In terms of estimating the effect of microjet, Plesset and Chapmann [84] proposed a model as shown in Equations (3.17) and (3.18) to calculate the microjet velocity and the water hammer pressure caused by the microjet,

$$V_j = 8.97 \left(\frac{H}{R_0}\right)^2 \sqrt{\frac{P_\infty - P_v}{\rho_l}} \tag{3.17}$$

$$P_j \approx V_j \rho_l c \tag{3.18}$$

where H is the distance between the bubble center to the bubble wall, which is assumed to be equal to the bubble radius R.

After achieving the results for shockwave and microjet, Newton's second law was used to simulate the resulting force F_R on the abrasive particles and calculate the particle velocity V_p as shown in Equation (3.19),

$$F_R - 6\pi\mu r_p V_p - \frac{1}{2}\xi \rho s {V_p}^2 = m_p \frac{dV_p}{dt} \tag{3.19}$$

where r_p is the radius of abrasive particles, m_p is the mass of abrasive particles, ξ is the resistance coefficient, s is the force area on the abrasive particle. The impact pressure of abrasive particles can also be calculated as in Equation (3.20),

$$P_p = \frac{1}{3}\left(\frac{5}{4}\rho_P\right)^{\frac{3}{5}}\left[\pi\left(\frac{1-{\nu_p}^2}{E_p}+\frac{1-{\nu_l}^2}{E_l}\right)\right]^{-\frac{2}{5}}{V_p}^{\frac{6}{5}} \quad (3.20)$$

where ρ_P is the density of the abrasive particles, ν_p and ν_l are the Poisson's ratio for abrasive particles and liquid media, and E_p is the elastic modulus for the abrasive particle.

According to Bitter's model in Equation (3.21) [85], deformation wear W_D due to the normal impact of abrasive particles is proportional to the kinetic energy,

$$W_D = \frac{m_p(V_p sin\alpha - V_{el})^2}{2\varepsilon} \quad (3.21)$$

Where ε is an empirical constant depending on the properties of both abrasive particles and workpiece material and α is the impact angle of the abrasive particle. Equation (3.22) is used to calculate the threshold velocity V_{el},

$$V_{el} = \frac{\pi^3}{2\sqrt{10}}EL^{5/2}\left(\frac{1}{\rho_P}\right)^{1/2}\left[\frac{1-{\nu_p}^2}{E_p}+\frac{1-{\nu_w}^2}{E_w}\right]^2 \quad (3.22)$$

where EL is the elastic load limit of the workpiece material, E_w and ν_w are the elastic modulus and the Poisson's ratio for the workpiece material.

3.5.2. Effect of Working Parameters on Material Removal

In order to develop a guide for selecting influencing parameters for experimental studies, some preliminary modeling results have been achieved using MATLAB R2022a.

Ultrasonic cavitation abrasive finishing is a relatively novel technique. Since the possible acceleration mechanism of abrasive particles is the growth and collapse of cavitation bubbles, achieving the bubble dynamics in the process is important. Figure 3.13 describes the evolution of bubble radius under ultrasonic vibration under different frequencies (Figure 3.13 (a)) and different amplitudes (Figure 3.13 (b)), which could serve as a starting point for calculating the impact velocity of abrasive particles.

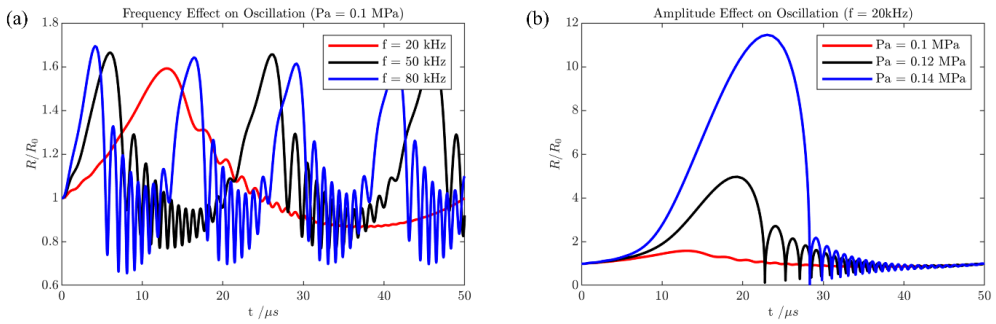


Figure 3.13 (a) Frequency and (b) amplitude effect on bubble dynamics

Figure 3.14 shows the calculation results for impact particle velocity (Figure 3.14 (a)) and pressure (Figure 3.14 (b)) due to both shockwave and microjet generated when cavitation bubbles collapse. The particle velocity can reach 130 m/s when the amplitude is 0.1 MPa, and the ultrasonic frequency is 20 kHz.

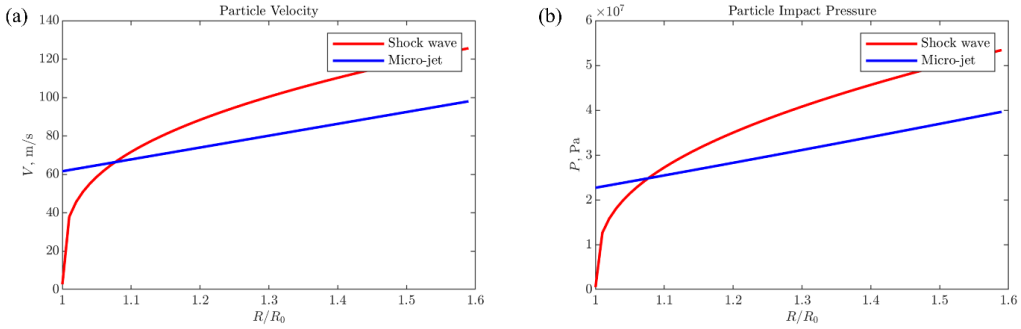


Figure 3.14 Particle (a) velocity and (b) impact pressure due to ultrasonic cavitation

Once particle velocity is achieved, it can be inserted into Bitter's model to calculate the material removal rate by the impact of abrasive particles. Figure 3.15 shows the relationship between the volumetric material removal by a single abrasive particle and the impact velocity generated by abrasive particles with different particle sizes. From the obtained values in the figure, it can be concluded that the volumetric material removal for single abrasive particle is on the order of 10^{-14}~10^{-15} cubic meters even if the particle velocity reaches 100 m/s. Although the particle amount in the solution can be significantly large (several millions) especially when working with particles with small sizes, the percentage of abrasive particles that will collide the surface and even cause surface material removal is limited. Therefore, material removal due to particle impact is still fairly small compared with electropolishing.

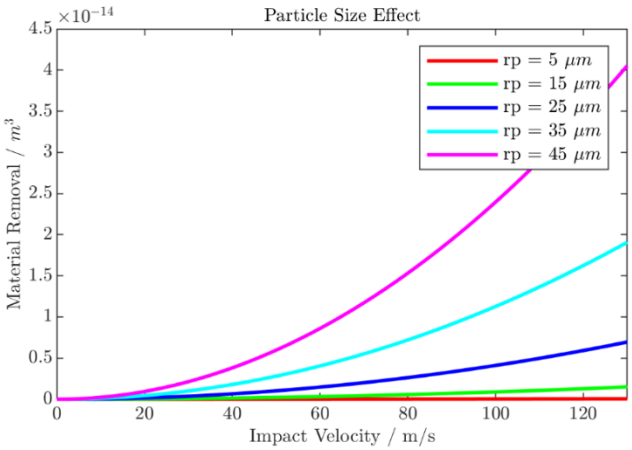


Figure 3.15 Effect of particle size on volumetric material removal

3.6. Summary

In this chapter, the physical mechanisms of electrochemical polishing and ultrasonic cavitation abrasive finishing were explained first. Then, both simplified analytical and numerical models based on electropolishing mechanisms were developed to account for influencing parameters and surface roughness evolution during the process. In addition, an analytical model on ultrasonic cavitation abrasive finishing was also presented, and modeling results were obtained for parameters used in the experiments. The models presented in this chapter could help with achieving a better understanding of the process mechanisms, while facilitating the parameter selection process in the following experiments.

4. Development of a Novel Hybrid Ultrasound Abrasive-Driven Electropolishing Technique

4.1. Chapter Overview

Although the average surface roughness can be reduced effectively (more than 80% roughness reduction) by electropolishing, large-scale surface waviness still remains an issue. To maintain the finishing efficiency while reducing the surface waviness, a novel hybrid surface finishing technique is designed, which involves the combination of electropolishing, ultrasonic vibration, and abrasion. Preliminary experiments to prove the feasibility of novel hybrid finishing methods were conducted on Ti6Al4V coupons manufactured via laser powder bed fusion (LPBF). Electropolishing, a combination of ultrasound and abrasion, and hybrid finishing were conducted for process optimization and comparison purposes. The effects of the voltage, inter-electrode gap, temperature, ultrasonic amplitude, abrasive concentration, and processing time were studied and optimized. When similar optimal arithmetic mean height values ($Sa \approx 1$ μm) are achieved for both processes, the arithmetic mean waviness values (Wa) obtained from hybrid finishing are much less than those from sole electropolishing after the same processing time, with the amount being 61.7% less after 30 min and 40.0% after 45 min. The graphical overview of this chapter is shown in Figure 4.1.

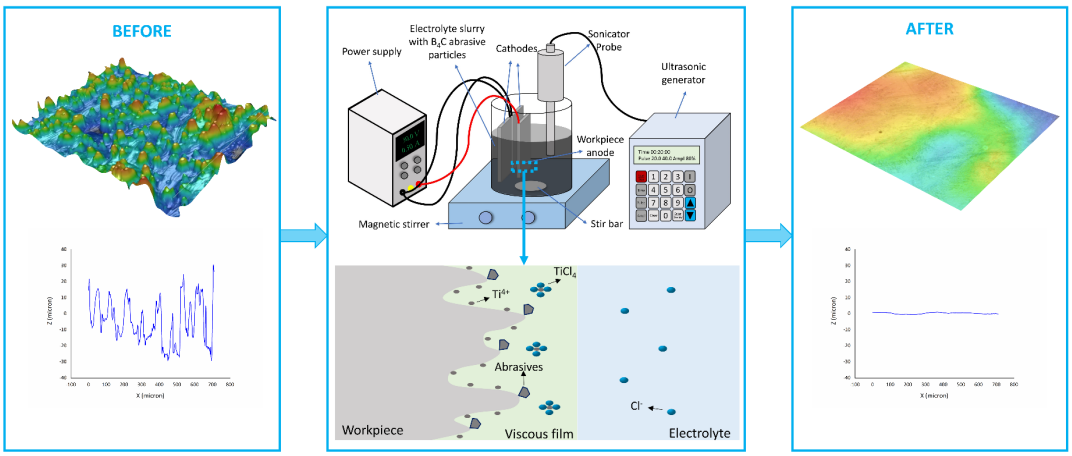


Figure 4.1 Graphical overview of Chapter 4

4.2. Experiments and Methods

4.2.1. Sample Preparation

The material selected for preliminary experiments is Ti6Al4V due to its unique mechanical properties, excellent chemical stability, and popularity in aerospace and biomedical applications [86]. Ti6Al4V grade 23 powder (AP&C Powder Metallurgy, Saint-Eustache, Canada) with a size distribution of 15–53 μm (with a D10, D50, and D90 of 19.5 μm, 35.5 μm, and 51.3 μm) was used for the LPBF process. Coupons with the dimensions of 10 mm × 25 mm × 2 mm were manufactured via LPBF (AM400, Renishaw plc, Wotton-under-Edge, United Kingdom). Optimal printing parameters were used to minimize the surface roughness of as-built parts, including up-skin, in-skin, and down-skin buildings, and contouring strategies, as shown in Table 4.1. Metal coupons were printed vertically so that as many coupons as possible could fit on the building plate. Meanwhile, different types of surface irregularities were observed on vertical surfaces for surface finishing trials. After printing, the specimens were cut from the substrate using a wire electrical discharge machining system (VL600QH, Sodick Inc., Schaumburg, United States). Before surface treatment, all the coupons were cleaned by sonicating in acetone for 10 min to remove the oily contaminants from the surface.

Table 4.1 Printing parameters for Ti6Al4V coupons

Category	Laser Power (W)	Scanning Speed (mm/s)	Hatch Distance (mm)
Hatch	185	1189	0.1
Contour	175.6	841	0.1
Upskin	160	1350	0.09
Downskin	90	2300	0.04

4.2.2. Measurement of Polarization Curve

Before conducting electropolishing experiments, a polarization curve (current density–voltage curve) was obtained to determine the optimal range of the working voltage for

the material system. To complete this, two printed Ti6Al4V coupons were immersed into the electrolyte solution and connected to both terminals of a power supply, respectively. The inter-electrode gap between the two coupons was kept constant at 1 cm. An eco-friendly alcoholic electrolyte consisting of 700 mL/L ethanol, 300 mL/L isopropanol, 60 g/L aluminum chloride, and 250 g/L zinc chloride [87] was used in this study. All the chemicals were purchased from Sigma Aldrich. The polarization curve was obtained by increasing the voltage from 0 to 90 V and recording the corresponding current value. Current density was achieved by dividing the measured current values by the surface area of the metal coupons.

4.2.3. Optimization of Electropolishing Parameters

Since the hybrid finishing technique was designed on the basis of electropolishing, the process parameters of electropolishing were optimized first. The same electrolyte used for measuring the polarization curve was used for the electropolishing study. To conduct electropolishing, a constant voltage was applied between the cathode and anode by a power supply (HY10010EX, VOLTEQ Equipment, San Jose, United States) equipped in an electropolishing station (E299, ESMA Inc., South Holland, United States). In each experiment, a printed coupon was connected to the positive terminal of the power supply as the anode workpiece for the electropolishing treatment. Two printed coupons were paralleled and connected to the negative terminal of the power supply as the cathode to maintain a 2:1 cathode-to-anode surface area ratio. Both the inert electrode and the workpiece were immersed in a 400 mL beaker filled with 250 mL of the electrolyte with adjusted inter-electrode gaps before each experiment. A hotplate and an ice bath were used to control the temperature of the electrolyte to study the temperature effect for electropolishing. Electrolytes were agitated at 300 rpm by a magnetic stirrer built into the hotplate to ensure complete mixing of the liquid. The experimental setup for conducting electropolishing experiments is shown in Figure 4.2 (a).

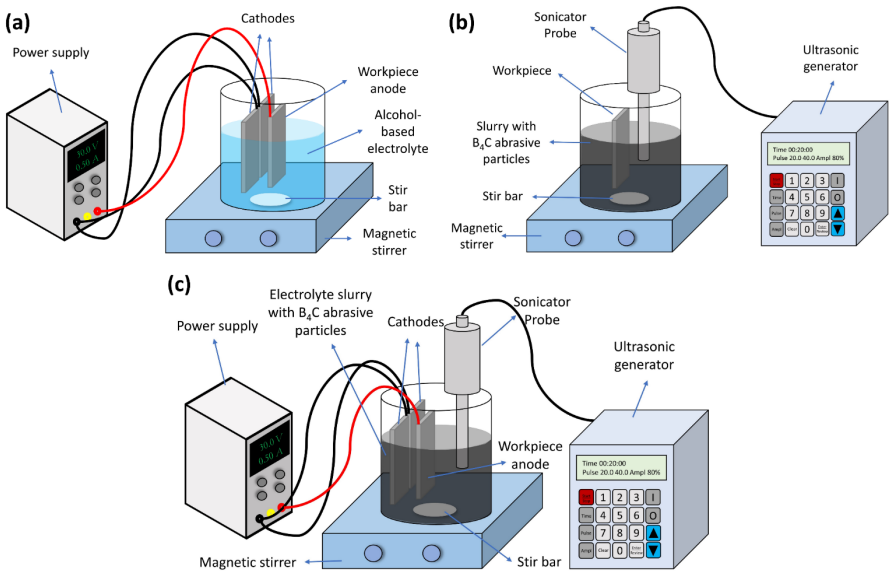


Figure 4.2 Schematic of experiment setup for (a) electropolishing, (b) surface finishing with ultrasound and abrasion, and (c) ultrasound abrasive-driven electrochemical hybrid finishing

Four parameters were selected to find the optimal working set for the material system, including voltage, which is determined from the polarization curve (25 V, 30 V, 35 V), electrolyte temperature (25 °C, 40 °C, 55 °C), the inter-electrode gap (5 mm, 10 mm, 15 mm), and electropolishing time (15 min, 30 min, 45 min). A 3-level Taguchi L9 design (electropolishing DOE) as shown in Table 4.2 was used to find the best combination of these four parameters to achieve the optimal electropolishing performance. The best parameter set to achieve the optimal roughness value was selected for the hybrid surface finishing.

Table 4.2 Taguchi L9 design for electropolishing DOE

Run	Voltage (V)	Temperature (°C)	Gap (mm)	Time (min)
1	25	25	5	15
2	25	40	10	30
3	25	55	15	45
4	30	25	10	45
5	30	40	15	15
6	30	55	5	30
7	35	25	15	30

8	35	40	5	45
9	35	55	10	15

4.2.4. Experimental Study on Ultrasound and Abrasion

Since ultrasound and abrasion were combined with electrochemical polishing in the design of the hybrid finishing technique, a set of experiments to study the combined effect of ultrasound and abrasion on surface roughness reduction without any electrochemical reactions was conducted. To this end, an ultrasonic processor (FB505 sonic dismembrator, Thermo Fisher Scientific, Waltham, United States) was used to generate ultrasonic waves with a frequency of 20 kHz. The high-frequency ultrasonic wave was transmitted to the horn tip through the transducer and caused a vibration at the horn tip at a maximum amplitude of 60 μm. The probe used in this study was a solid tip probe with a tip diameter of 19.1 mm. Metal coupons were immersed in a beaker filled with an abrasive slurry. For the preliminary trials, the abrasive slurry was prepared by dispersing 20 g B_4C abrasive particles with an average particle size of 10 μm in 200 mL deionized water. To achieve a uniform mixing behavior, the slurry was stirred at a constant speed on a magnetic stirrer. An ultrasonic duty cycle of 80% in a pulsed mode was selected in the preliminary trial to provide the system with enough power while preventing overheating. The beaker was placed in an ice bath so that excessive heat generated during the process could be effectively removed. Figure 4.2 (b) shows the schematic of the experimental setup. Surface roughness evolution of the treated coupon with time was measured and recorded.

4.2.5. Optimization of Hybrid Surface Finishing

The hybrid ultrasound abrasive-driven electrochemical polishing was conducted in the same alcoholic electrolyte as in the electropolishing study with the dispersion of B_4C abrasive particles with an average particle size of 10 μm in different weight concentrations. The total amount of the polishing slurry was 250 mL. The schematic of the experimental setup is shown in Figure 4.2 (c). The distance between the ultrasonic

probe and the workpiece was kept at 5 mm. The ultrasonic probe was placed on a holder fixed to a lab stand. The optimal electropolishing parameters obtained from the electropolishing DOE were selected as the electropolishing working conditions in the hybrid treatment, while all the other conditions remained the same. Meanwhile, an ultrasonic probe was connected to the ultrasonic generator with the probe tip immersed in the electrolyte. The power supply and the ultrasonic processor were switched on and off at the same time to study the synergistic effect of all the components involved in the process.

After determining the optimal working set for the electropolishing process, three other parameters were selected in order to investigate the influencing parameters of the hybrid technique, including the processing time (15 min, 30 min, 45 min), ultrasonic amplitude (70%, 80%, 90%), and abrasive concentration of the slurry (5%, 10%, 15%). A Taguchi L9 orthogonal array (hybrid DOE) as shown in Table 4.3 was generated based on these influencing factors.

One thing worth noting is that due to the rapid heat generation that resulted from the high-power ultrasound, and although an ice bath and a hotplate were used to try to manually maintain the temperature at 40 °C according to the optimal electropolishing parameter set, a fluctuation in the temperature existed, with the temperature being in the range of 37–43 °C during all the hybrid processes.

Table 4.3 Taguchi L9 design and output response for hybrid DOE

Number	Time (min)	Ultrasonic Amplitude (%)	Abrasive Concentration (%)
1	15	70	5
2	15	80	10
3	15	90	15
4	30	70	10
5	30	80	15
6	30	90	5
7	45	70	15
8	45	80	5
9	45	90	10

4.2.6. Surface Roughness Characterization

For both as-built samples and finished samples, surface images were taken and surface roughness values were measured using a 3D laser scanning confocal micro-scope (VK-X250, Keyence, Osaka, Japan). To characterize both the surface roughness and the surface waviness in the following section, five positions were measured for each coupon as shown in Figure 4.3 and the average and standard deviation of the five values were calculated to present the results. ISO 25178 [88] was followed when characterizing the surface roughness. A laser beam scans the xy plane of the sample surface, while the accumulation of reflection information along the z-axis constitutes the confocal image for roughness measurement. In order to investigate the average surface roughness change of the printed samples, the arithmetical mean height (Sa) was measured and compared in this research. Surface defects and irregularities which result in different levels of surface roughness before surface finishing were also characterized with a scanning electron microscope (SEM) (VEGA3, TESCAN GROUP, Brno, Czech Republic).

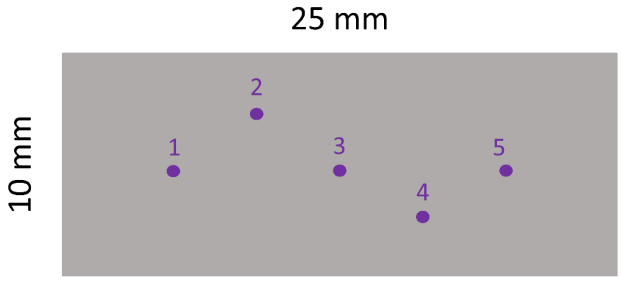


Figure 4.3 Locations of surface roughness and surface waviness measurements

4.2.7. Investigation of Surface Waviness

To characterize the surface waviness of the finished parts, line roughness profiles were measured with Keyence VK-X250. Line waviness profiles were obtained by applying a waviness filter to line roughness profiles, which eliminates the small-scale fluctuations while extracting the signals with a larger wavelength. Arithmetic mean waviness (*Wa*) values under 4 different treatments were measured and compared. Three

replications of each treatment were conducted and the line waviness values of five different locations were measured for each replicate. The optimal electropolishing parameters achieved from the electropolishing DOE including the voltage, inter-electrode gap, and electrolyte temperature were used. The optimal ultrasonic amplitude and abrasive concentration obtained from the hybrid DOE were selected as well. A detailed parameter selection is shown in Table 4.4.

Table 4.4 Parameter Selection for Surface Waviness Investigation

Sample Name	Type of Treatment	Time	Other Parameters
E-30	Electropolishing	30 min	Voltage 30 V, Temperature 40±3 ºC, Inter-electrode Gap 5 mm, Ultrasonic Amplitude 80%, Abrasive Concentration 10%
E-45	Electropolishing	45 min	
H-30	Hybrid Finishing	30 min	
H-45	Hybrid Finishing	45 min	

4.3. Results

4.3.1. Surface Analysis of As-built Samples

Figure 4.4 (a) shows the photo of the as-built coupon printed vertically with reference to the building plate. Figure 4.4 (b,c) show the 3D height profile and laser optical image of the as-built surface. The average initial surface roughness of the as-built vertical surfaces in this batch is 11.50 ± 0.81 μm. The high surface roughness for the as-built surface was caused by different types of surface defects and surface irregularities, as shown in the SEM images in Figure 4.5. Partially melted particles are the primary cause of high surface roughness, as unmelted metal powders adhere to the surface at extremely high temperatures [89], with a larger attaching tendency for finer particles [9]. The balling effect as well as the formation of liquid spatter also contribute to the high surface roughness, resulting from the tendency of the melt pool track to minimize its surface energy due to liquid surface tension [12]. Apart from these, surface cracks and solidified melting tracks also lead to the increase in surface roughness.

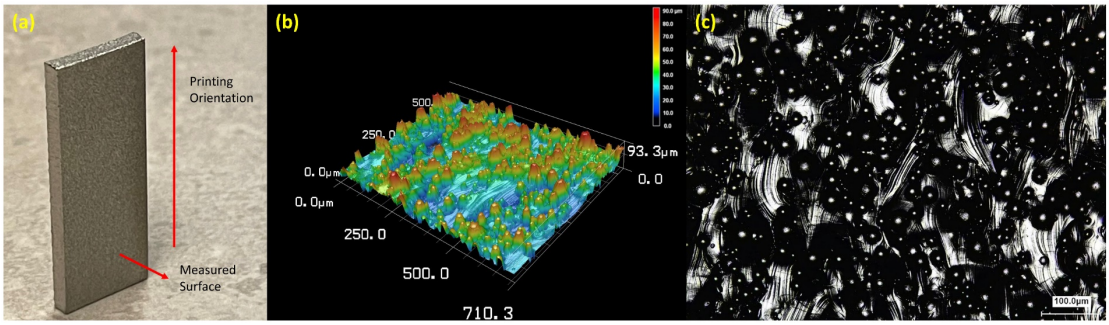


Figure 4.4 Images of as-built coupons: (a) camera image; (b) 3D height profile; (c) laser optical surface image

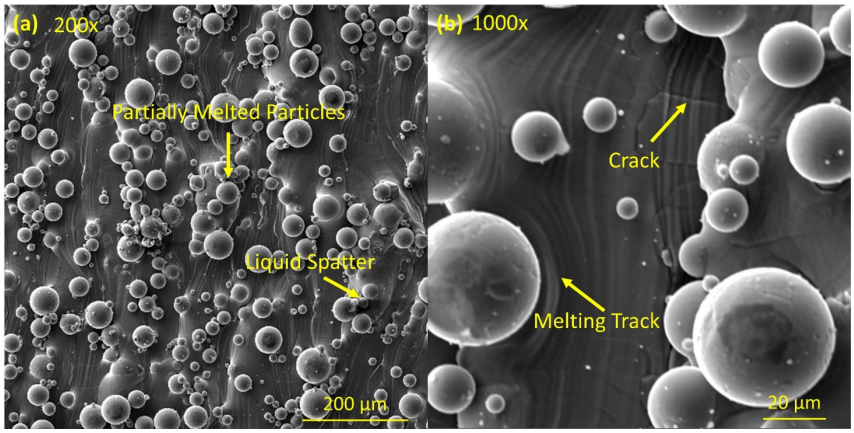


Figure 4.5 SEM images of as-built surface (a) 200×; (b) 1000×

4.3.2. Polarization Curve

As discussed earlier in Section 3.2.1, a polarization curve always needs to be measured for locating the optimal working voltage of a new electrolyte-electrode system. Figure 4.6 is the measured polarization curve of the material system in this work. The current density keeps increasing within the voltage range of 0–20 V, suggesting that etching instead of polishing happens in this voltage range. From 20 V to 25 V, the current density increases at a much lower increasing rate with a slight decrease before the voltage reaches 25 V, where passivation takes place. From 25 V to below 35 V, the current stays relatively stable, which corresponds to the limiting current plateau region and indicates that the optimal working voltage should exist in the 25–35 V range. The current density increases again after 35 V, showing that the process enters the gas evolution region.

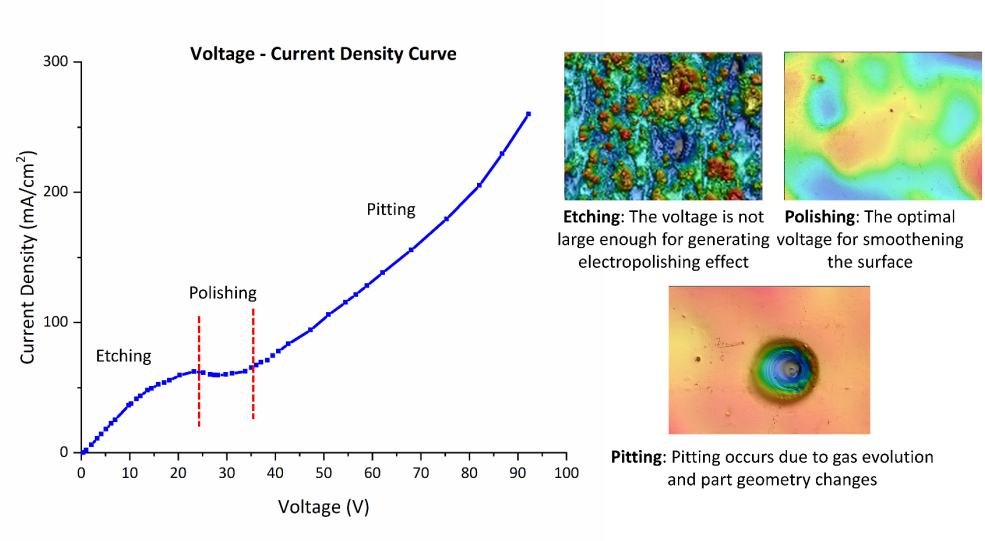


Figure 4.6 Polarization curve achieved from electropolishing experiment

4.3.3. Analysis of Electropolishing

Since the goal of the experiment is to reduce the surface roughness of printed coupons, surface roughness reduction ($\Delta Sa\%$) as calculated in Equation (4.1) was set as the response for data analysis, where Sa_0 is the initial roughness and Sa_f is the final roughness. To analyze a Taguchi orthogonal array design, signal-to-noise (S/N) ratios calculated in Equation (4.2) following a the-larger-the-better standard were used for evaluating the process performance.

$$\Delta Sa_{\%} = \frac{Sa_0 - Sa_f}{Sa_0} \times 100\% \tag{4.1}$$

$$S/N = -10\log_{10}\left(\frac{1}{n}\sum_{i=1}^{n} 1/{Sa_i}^2\right) \tag{4.2}$$

The Taguchi orthogonal array listed in Table 4.2 was analyzed based on the mean value for the surface roughness reduction and signal-to-noise ratio, as shown in Figure 4.7. According to the results, in the three-level Taguchi design, when the voltage is 30 V, the temperature is 40 °C, the inter-electrode gap is 5 mm, and the polishing time is 45 min, the largest S/N ratio and the largest mean for surface roughness reduction can be achieved. Therefore, these parameters were selected to conduct further hybrid treatment.

Figure 4.8 presents 3D surface images achieved by a Keyence laser profilometer after nine treatments.

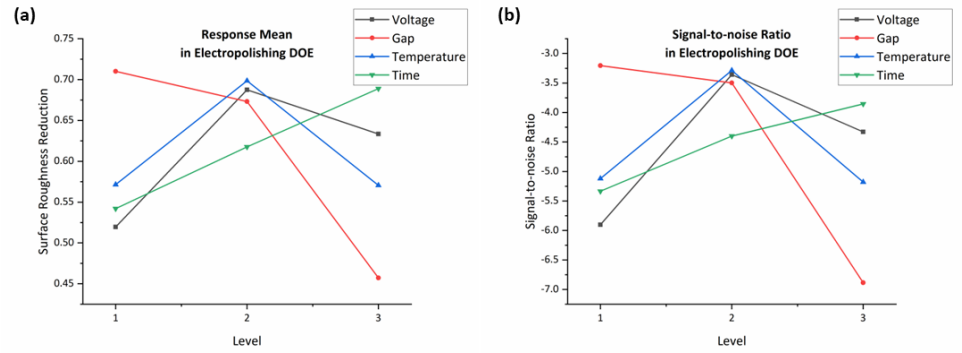


Figure 4.7 Main effect plots in electropolishing DOE for (a) response means and (b) S/N ratios

Among all the tested influencing parameters, electrical voltage or the corresponding current density is the most significant influencing parameter for optimizing electropolishing performance. As described before, a low current density results in direct dissolution, while a high current density might lead to pit formation. If the voltage is lower than the optimal working voltage, the ionic mass transfer rate is higher than the anodic dissolution rate, and the polishing and leveling effect cannot be achieved. If the voltage is too high, excessive heat would be generated in the electrolyte, resulting in rapid metal dissolution and vigorous gas evolution, which leads to the accelerated formation of pitting corrosion and expeditious decomposition of the electrolyte solution.

The inter-electrode gap is another significant parameter. When the distance between the cathode and anode is large, the current generated in the electrolyte is not large enough, due to the large electrolyte resistance; thus, achieving the desired polishing effect is difficult. Therefore, the inter-electrode distance should be small enough to achieve enough current density and improved electropolishing efficiency. However, if the distance is too small, high local current density will lead to a rapid increase in electrolyte temperature, which may cause detrimental effects on the metal surface [90]. Electropolishing performance also increases with the temperature since the temperature

increase helps accelerate the diffusion and migration of dissolved ions in the electrolyte. However, when the temperature reaches a certain point, electropolishing performance drops when the temperature further increases, due to the fact that etching pits may form on the surface at elevated temperatures. Moreover, surface roughness decreases with time in the feasible time range.

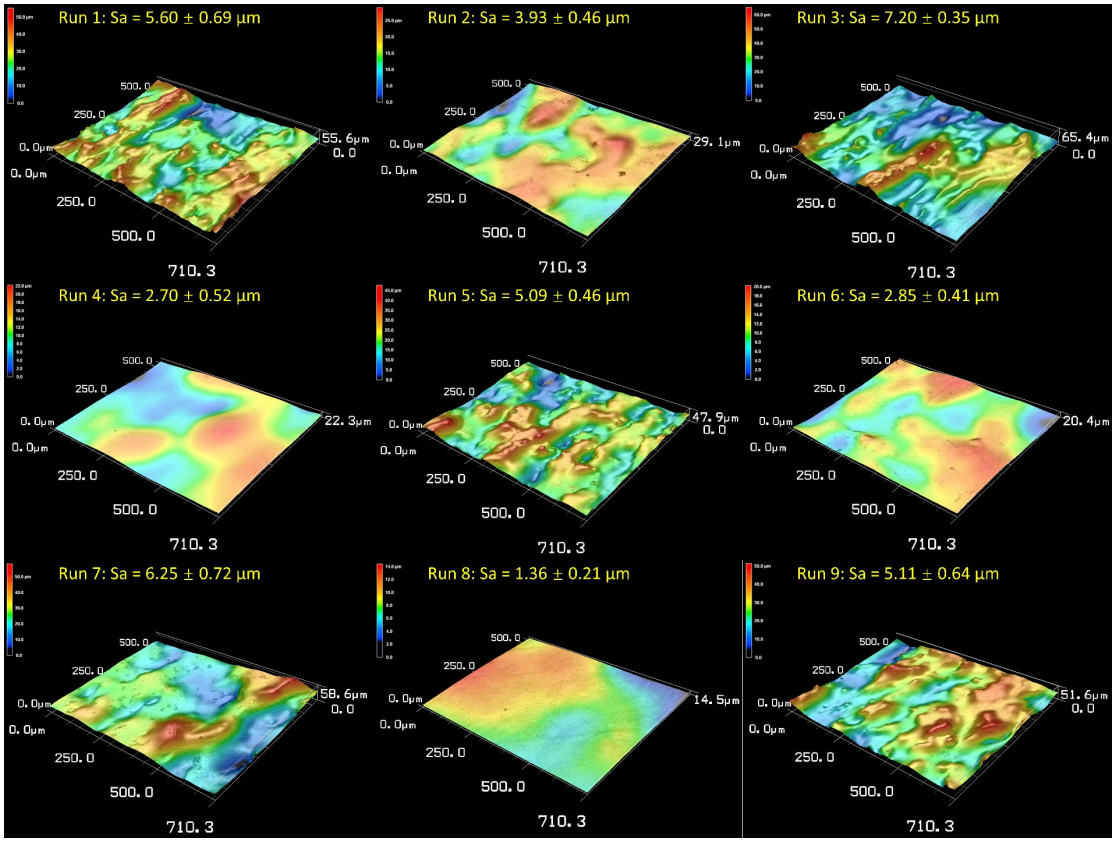


Figure 4.8 Three-dimensional surface images for samples in electropolishing DOE

Mass reductions achieved from the nine electropolishing parameter sets were also used to compare with the calculated results from Faraday's Law, as shown in Figure 4.9, where normalized mass reduction was calculated by dividing the real mass reduction by the maximum value in the dataset with nine different experimental parameters. The comparison between experimental results and calculation results exhibits a consistent trend in terms of mass reduction with varying working parameters.

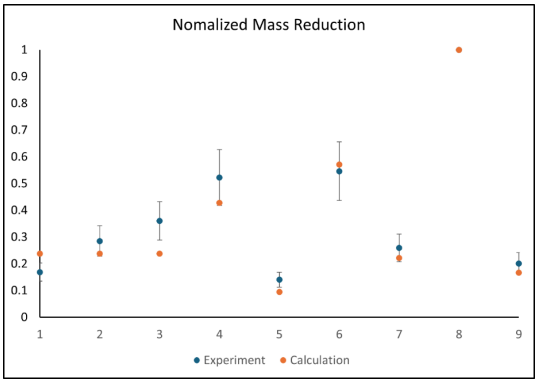


Figure 4.9 Comparison between experimental results and calculation results on Faraday's Law

4.3.4. Effect of Ultrasound and Abrasion on Surface Finishing

In order to study the combined effect of ultrasonic vibration and abrasion on the surface roughness reduction, a surface roughness evolution curve was obtained after conducting the sole process for 8 h, as shown in Figure 4.10. The figure shows that the surface roughness of the part decreases rapidly in the first two hours and then becomes relatively stable afterward. Figure 4.11 presents and compares 3D images of the as-built part surface (Figure 4.11 (a)) and the surface after 1 h (Figure 4.11 (b)) and 4 h (Figure 4.11 (c)) of treatment. While some partially melted powders can be removed from the metal surface, only 27% of surface roughness reduction was achieved. Due to the fact that no satisfying result was achieved from this method during the screening phase, no complete DOE was designed and conducted for this process. According to the preliminary results, ultrasound and abrasion alone do not have the capability to effectively reduce the surface roughness of the AM metal parts. However, when combining these with electrochemical surface finishing, synergistic effects are induced, improving the surface quality and the process efficiency at the same time.

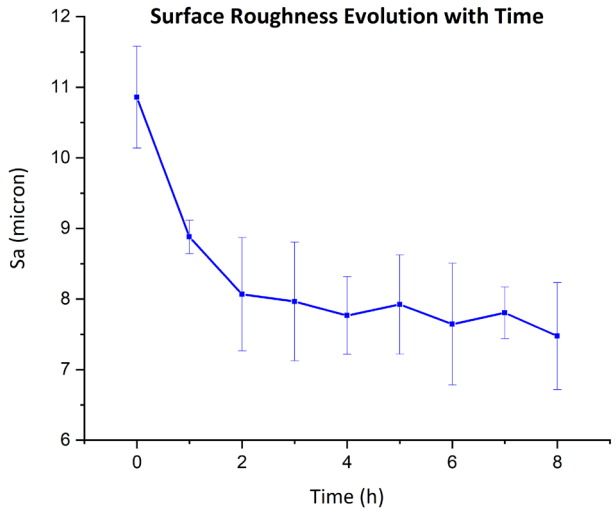


Figure 4.10 Surface roughness evolution with time under ultrasound and abrasion

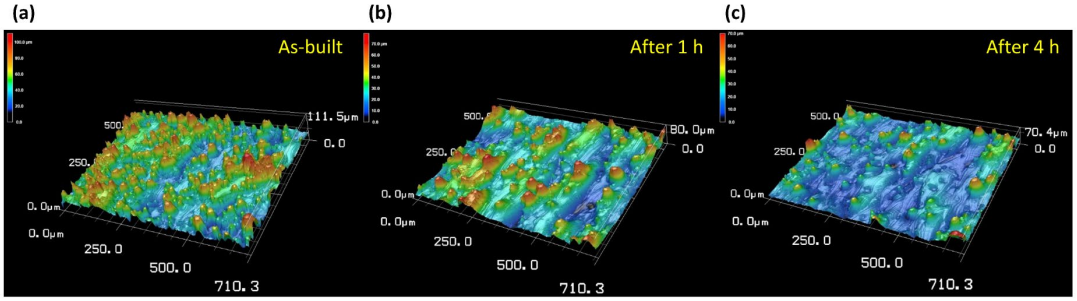


Figure 4.11 Three-dimensional images of (a) as-built surface; (b) surface after 1 h treatment by ultrasound and abrasion; and (c) surface after 4 h treatment by ultrasound and abrasion

4.3.5. Analysis of Hybrid Finishing Technique

Figure 4.12 show the main effect plots for response means and for S/N ratios when analyzing the surface roughness for the hybrid DOE as shown in Table 4.3. According to the results, in the three-level Taguchi design, when the process time is 45 min, the ultrasonic amplitude is 80%, and the abrasive concentration is 10%, the largest *S/N* ratio and the largest mean for surface roughness reduction can be achieved. However, the influence of ultrasonic amplitude and abrasive concentration is less significant than processing time in the selected parameter range. Figure 4.13 presents 3D surface images achieved by a Keyence laser profilometer after nine treatments.

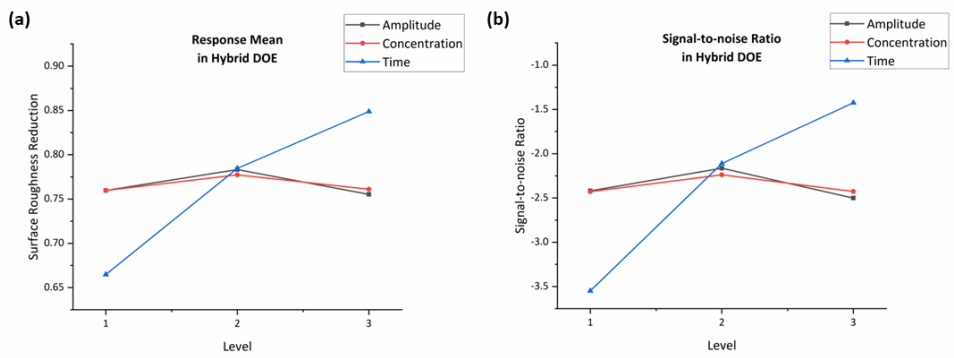


Figure 4.12 Main effect plots in hybrid DOE for (a) response means and (b) *S/N* ratios

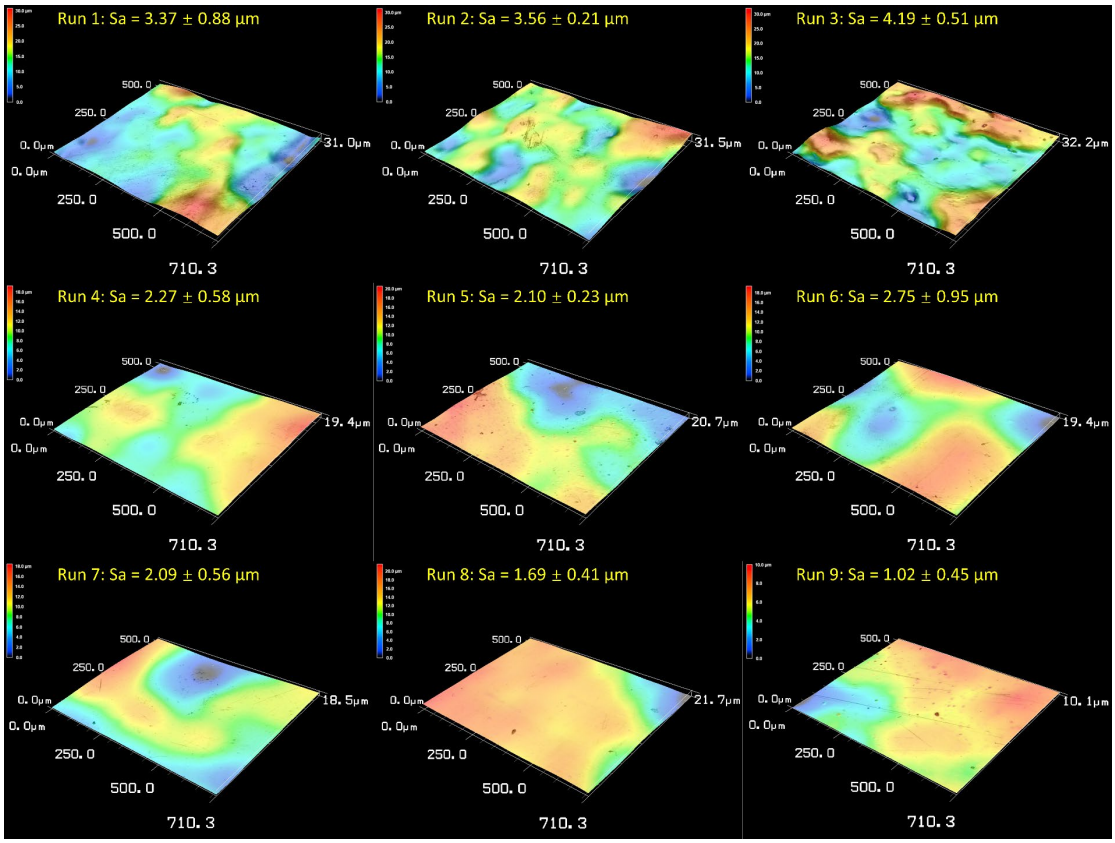


Figure 4.13 Three-dimensional surface images for samples in hybrid DOE

Similar to electrochemical polishing, processing time is an important influencing factor for the hybrid finishing process. If the finishing time is too short, it is not adequate to generate effective polishing footprints on the part surface. The results show that hybrid finishing is able to decrease the *Sa* value of the part surface to ~1.02 µm after 45 min. Both ultrasonic amplitude and abrasive concentration have a slight impact on the *Sa* reduction. If the ultrasonic amplitude is not high enough, the vibration might not be

substantially large for accelerating abrasive particles in the slurry, resulting in a low material removal efficiency. In addition, it is challenging for low-amplitude ultrasound waves to provide enough power to ensure uniform ionic mass transport for electrochemical polishing. However, a high ultrasonic amplitude may generate a huge amount of localized heat, causing damage to the metal surface while making it difficult to control the electrolyte temperature. If the abrasive concentration in the slurry is too low, the lack of abrasive particles in the slurry might not initiate obvious abrasion and peening on the surface for changing the surface condition. However, if the concentration is too high, abrasive particles could be embedded in the part surface, which might lead to a further increase in surface roughness. Meanwhile, the addition of abrasive particles in the electrolyte slurry also increases its viscosity while decreasing its conductivity [91][92], leading to the deterioration in the electropolishing performance.

4.3.6. Comparison between Electropolished Surface and Hybrid Finished Surface

To analyze surface waviness, a waviness filter was applied to the line profile to extract large-scale surface waviness while eliminating the small-scale roughness signal. Figure 4.14 shows surface waviness profiles after electropolishing and hybrid finishing under optimal working parameters for different processing times as shown in Table 4.4. Increasing the finishing time from 30 min to 45 min for electropolishing and hybrid finishing decreases the surface waviness by 66.5% and 47.4%, respectively. Compared with electropolishing, hybrid finishing has the capability to provide a surface with a similar surface waviness in a shorter time, with the average *Wa* value of 0.83 μm after electropolishing for 45 min, while the same value is 0.94 μm after hybrid finishing for 30 min. After process optimization for both processes, although similar Sa values are obtained, the surface waviness of hybrid technique-treated samples is much less than the electropolished samples, as presented in Figure 4.15.

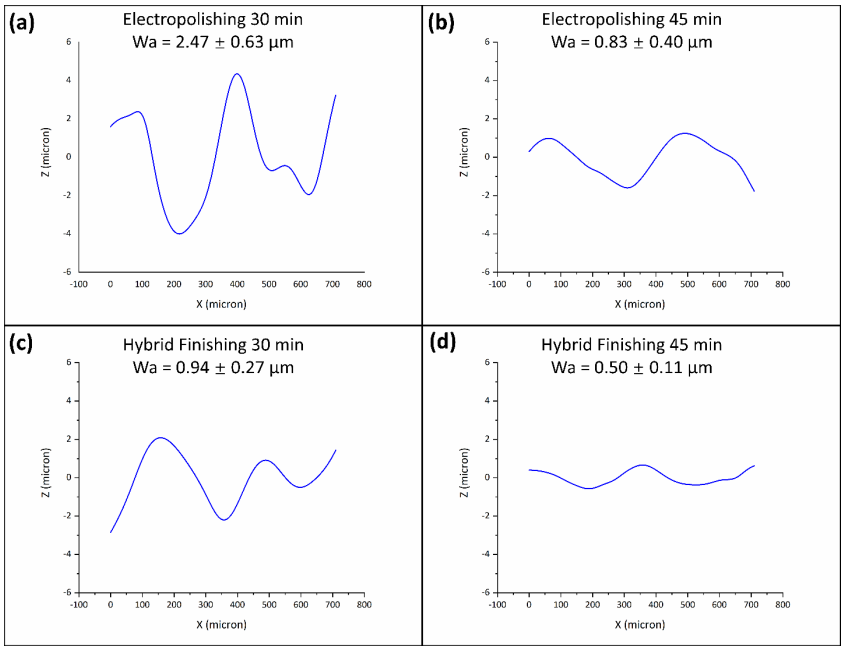


Figure 4.14 Surface waviness profile for (a) electropolishing for 30 min; (b) electropolishing for 45 min; (c) hybrid finishing for 30 min; (d) hybrid finishing for 45 min

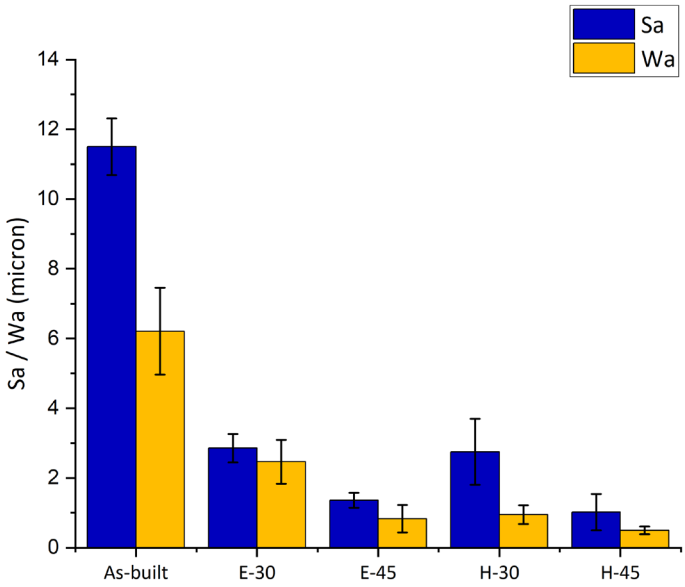


Figure 4.15 Surface roughness and waviness comparison for electropolishing and hybrid finishing

4.4. Discussions

There are multiple causes of the large-scale surface waviness of electropolished metal

AM parts, from the perspectives of both AM and electropolishing. The stair-stepping effect is a main type of surface irregularity for AM parts. It is created due to the layer-by-layer nature of the process, where a larger layer thickness may result in visible discontinuities on the part's surface, resulting in large surface waviness. Although electropolishing could eliminate the small-scale surface roughness effectively, it seems not to be efficient enough to remove the surface waviness via merely electropolishing. From another perspective, the electropolishing process could introduce surface waviness as well due to non-uniform mass transfer. When there are localized concentration variations in the electrolyte flow, non-uniform distribution of the current density occurs, which would lead to uneven material dissolution and, consequently, the formation of surface waviness.

In the electropolishing process, a voltage is applied between the workpiece anode and the inert cathode; Ti atoms on the workpiece surface dissolve in the electrolyte by being oxidized to Ti^{4+} ions. In order to maintain the electrical neutrality of the electrolyte, Cl^- ions in the bulk electrolyte migrate to the workpiece surface and complex with Ti^{4+} to form $TiCl_4$. $TiCl_4$ is a viscous liquid, which forms a viscous layer with a higher electrical resistivity compared to the bulk electrolyte adjacent to the workpiece anode[93]. According to the viscous film theory [73], due to the high surface roughness of the as-built workpiece, the thickness of the viscous layer at the valley is higher than the thickness at the peak. Accordingly, the viscous layer at the valley has larger electrical resistance compared with the viscous layer at the peak, resulting in a potential difference at different surface locations, leading to a leveling and polishing effect. With the progress of the aforementioned process, the surface roughness as well as the surface waviness decreases with time, while the uniformity of the waviness distribution also increases. Although electropolishing has the capability to reduce the surface roughness and waviness, when the processing time reaches the threshold limit, instead of polishing the surface and further reducing the surface waviness, overpolishing occurs with pits forming on the surface. The mechanism is shown in Figure 4.16.

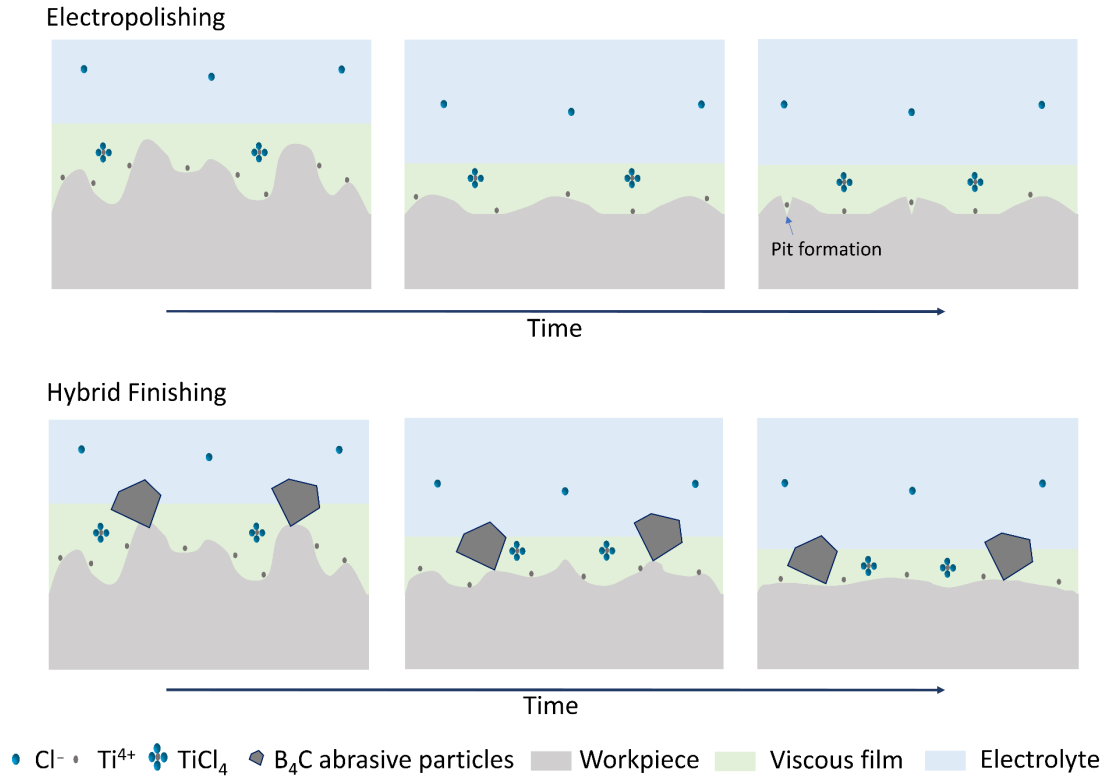


Figure 4.16 Surface finishing mechanism for electropolishing and hybrid finishing

While electropolishing plays the main role in material removal, abrasive particles accelerated by the ultrasonic cavitation help reduce the surface roughness by cutting and peening, also as shown in Figure 4.16. When ultrasonic energy is applied to the liquid medium, the pressure of the ultrasound wave vibrates under the ultrasound frequency. A reduction in the liquid's static pressure to below its vapor pressure leads to the formation and growth of cavities or "gas bubbles", which would collapse when the pressure inside the bubble increases and reaches the threshold pressure. When adding abrasive particles into the liquid medium, cavitation bubble collapse accelerates the abrasive particles in the slurry, leading to the impact of abrasive particles on the metal surface, which generates abrasive erosion on the metal surface.

The high initial kinetic energy of abrasive particles could be achieved due to the formation of a shockwave and micro-jet in the ultrasonic cavitation, which has been verified by numerical simulations [79]. When abrasive particles impact the metal surface, material removal with different patterns happens under different impact angles.

When the particle impacts the metal surface with a shallow impact angle, cutting acts as the main mechanism, as shown in Figure 4.17 (a). Abrasive particles with high initial speed cut the surface bumps and lead to the reduction in surface waviness. On the other hand, if the impact angle is large, or the abrasive particles vertically impact the surface bumps, peening instead of cutting occurs on the metal surface, which creates localized plastic deformation and may possibly benefit with a reduction in surface roughness (Figure 4.17 (b)). At the same time, the ultrasonic cavitation itself might also contribute to the roughness and waviness reduction to some extent (Figure 4.17 (c)). When the gas bubbles form and grow close to the surface protrusions, high shear stress could be generated due to bubble collapse, leading to crack propagation on the surface bumps and eventually resulting in material removal.

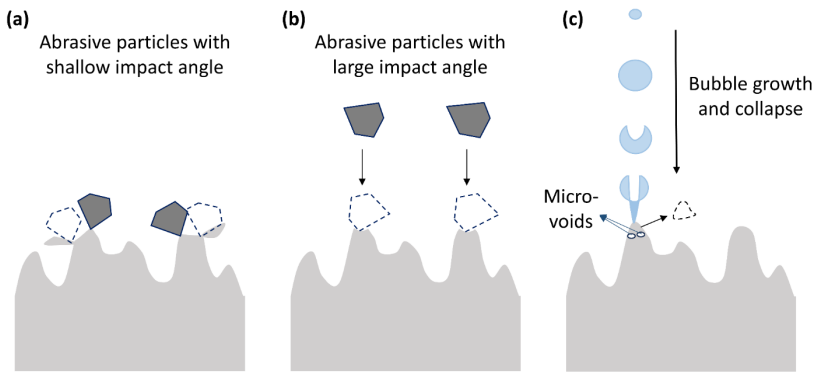


Figure 4.17 Mechanism for roughness removal due to ultrasound and abrasion: (a) cutting due to shallow impact angle; (b) peening due to large impact angle; (c) micro-void formation and material removal due to cavitation bubble collapse

In addition to the aforementioned mechanisms for reducing surface roughness, we propose another possible mechanism for the hybrid finishing technique to mitigate surface waviness, attributed to the synergistic effect of electropolishing, ultrasound, and abrasives. Given that solid surfaces in the liquid electrolyte solution are the preferred sites for cavitation to occur, the localized bubble density near the metal surface may be higher than in other areas of the bulk electrolyte during treatment. Moreover, bubbles and abrasives situated at the wave trough are less likely to move freely, potentially

resulting in higher concentrations of abrasive particles and cavitation bubbles at the metal surface compared to the bulk electrolyte, as shown in Figure 4.18. The presence of a higher concentration of particles at the wave trough increases the viscosity in this region, maybe leading to a decrease in ionic conductivity compared to the wave crest. Consequently, the application of ultrasound and abrasive particles may generate a "synthetic viscous layer" at the metal surface on a larger scale, adjusting the localized ionic conductivity of the electrolyte during the electropolishing process and thus reducing surface waviness.

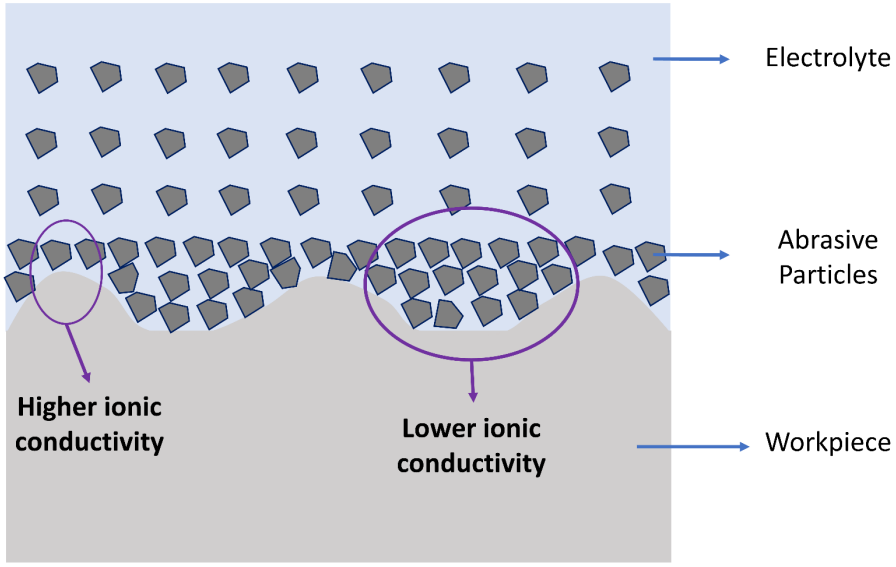


Figure 4.18 Hypothesis for waviness removal due to synergistic effect of electropolishing, and application of ultrasound and abrasive particles

Although the experimental results in this study are achieved on the rectangular coupons, this method is also a promising candidate for surface finishing of curved and conformal surfaces, and other types of external surfaces with complicated geometries, which cannot be achieved by conventional grinding and cutting. Figure 4.19 shows the pictures of the cylinder surface after the hybrid process. Due to its capability of polishing curved surfaces, the proposed method has the potential for various applications, such as surface finishing of printed implants for biomedical applications and reducing the roughness of engine components for the automotive or aerospace and aviation sectors. The next step of this study will be to adjust the method for improving

the surface quality of internal channels, which will be beneficial for heat exchangers and conformal cooling passages for energy applications.

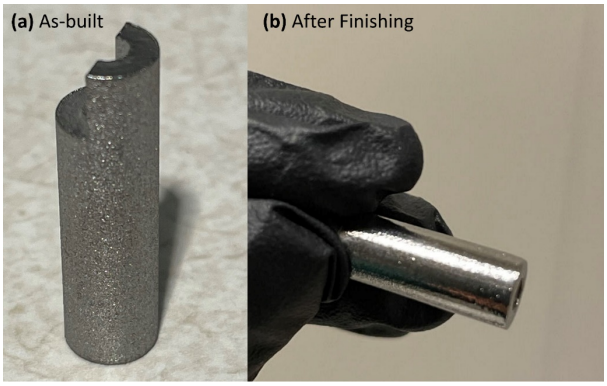


Figure 4.19 (a) Camera picture of as-built cylinder surface; (b) camera picture of cylinder surface after hybrid finishing

4.5. Summary

In this research, an experimental feasibility study was carried out to shed some light on the general concept of the novel hybrid ultrasound abrasive-driven electrochemical surface finishing method. The preliminary results prove the feasibility of the idea. To synergistically study the effect of different processes involved, electropolishing, ultrasound/abrasion, and hybrid surface finishing were conducted on the LPBF-made Ti6Al4V coupons when the resultant surface roughness was compared. The conclusions are as follows:

(1) A smooth and reflective surface could be achieved after both the electropolishing and hybrid treatment, with the optimal Sa values of 1.36 ± 0.21 μm and 1.02 ± 0.45 μm, respectively.

(2) No evidence showed that the combination of ultrasound and abrasion is capable of effectively reducing surface roughness.

(3) The introduction of ultrasound and abrasion into electropolishing has the capability to reduce the surface waviness further compared to electropolishing, with the *Wa* value being 0.83 ± 0.40 μm for electropolishing and 0.50 ± 0.11 μm for hybrid finishing after

45 min.

Although the hybrid treatment shows promising potential for surface finishing of AM parts, temperature control remains a challenge in terms of scaling it up due to the rapid heat generation when introducing ultrasound and abrasion into electrochemical surface finishing. In addition, process optimization for finishing complex parts with internal channels is another challenge that needs to be solved.

5. Feasibility of 3D-Printed Polymeric Covers for Electrode Wires in Electropolishing Internal Channels

5.1. Chapter Overview

This work discloses a novel setup and procedure for electropolishing of internal channels of additively manufactured components. A specially designed and printed polymeric cover was assembled with a flexible stainless steel 316 wire to facilitate electropolishing of internal channels with various curvatures. Experimental studies were conducted to assess the feasibility of the process. The presence of curvatures was found to influence the formation and removal of conductive solid reaction products, thus affecting the electropolishing performance accordingly. A maximum surface roughness Sa reduction from 10.86 ± 0.50 µm to 1.44 ± 0.46 µm was obtained for straight channels, while Sa values for curved channels with curved values of 0.04 and 0.08 were decreased to 2.22 ± 0.14 µm and 3.53 ± 1.04 µm. Following that, a numerical simulation was conducted for optimization of wire covers, and the performance of three designs were analyzed and compared. While the methods show great potential on electropolishing curved internal channels, challenges need to be solved for improving the electropolishing performance and reducing the limit of the channel size that can be electropolished. Figure 5.1 is the graphical overview for Chapter 5.

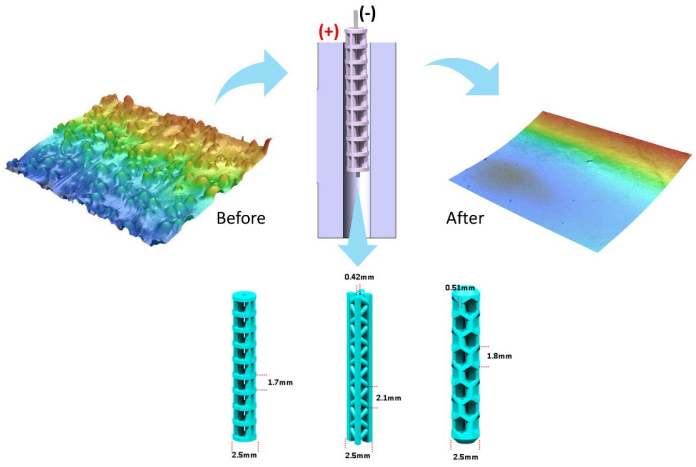


Figure 5.1 Graphical overview of Chapter 5

5.2. Experiments and Methods

5.2.1. Introduction of Polishing Concept

To electropolish internal channel walls, a cathode electrode must be inserted into the channel for having the maximum ionic transport between the workpiece anode and the tool cathode. For achieving optimal polishing performance, the distance between the two electrodes should relatively remain the same throughout the channel so that a uniform current distribution could be obtained on the polished surface. However, when a flexible wire is inserted into the straight channels, it is challenging for maintaining the shape of the wire - some parts of the wire might be closer to the channel walls, while others move further away, as shown in Figure 5.2 (a), leading to a non-uniform current distribution. In addition, in the case of curved channels, inserting a flexible wire without any insulating structure often results in short circuits.

To address these issues, a novel tool electrode was developed, consisting of a flexible wire combined with specially designed flexible polymeric wire covers. The purpose of this design is to maintain a constant distance between two electrodes while allowing for the electrolyte flow, therefore preventing short circuits and ensuring a relatively uniform current distribution. The general concept of the proposed innovative tool electrode is illustrated in Figure 5.2 (b).

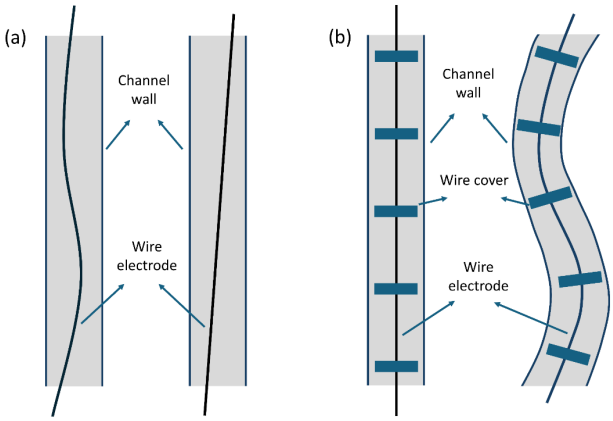


Figure 5.2 Cross-section of internal channels: (a) Non-uniform distance between the wire and the channel wall when inserting the wire directly into the channels; (b)

5.2.2. Fabrication of Samples with Internal Channels

Ti6Al4V was selected in this work due to its wide range of applications in the aerospace and biomedical industries, resulting from its excellent mechanical properties, chemical stability, and corrosion resistance [86]. Ti6Al4V cylindrical samples (AP&C powders with 0.1% carbon contaminants), each 40 mm in length with internal channels of 4 mm in diameter, were fabricated using laser powder bed fusion (LPBF) with an EOS M290 machine. Both straight (S) and curved channels were printed, as shown in Figure 5.3. To develop a preliminary benchmark, curved channels with three different curvatures (C1, C2, C3) were used for surface finishing tests. The curvature values were 0.04, 0.08 and 0.14, corresponding to radii of curvature of 25.27 mm, 12.59 mm and 7.21 mm, respectively. The printing process was carried out along the length of the cylinder, with the corresponding parameters listed in Table 5.1.

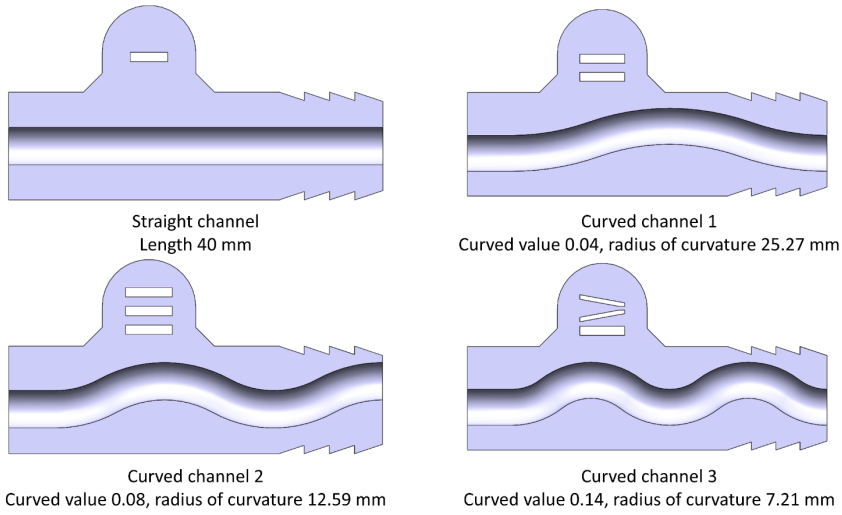


Figure 5.3 Shape of printed straight and curved channels

Table 5.1 Printing parameters for cylinders

Category	Laser Power (W)	Scanning Speed (mm/s)	Hatch Distance (mm)
Hatch	200	1300	0.1
Contour	100	500	0.1

5.2.3. Fabrication of Tool Electrode

Given the proven effectiveness of using 316-type stainless steel (SS316) as the cathode for electropolishing Ti6Al4V parts, SS316 wire with a diameter of 0.3 mm was selected as the cathode for the electropolishing tests due to its low price and popularity. To prevent direct contact between the Ti6Al4V workpiece anode and the SS316 wire cathode while enabling the electrolyte to flow through the gap between the two electrodes, a polymeric cover was designed and fabricated using a Stratasys J750 PolyJet printer. The printing process was conducted at ambient temperature and humidity, with a layer thickness of 27 microns. The cover was printed using a combination of hard (VeroBlackPlus) and soft (Agilus30Clear) materials to ensure adequate strength during usage as well as possess the suitable flexibility to accommodate the bending requirements in curved channels. The disks in the fixture were printed with hard polymers, while the connecting bridges were printed with flexible rubbers. Figure 5.4 provides the CAD design of the polymeric cover, the camera picture of its assembly with the SS316 wire, and the SEM images of both the cover and the wire.

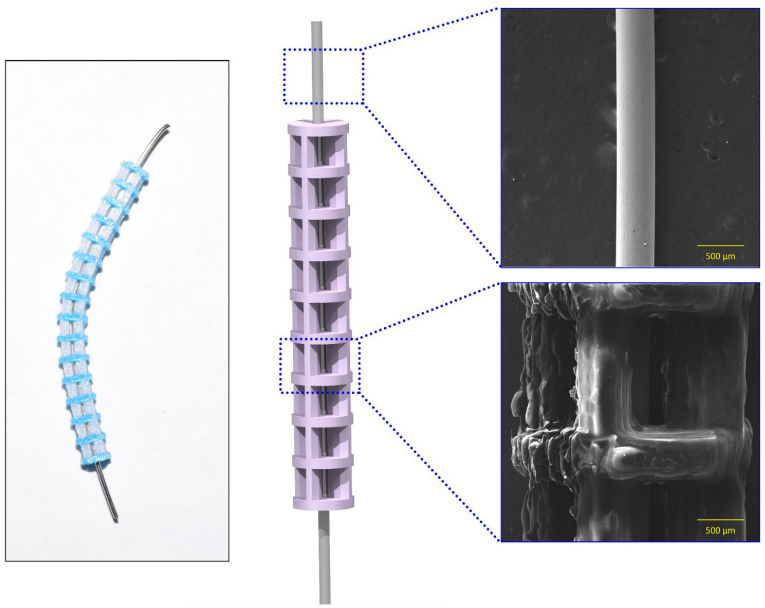


Figure 5.4 Images for tool electrode, including camera picture for wire-cover

assembly (blue disk was printed with hard material, and the white bridge was printed with flexible material), CAD design for printed polymeric wire cover, SEM image for wire cover and the SS316 wire

Before starting electropolishing tests, a compatibility study was conducted to evaluate the interaction between the wire covers and the electrolyte. Fresh electrolyte was prepared, and wire covers were immersed in the solution for 1, 2, 5, and 24 hours. After immersion, the wire covers were rinsed with water, dried thoroughly in an airflow, and their mass changes were calculated for each immersion period.

5.2.4. Electropolishing Tests

The experimental setup for electropolishing internal channels consisted of the electrolyte, a pump for creating flow and circulation of the electrolyte, and a power supply to provide the power source for the electrochemical reaction. The electrolyte used in the study was an environmentally friendly electrolyte for polishing titanium alloy, containing 250 g/L zinc chloride, 60 g/L aluminum chloride, 700 mL/L ethanol and 300 mL/L isopropanol. To pump the electrolyte into the internal channels, a peristaltic pump (Kamoer DIP1500) was operated at a constant flow rate of 300 mL/min. A 300 mL electrolyte solution was used for each run, and fresh solutions were prepared for electropolishing new samples. A custom sample holder was designed, and 3D printed with a Stratasys J750 printer, to fix the samples while providing a consistent method for connecting the wires. Figure 5.5 is the schematics of the experimental setup for the electropolishing tests.

A power supply (Korad KC6403) with data-logging functions was used to apply a constant voltage while recording the current during electropolishing tests. The real-time current of each test was monitored to assess the influence of current density on the surface finishing performance. To maintain a constant temperature range (25-35 ºC), the electrolyte reservoir was placed in a water bath at room temperature throughout the tests. Prior to each test, all samples were sonicated in isopropanol in an ultrasonic bath for 10 minutes to remove loose powder and oily contaminants from their surfaces.

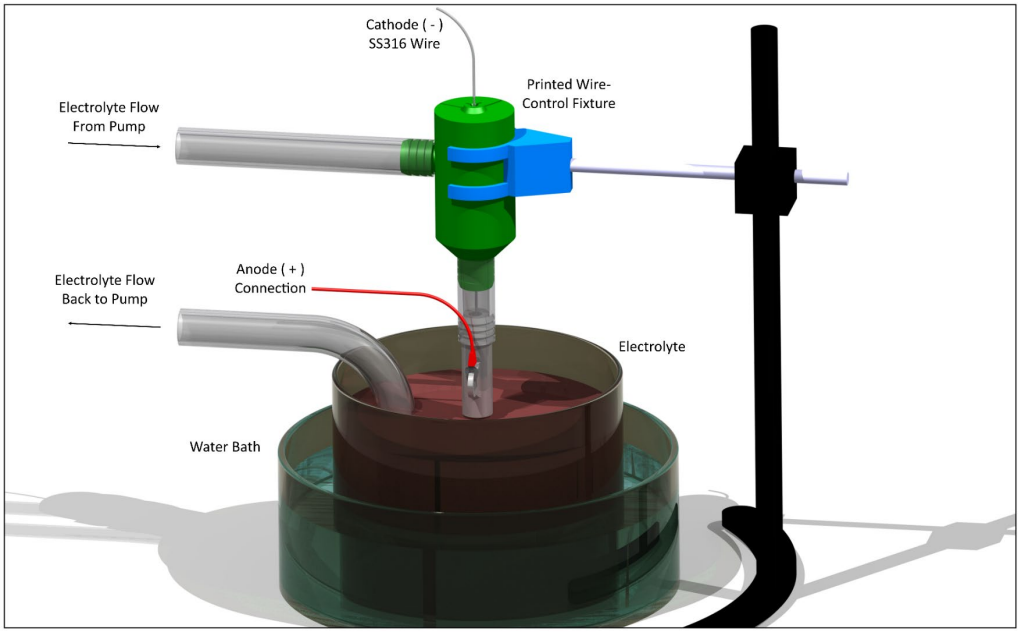


Figure 5.5 Schematics of the experimental setup with electrolyte flow

Before conducting electropolishing tests, the optimal working voltage used in the tests was determined. According to preliminary experiments conducted by the authors [94] on the same material system, the ideal voltage range for electropolishing Ti6Al4V in the current electrolyte was between 25 V and 30 V. Therefore, 25 V and 30 V were selected for initial testing on straight channels. Electropolishing performance under these two voltages was compared after a surface treatment of 20 minutes with bare SS316 wires inserted and fixed in the straight channels without wire covers. The voltage that led to the best surface quality was then used for the subsequent experiments on both straight and curved channels using the polymeric wire covers.

Table 5.2 Test Parameters

Voltage	25 V (Selected), 30 V
Electrolyte composition	250 g/L zinc chloride, 60 g/L aluminum chloride, 700 mL/L ethanol and 300 mL/L isopropanol
Channel diameter	4 mm
Channel curved value	0, 0.04, 0.08, 0.14
Wire diameter	0.3 mm
Wire cover diameter	2.5 mm
Temperature	25-35 ºC
Flow rate	300 mL/min

Accumulated processing time	20 min

Following the selection of the working voltage, electropolishing tests were conducted using the novel flexible cathodic electrodes on samples S, C1, C2 and C3 with the experimental setup shown in Figure 5.5. Surface roughness evolution during the process was measured using the straight channel. The electropolishing process was conducted for a total accumulated processing time of 20 min for both straight channels and curved channels to compare the surface quality of the polished surfaces and the as-built surface. In cases where curved channels experienced short-circuiting behavior during the process, wire cover and cathode were removed, cleaned, and reinserted into the channel to continue the electropolishing test. Current density versus time (i-t) curves were recorded during each test. Table 5.2 lists all the experimental parameters used in this study.

5.2.5. Surface Characterization

After electropolishing, the samples with internal channels were cut in half with a wire electrical discharge machining system (Sodick VL600QH) to facilitate surface characterization of the polished channel walls. Laser scanning confocal microscopy was used for surface roughness characterization due to its largest capability for detecting different types of surface textures, compared with other techniques including structured white light triangulation, coherence scanning interferometry and contact stylus[95]. According to ISO 25178 [88], surface roughness was measured by the reflection along the z-axis when the surface is scanned by a laser beam. Based on this mechanism, surface images and surface roughness values were acquired by a 3D laser scanning confocal microscope (Keyence VK-X250) under the magnification of 20×. To compare the surface roughness of the polished surface, arithmetical mean height (Sa) and maximum height (Sz) values were measured at five different locations for each sample, with each location covering an area of 0.71mm×0.5mm. Figure 5.6 demonstrates the locations for measurements with respect to their building direction

and the electrolyte flow direction for each channel geometry. The average and standard deviation of Sa and Sz values were then used to quantify the surface quality of the channels. The roughness values presented in this paper have been processed using a filter to remove curvatures resulting from the cylinder's radius. The image of the whole channel was obtained by the stitching function of a digital microscope (Keyence VHX-7000). Additionally, for examining surface defects and irregularities before and after electropolishing, surface quality was also characterized at higher magnifications using a scanning electron microscope (SEM) (TESCAN VEGA3).

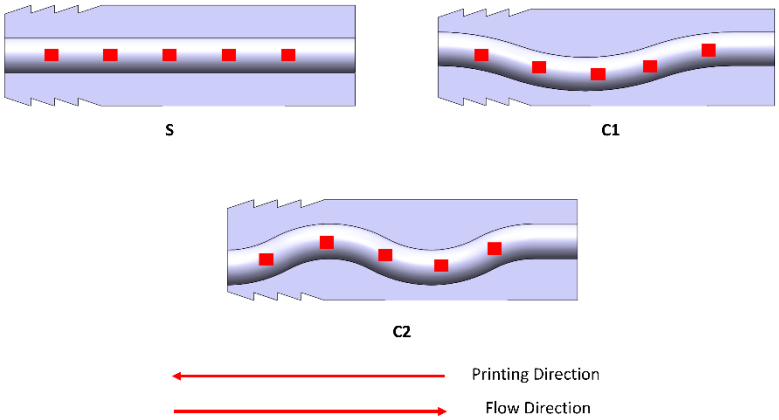


Figure 5.6 Locations for internal channel surface roughness measurements

5.3. Results and Discussion

5.3.1. As-built Surface Analysis

The as-built channel surface possesses a relatively high average surface roughness (*Sa* = 10.86 ± 0.50 µm, *Sz* = 105.06 ± 6.26 µm) due to various surface features presented on it. The 3D surface profile and the SEM image of the as-built surface features of the straight channel are shown in Figure 5.7. As can be seen from Figure 5.7 (b), the whole as-built surface was covered with partially melted particles, caused by unmelted metal powders adhering to the metal surface at extremely high temperatures. The formation of liquid spatter also contributed to the high initial surface roughness, since the melt pool track has the tendency to minimize the surface energy due to the existence of liquid

surface tension. Additionally, surface defects including cracks and pores as well as solidified melting tracks also lead to the increase of the surface roughness. Due to the fact that the change in build angles might cause the difference in surface roughness, surface profiles with roughness data for different channel curvatures are presented in Figure 5.8 for comparison purpose. The picture illustrates that straight channel surface shows a higher density of adhered particles, with slightly higher *Sa* and *Sz* values.

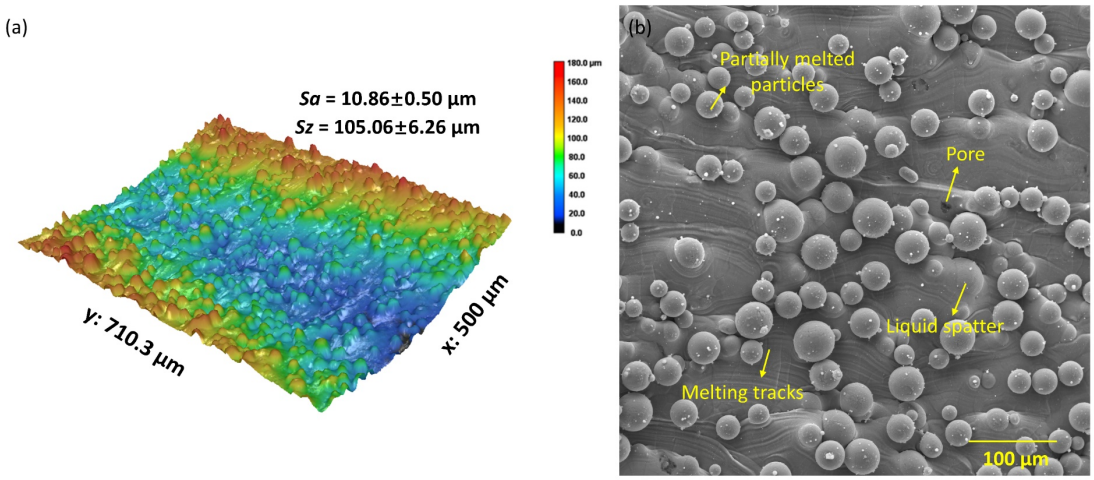


Figure 5.7 (a) 3D profile and (b) SEM image of as-built surface features

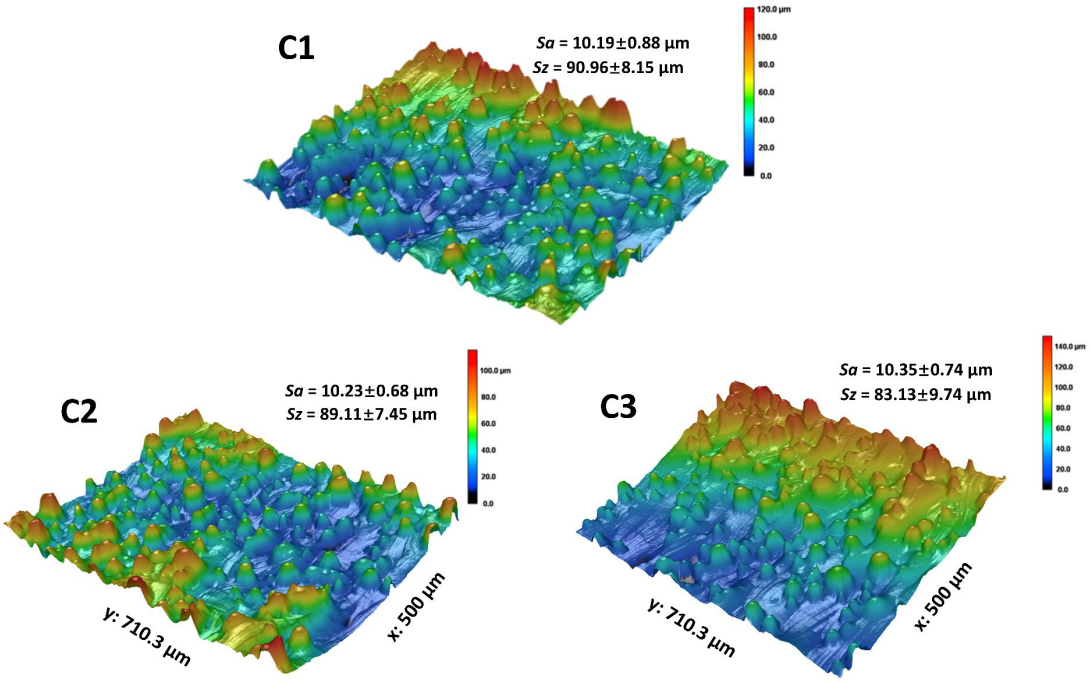


Figure 5.8 Comparisons of initial roughness for different curvatures

5.3.2. Compatibility between the Wire Cover and the Electrolyte

A compatibility study was conducted to evaluate the interaction between the wire covers and the electrolyte prior to performing electropolishing tests. Fresh electrolyte was prepared, and wire covers were immersed in the solution for 1, 2, 5, and 24 hours. Figure 5.9 shows the mass increase of the wire cover after different immersion periods. Camera pictures of the wire covers (Figure 5.10) illustrate their shape integrity following the treatments. The results revealed different degrees of shape expansion depending on the immersion duration, suggesting absorption of salt components into the polymeric network.

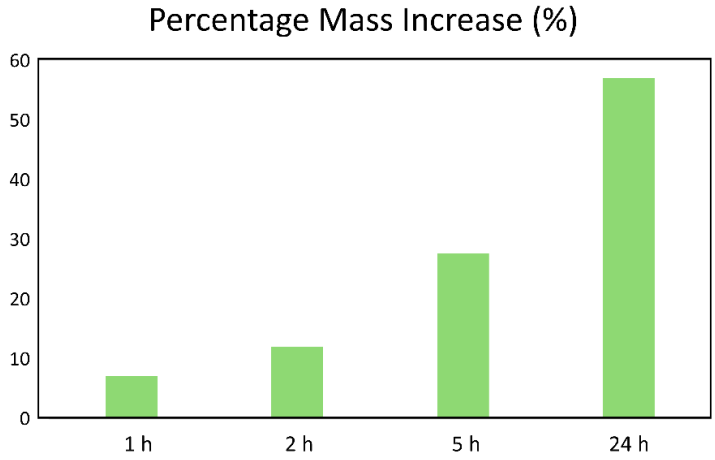


Figure 5.9 Percentage mass increase of wire covers at different immersion durations

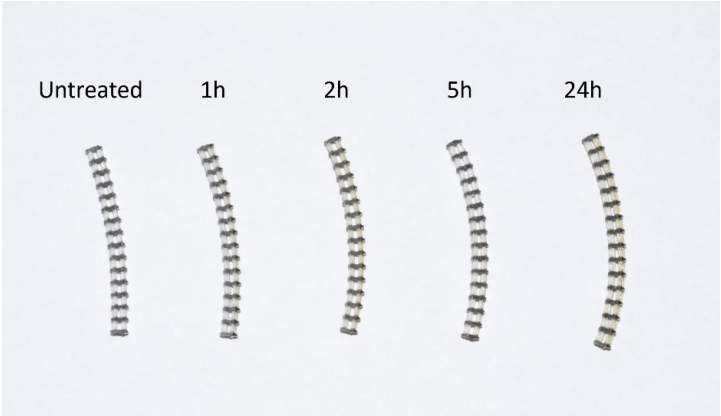


Figure 5.10 Camera pictures of wire covers at different immersion durations

5.3.3. Effect of Voltage

Figure 5.11 demonstrates the 3D profile of the straight channel surface after electropolishing at 25 V and 30 V for 20 min, both of them starting from as-built surface shown in Figure 5. Although the Sa values are within the similar range, measuring 1.24 ± 0.20 µm and 1.56 ± 0.21 µm respectively, the limited channel size results in a relatively low inter-electrode distance compared to the electropolishing of external surfaces, which leads to the formation of numerous pits on the surface when polished at 30 V. On the contrary, the surface polished at 25 V appears relatively smooth with fewer surface defects presenting, proved by the significantly lower Sz value of 18.94 ± 7.55 µm compared with the value of 37.17 ± 21.86 µm for the surface polished at 30 V. Based on these observations, 25 V was selected as the working voltage for polishing channels with all types of curvatures.

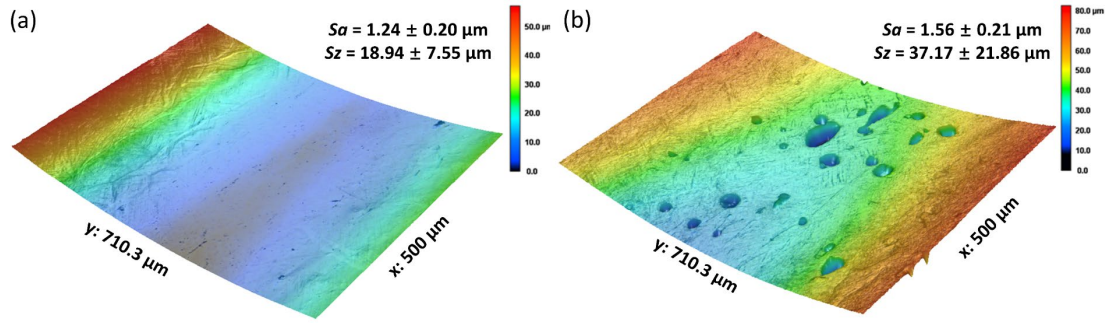


Figure 5.11 3D profile of channel surface after polishing at (a) 25 V and (b) 30 V

Figure 5.12 exhibits SEM images of surface defects after polishing at 30 V without using wire covers. The surface displays a distinctive topology with numerous pits and voids of various sizes and shapes. Meanwhile, the evidence of particle collapse has been observed in Figure 5.12 (b). This type of surface defect is likely due to, more gas bubbles, generated in the electrolyte at the higher voltage. Given the small inter-electrode distance resulted from the limited channel size, the presence of the bubbles plays a critical role on modifying the localized electrolyte conductivity through bubble shielding and broken bubble tunneling effect [96]. Consequently, the pit formation might occur due to increased material dissolution rate at locations with a more

concentrated electric field.

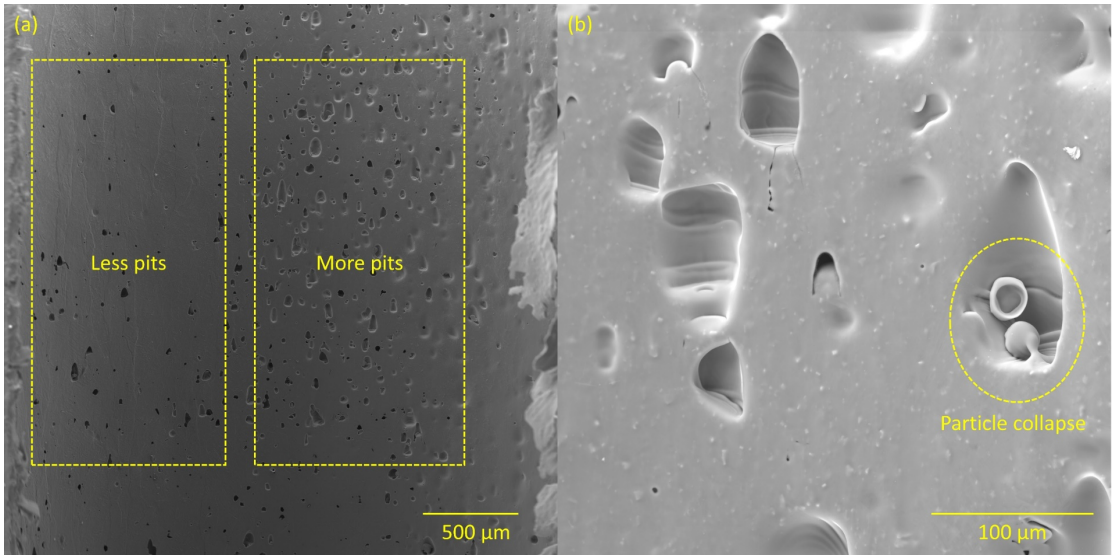


Figure 5.12 Non-uniform and pitting surface after electropolishing at 30V at (a) lower magnification (200x) and (b) higher magnification (1600x)

In addition, as shown in Figure 5.12 (a), the distribution of pits and defects is not even across the surface. When the wire is inserted into the straight channel without any cover, its centre distance with respect to the wall normally fluctuates constantly with the electrolyte flow. Some areas of the surface are closer to the wire electrode, while others are further away, which leads to a non-uniform current density distribution and inconsistent surface quality. Therefore, it is essential to design an appropriate wire cover to maintain a uniform gap between the wire and the channel wall.

5.3.4. Surface Roughness Analysis

Surface profiles were captured after electropolishing tests using the novel integrated cathodes, and surface roughness values were measured after electropolishing for different time until the surface became smooth. Figure 5.13 shows the 3D surface profiles of the channel walls at different stages of electropolishing, with the corresponding surface roughness values, *Sa* and *Sz,* presented in Figure 5.14. The parameter *Sa* represents the arithmetic mean height, which is the average of the absolute values of height deviations at each point from the reference plane. *Sz* stands for the

maximum height, which measures the vertical distance between the top of the highest peak and the bottom of the deepest valley.

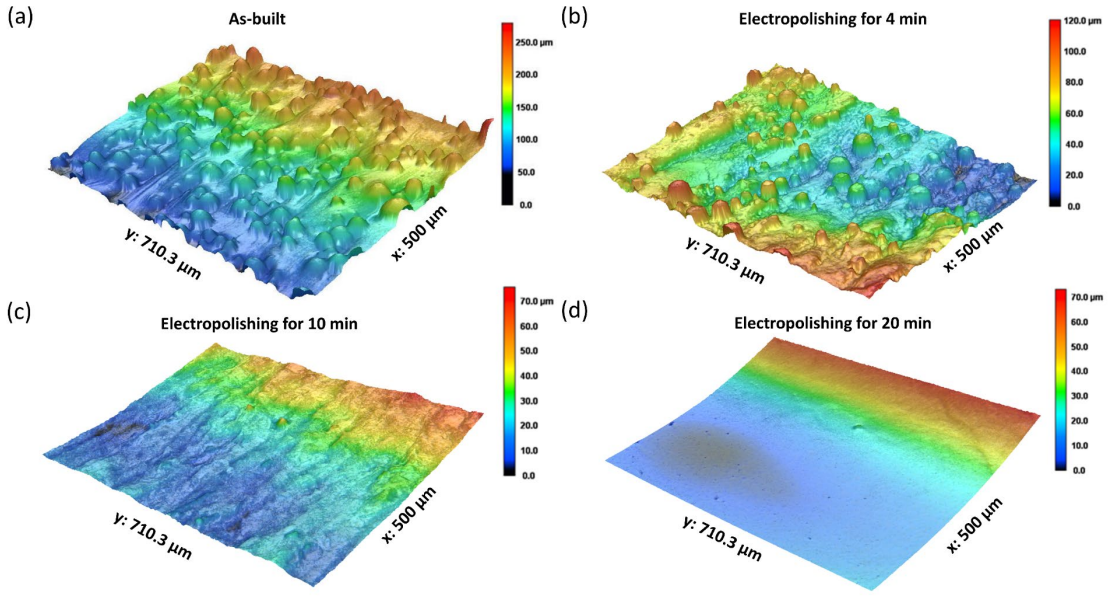


Figure 5.13 3D surface profile for (a) as-built sample and samples after electropolishing after (b) 4min, (c) 10 min and (d) 20 min

The as-built channel walls exhibited a variety of surface irregularities, such as partially melted particles, stair-stepping effects and visible melting tracks, as shown in the SEM image in Figure 5.7 (b). These defects result in a high initial surface roughness, with *Sa* at 10.86 ± 0.50 µm and *Sz* at 105.06 ± 6.26 µm. After 4 minutes of electropolishing, some of the partially melted particles were removed, leading to a reduction of Sa value to 7.62 ± 1.02 µm, and *Sz* value to 68.68 ± 4.94 µm. With the continuous operation of electropolishing, a majority of the partially melted particles on the channel wall surface were removed, leaving the surface with noticeable waviness (roughness with a wavelength of larger than 50 µm) after 10 minutes, with a *Sa* value of 3.79 ± 1.40 µm and a *Sz* value of 45.16 ± 14.07 µm. Finally, after 20 minutes of electropolishing, a smooth surface was obtained, with *Sa* reduced to 1.44 ± 0.46 µm and *Sz* to 16.25 ± 4.79 µm. Figure 5.15(a) and (b) illustrate the SEM image of the channel surface after electropolishing for 20 min at magnifications of 200× and 1000×. Surface irregularities were effectively removed from the surface compared with the as-built surface in Figure

5.7(b).

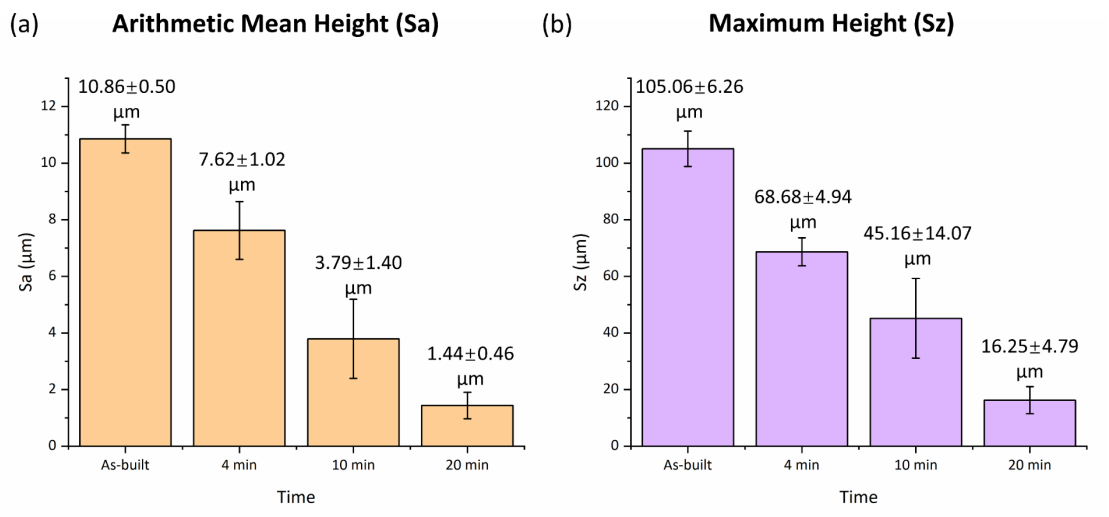


Figure 5.14 Different types of surface roughness evolution with time: (a) arithmetic mean height (*Sa*); (b) maximum height (*Sz*)

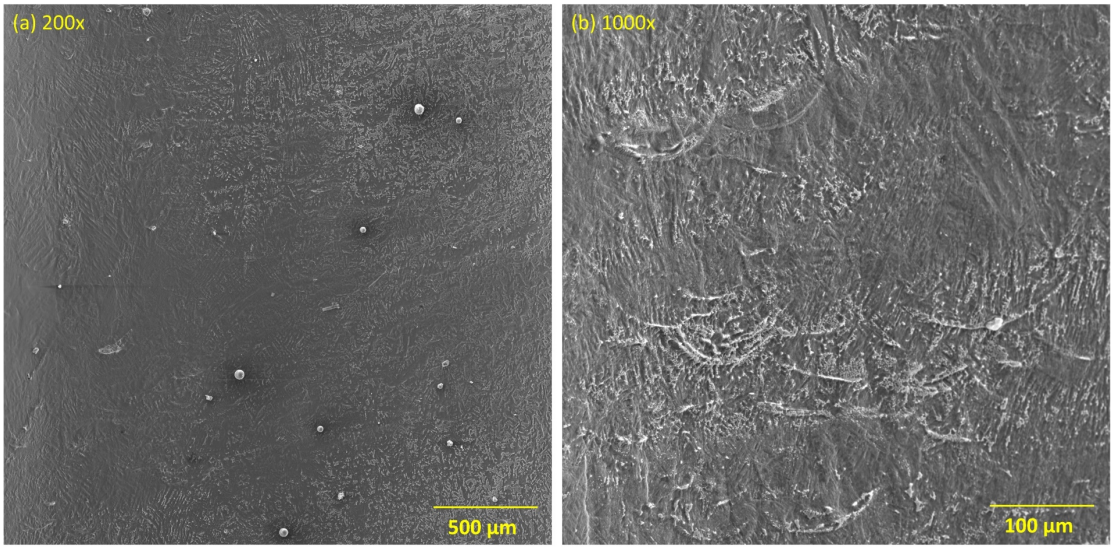


Figure 5.15 SEM images of polished surface under different magnifications:

(a) 200x and (b) 1000x

5.3.5. Failure Mechanism and Defect Formation

During the electropolishing process, material removal from the workpiece surface leads to the formation of conductive solid reaction products on the surface of the cathodic electrode. If these solid particles are not removed efficiently, they can gradually reduce

the inter-electrode gap, causing non-uniform polishing, and potentially leading to a short circuit. To quantitatively characterize the formation, accumulation and removal of reaction products in channels with different curvatures, the real-time current density for electrochemical reactions is illustrated in Figure 5.16.

For all channels, current density sharply increases at the initial stage of electropolishing, primarily due to the initial removal of partially melted particles and the accumulation of solid particles in the gaps of the wire covers. For straight channel S, the current reaches the maximum of the power supply after ~100 seconds of electropolishing due to the accumulation of the solid particles, followed by a drop after ~400 seconds due to their sudden removal. In contrast, for all curved channels, current density experiences a sharp increase and then the system becomes short circuited afterwards. The time until a short circuit occurs varies as it is a stochastic process, heavily dependent on the positioning of the wire and wire covers, while being dependent on many environmental and process disturbances. Figure 5.17 and Figure 5.18 provide the current density curves for electropolishing C1 and C2 while trying to maintain all the other parameters the same, indicating the stochastic nature of the process.

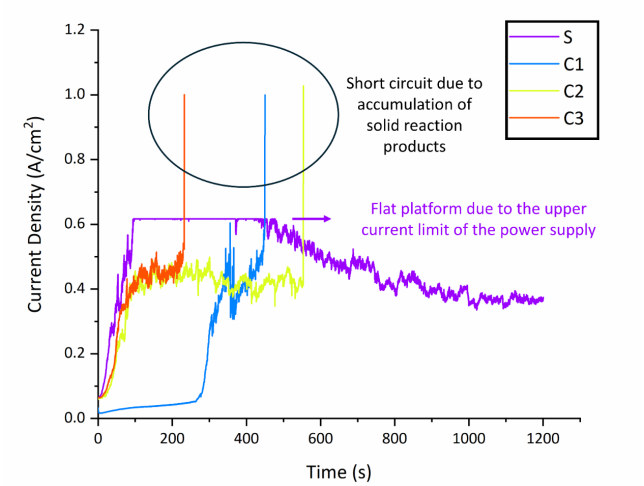


Figure 5.16 Current density curve for electropolishing internal channels with different curvatures

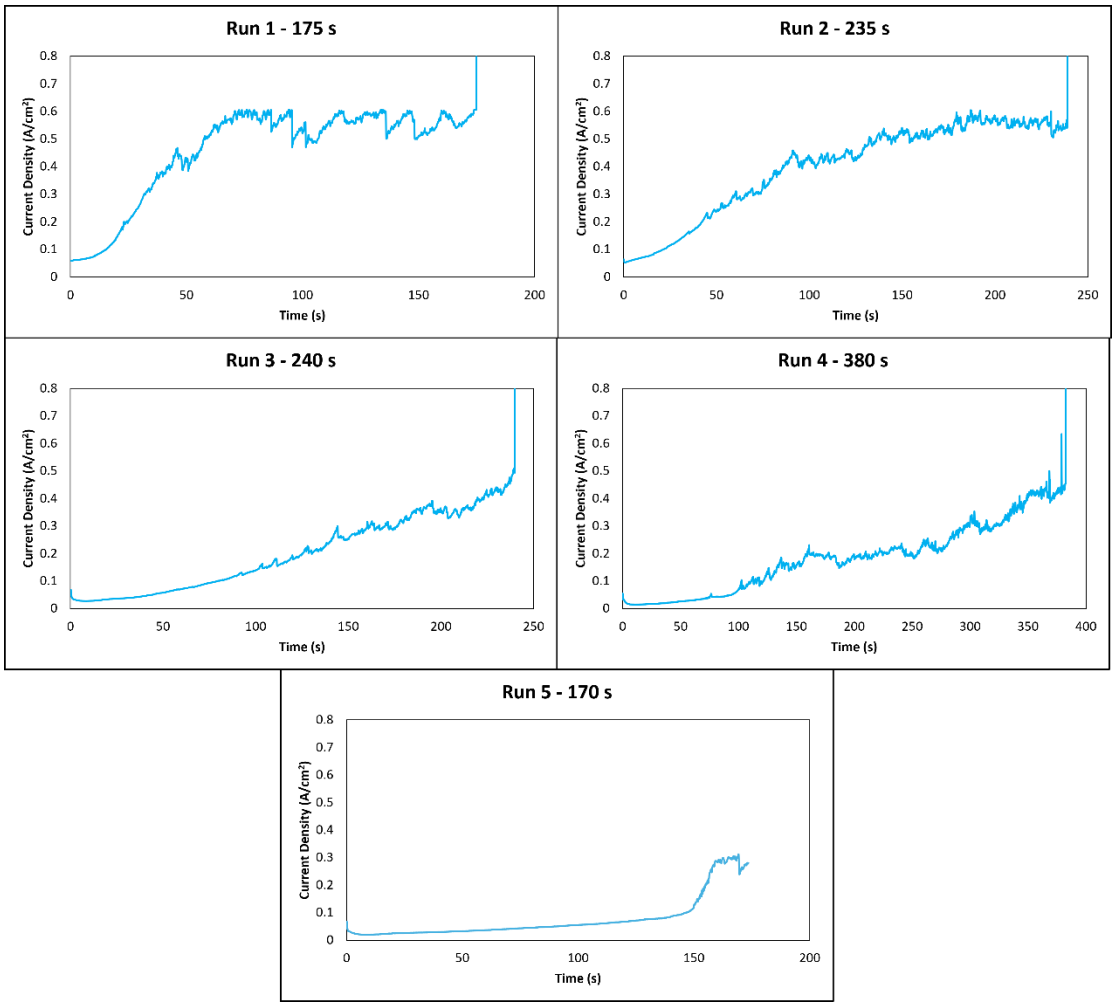


Figure 5.17 Current densities measurements during electropolishing C1

When a short circuit occurs, footprints of current overflow can form on the metal surface, as shown in Figure 5.19 (a), deteriorating the surface quality. Similarly, when the system operates under an extremely small inter-electrode gap for an extended period of time, localized temperatures might rise due to Joule heating, causing surface melting and creating surface tracks, as observed in Figure 5.19 (b). High localized current densities can also lead to pit formation on the channel surface, as illustrated in Figure Figure 5.19 (c).

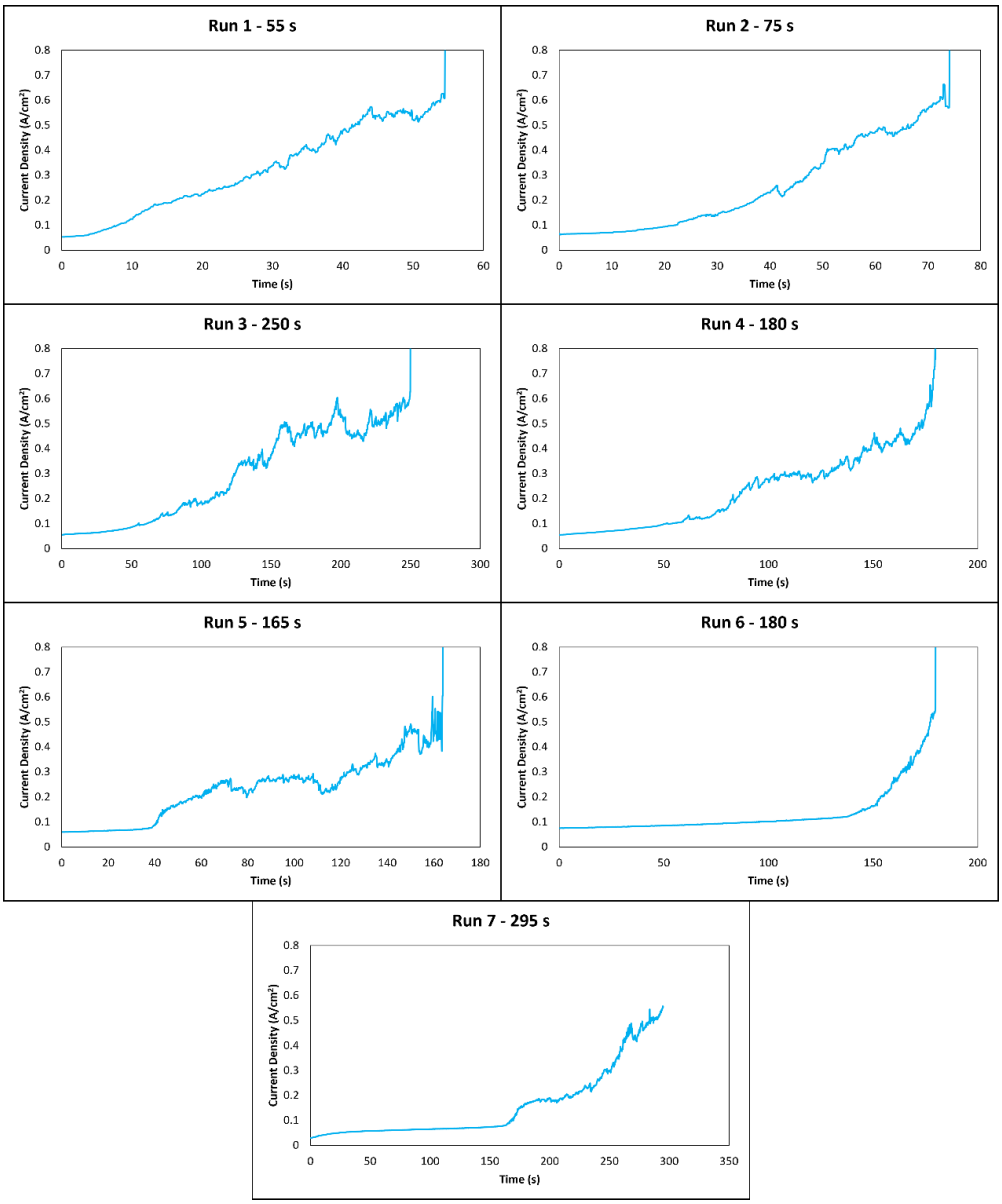


Figure 5.18 Current densities measurements during electropolishing C2

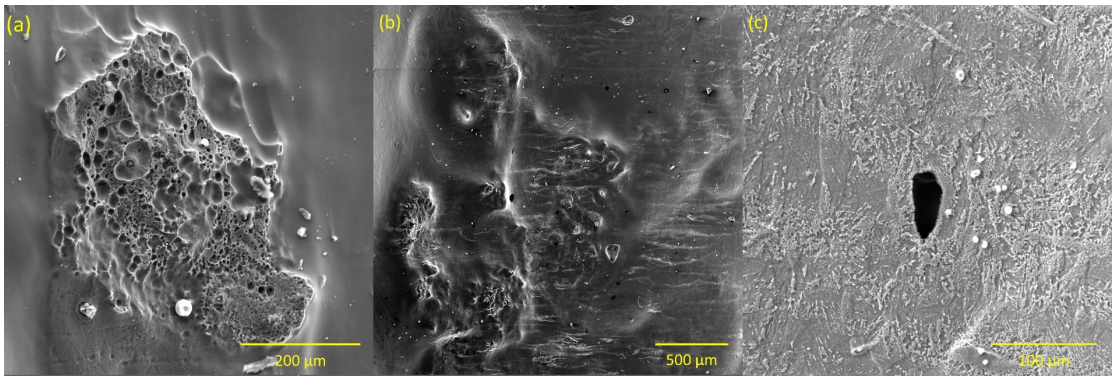


Figure 5.19 Surface defects due to (a) short circuit; (b) melting due to high localized temperature; (c) pit formation

5.3.6. Effect of Channel Curvatures

Due to the small channel size and the specific design of the wire covers, the relative rates of accumulation and removal of these conductive particles vary with the channel curvature, resulting in different current distributions and electrolyte flow qualities, which affect the electropolishing performance. When electropolishing the straight channel, the flow has the highest efficiency for removing reaction products because of the absence of turns and curves. In addition, with the SS316 wire and the polymeric covers inserted into the straight channel, the hard disks of the wire covers are evenly distributed along the flexible wire, since they do not need to bend or adapt to any curvature. On the other hand, the wire covers need to be bent and compressed for adapting to curvatures when electropolishing curved channels, leading to increased non-uniformity of the process.

Figure 5.20 exhibits the 3D profiles of electropolished surfaces for straight channel, and curved channels with the curved value of 0.04 and 0.08, along with the surface roughness values of the channels with the three curvatures. With the increase of the channel curvature, the average surface roughness value increases, and the non-uniformity of the surface quality also increases. The results presented in Figure 5.20 were achieved after an accumulation of electropolishing time of 20 minutes, with a few short circuits occurring during the process (the wire covers were taken out, cleaned and reinserted into the channel when the short circuit occurred). For the sample with the largest curvature (C3) shown in Figure 5.3, the electropolishing process failed in very short time period due to the lack of electrolyte flow for removing the conductive products, therefore the results for C3 were not presented here.

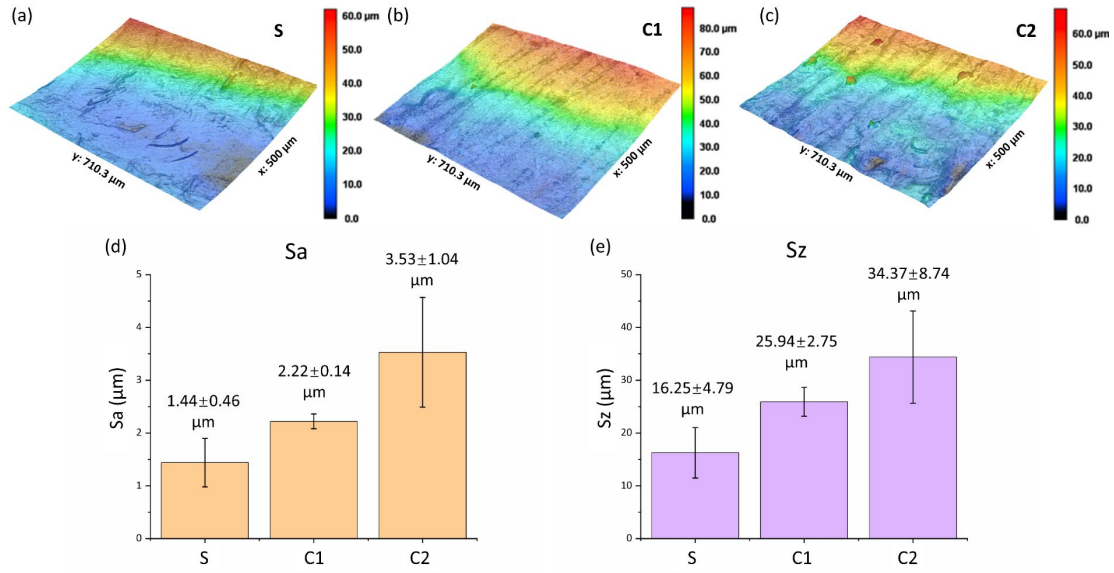


Figure 5.20 Effect of channel curvature on surface roughness after electropolishing for 20 minutes: (a-c) 3D surface profile of channels with different curvatures; (d-e) surface roughness values of electropolished surface

Due to the inherent complexity and stochastic nature of the process, such as the unpredictable positioning of the wire in the channel and the distribution of conductive reaction products, the resulting channel surface might not be uniformly polished. Figure 5.21 presents microscope images of the polished internal channels for two different curvatures (C1 and C2) after an accumulated electropolishing time of 20 min. The presence of the wire cover reduces the uniformity of the current density distribution, compared with the picture of the straight channel shown in Figure 5.22. The stress distribution in the SS316 wire makes it almost impossible to position the wire exactly along the centerline of the curved channel. In addition, the flexibility of the bridge material in the wire cover affects the gap between disks when the wire is inserted into the channel because of compression and bending of the wire cover. Furthermore, the accumulation and removal of conductive solid reaction products are also unpredictable. These factors collectively contribute to the non-uniformity of the surface after electropolishing.



Figure 5.21 Microscope images of electropolished (a) C1 and (b) C2

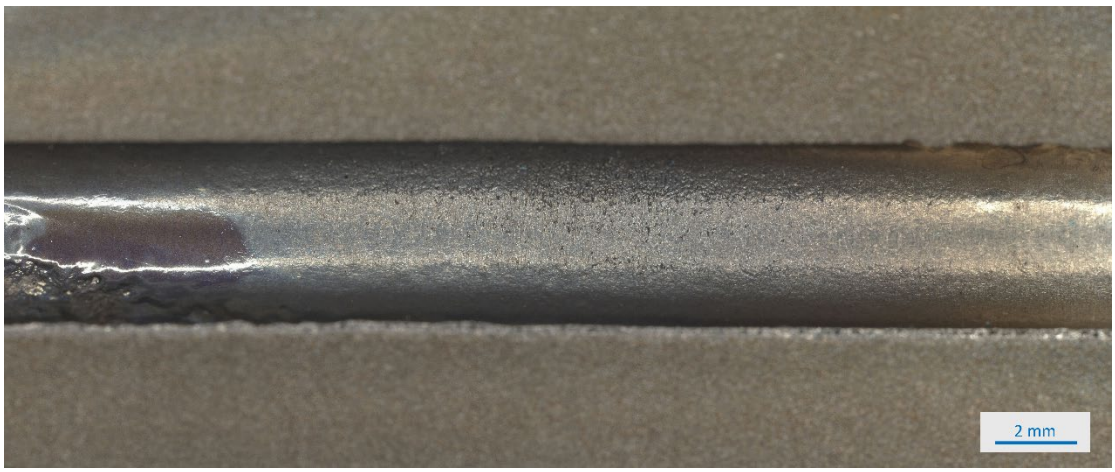


Figure 5.22 Microscope picture of the straight channel

SEM images in Figure 5.23 also show the non-uniformity of the electropolished surface due to channel curvatures. For both C1 and C2, there are less polished and more polished areas on the surface, where the Sa value for the more polished area is 1.30 ± 0.24 µm, while the Sa value of the less polished area is 5.11 ± 1.43 µm. Besides surface roughness reduction, a comparison made between the as-built sample and the polished sample shows a thickness reduction of 200 µm according to Figure 5.24.

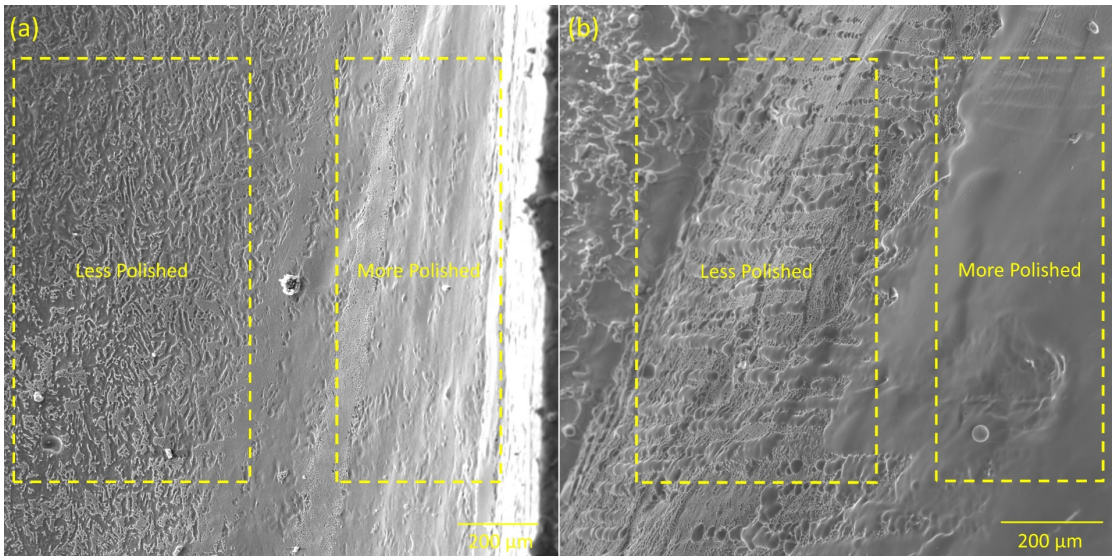


Figure 5.23 SEM images of non-uniformity of the polished channel surface for (a) C1 and (b) C2, with a Sa value of 1.30 ± 0.24 µm for the more polished areas and 5.11 ± 1.43 µm for the less polished areas

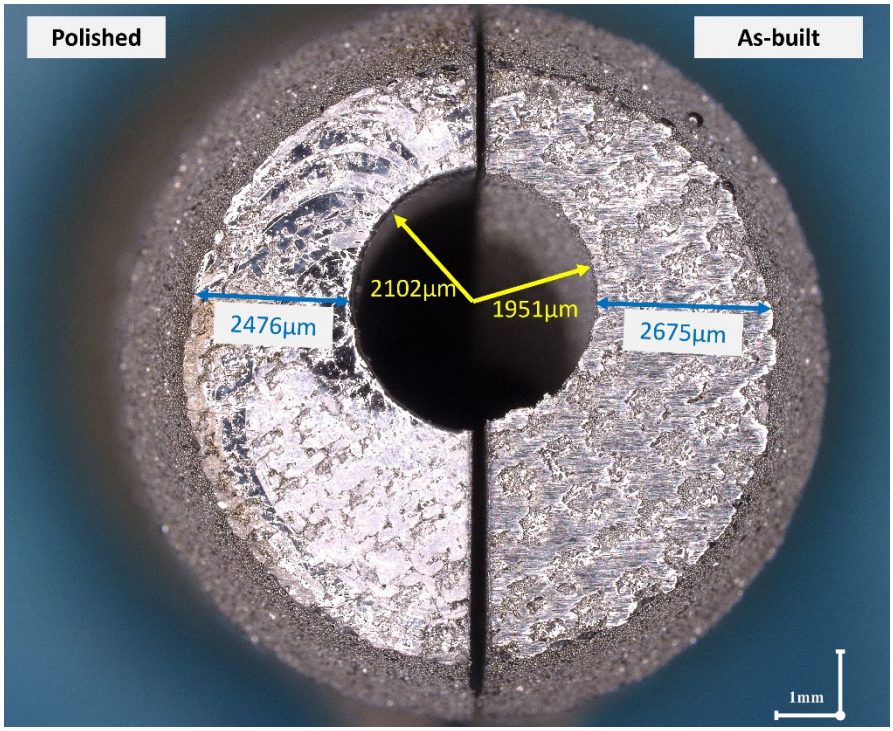


Figure 5.24 Comparison of polished and non-polished samples (image taken from C2)

5.3.7. Effect of Ultrasonic Vibration

In order to remove the conductive solid reaction products more effectively and prevent

the short circuit during the electropolishing process, a trial with ultrasonic vibration was conducted. However, for Ti6Al4V samples with carbon contaminants, the results are not promising. Without ultrasonic vibration, an accumulation time of 20 minutes leads to a noticeable reduction of surface roughness as discussed above. On the contrary, when applying ultrasonic vibration, intense localized heat generated via ultrasonic cavitation creates a large number of pits on the channel wall instead of polishing the surface, as shown in Figure 5.25. The results greatly differ from those presented in Chapter 4 due to two possible reasons. On the one hand, the relatively small inter-electrode gap between the wire electrode and the channel wall results in significant Joule heating, which increases the localized temperature, and this temperature further increases as a result of ultrasonic cavitation, leading to the formation of pitting corrosion. On the other hand, Ti6Al4V used in Chapter 4 is the pure alloy without any contamination, while the alloy used in this test is Ti6Al4V contaminated with carbon, thus the sonochemistry might be altered due to the composition change.

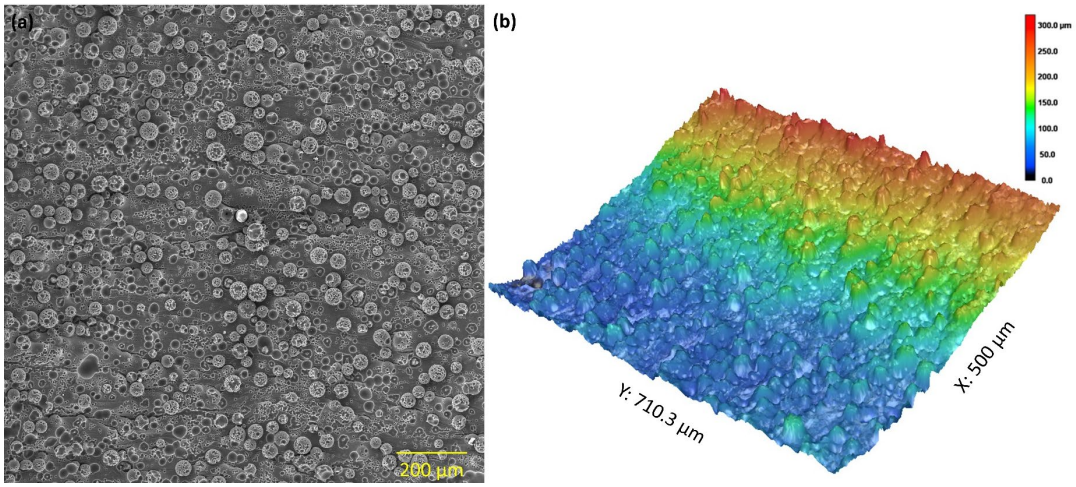


Figure 5.25 (a) SEM and (b) 3D profile of pitting formation at the channel wall under ultrasonic cavitation

5.4. Numerical Simulation for Design Optimization

5.4.1. Design Optimization and Model Description

As stated in the previous experimental sections, achieving a uniform surface finish via

the proposed method remains challenging due to the presence of wire covers, and the accumulation of conductive reaction products leading to short circuit behaviors. Therefore, it is crucial to design wire covers that ensure a more uniform current density distribution and facilitate the removal of the solid reaction products through an increased flow rate. The design of wire cover should be based on the structure that could maximize the opening area to promote uniform electrolyte flow within the internal channel. The size of components contained in the wire covers should be as small as possible so that electropolishing rate would not be reduced due to a decreased current density. Meanwhile, the component should be strong enough for maintaining the shape integrity during the electropolishing process. Due to the aforementioned criteria, a minimum structure thickness of 400μm has been selected. In addition to the design used in the experiments, two new designs have been developed, referred to as simple cubic (SC), centered cubic (CC) and hexagonal (H) respectively, as shown in Figure 5.26.

In order to compare the performance of the three wire covers, a numerical simulation was conducted using electrochemistry module and fluid dynamics module in COMSOL Multiphysics 6.2[78]. A corresponding 3D model was used for design optimization of wire covers. To achieve the balance between the modeling accuracy and the computational cost, some simplifications and some assumptions were considered:

(1) The model is based on a 3D geometry.

(2) Transport of ions and gas species, as well as the electrode kinetics during the electropolishing process are neglected. Primary current distribution considering the electrolyte resistance is used for the model.

(3) Laminar flow is assumed for the flow simulation.

(4) The polymeric cover and the wire are assumed to be stationary during the process. The shape of the channel, the wire and the cover remain unchanged throughout the whole process.

(5) Stationary analysis was performed to compare the performance of the three wire

covers.

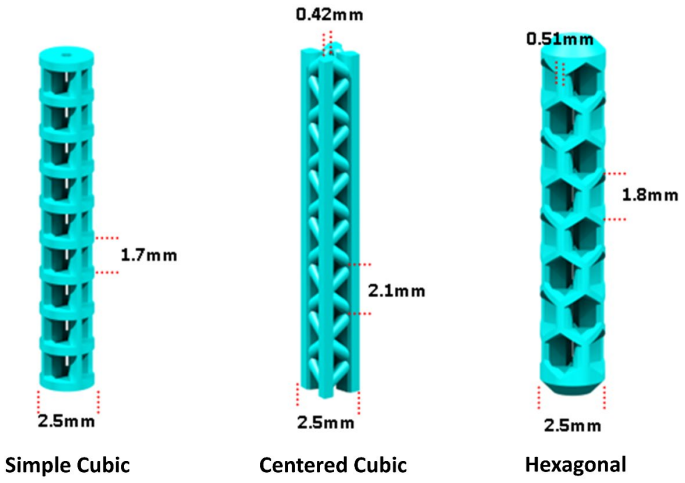


Figure 5.26 Three designs of wire covers

5.4.2. Governing Equations

For the current distribution simulation, a primary current distribution interface was selected, where the current density (j) equals the non-Faradaic current caused by electrolyte resistance ($j_{electrolyte}$), which follows Ohm's law:

$$j = j_{electrolyte} = -\sigma_{electrolyte}\nabla\phi_{electrolyte} \tag{5.1}$$

where $\sigma_{electrolyte}$ is the conductivity of the electrolyte, and $\phi_{electrolyte}$ stands for the electrolyte potential.

For the flow simulation, the Navier-Stokes equation was used as the governing equation including momentum conservation and mass conservation:

$$\rho\left[\frac{\partial \boldsymbol{u}}{\partial t} + \boldsymbol{u}\cdot(\nabla \boldsymbol{u})\right] = -\nabla p + \mu\nabla^2\boldsymbol{u} \tag{5.2}$$

$$\nabla\cdot\boldsymbol{u} = 0 \tag{5.3}$$

where, ρ is the density of the electrolyte, μ is the dynamic viscosity of the electrolyte, $\boldsymbol{u}$ is the velocity field of the flowing electrolyte, and p is the pressure.

5.4.3. Boundary Conditions and Mesh Independence Analysis

Current and flow distributions for internal channels were simulated using three wire

cover designs. In addition, the geometry with a bare wire inserted into the channel was also simulated as the current density reference. Figure 5.27 demonstrates the modeling geometry with boundary conditions for all the conditions. Parameters used in the simulation are listed in Table 5.3.

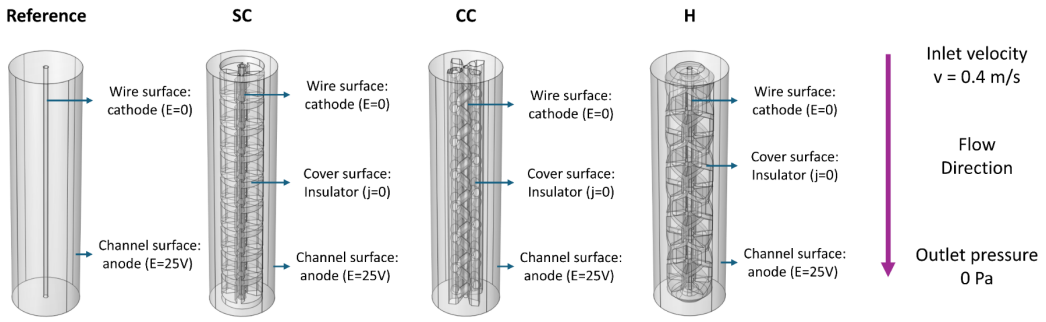


Figure 5.27 Geometries and boundary conditions using SC, CC and H for electropolishing internal channels

Table 5.3 Parameters Used for Numerical Simulation

Parameter Name	**Value**
Electrical Voltage	25 V
Electrolyte Conductivity	7 S/m
Fluid Density	789 kg/m^3
Fluid Dynamic Viscosity	2 mPa·s
Inlet Velocity	0.4 m/s

Physical-controlled mesh was used for the simulation. Mesh independence analysis was performed for all the three geometries. Average outlet velocity was used for the analysis. The mesh was selected when the %change for the outlet velocity is less than 1% after mesh refinement. Figure 5.28 provides detailed information about the mesh used in the study.

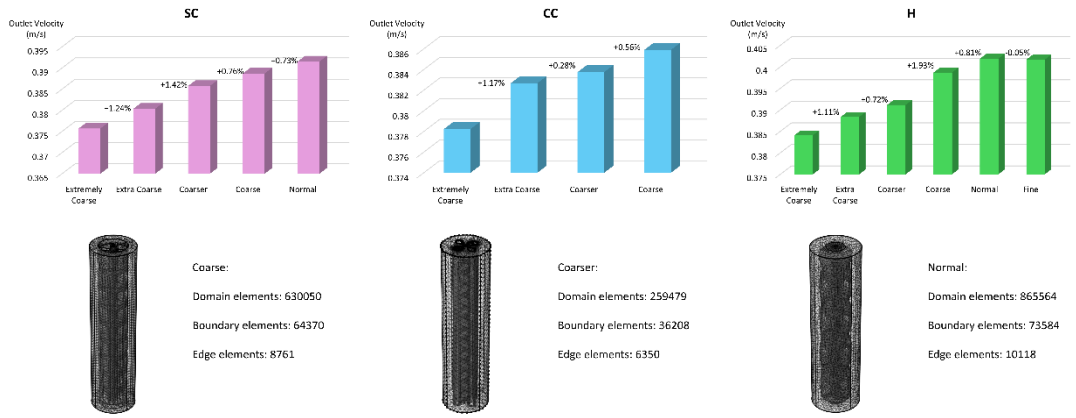


Figure 5.28 Mesh information for numerical modeling

5.4.4. Modeling and Optimization Results

For characterizing wire covers and selecting the best wire cover design, a set of optimization criteria has been created from the aspects of current density distribution and flow distribution.

In terms of current density distribution, a current density value computed using the reference geometry has been used as the reference current density. A normalized current density achieved by the ratio between the obtained current density with wire covers and the reference current density was used for computing current density distribution. The introduction of normalized current density accounts for the reduction of current density values due to the presence of wire covers. Therefore, the wire cover with the highest normalized current density should be selected, since the presence of the wire cover deteriorates the electropolishing performance the least. In spite of a higher normalized current density, the current density should have a uniform distribution to achieve a uniform surface finishing.

Besides current density distribution, it is also necessary to consider the flow distribution. As stated in the experimental sessions, the amount of flow is significant, since conductive solid reaction products need to be removed for preventing short circuit for the electropolishing process to continue. Therefore, another important criterion is that the flow in the areas inside the wire covers (i.e. the flow close to the wires) should be

as high as possible for particle removal.

Figure 18 presents the normalized current density distribution of the reference geometry and three geometries with wire covers. Compared with the completely uniform current density distribution achieved by the reference geometry, inserting all types of wire covers leads to the reduction of current density and the introduction of distribution non-uniformity. Wire covers SC and H result in higher current density values. In contrast, the current density distribution of inserting the wire cover CC is more uniform than inserting the other two covers.

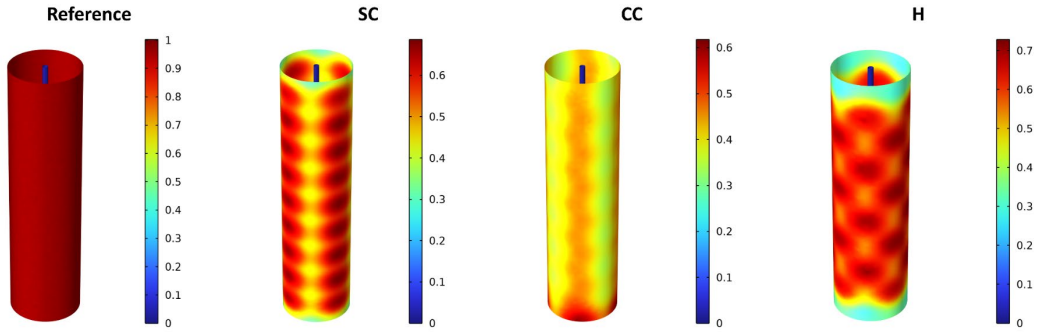


Figure 5.29 Normalized current density distributions for reference geometry, and channels with SC, CC and H

For further quantitating the normalized current density distributions, curves of normalized current density values are plotted along the length of the channels, as shown in Figure 5.30. For SC and H, 30% to 40% of the current density are reduced due to the insertion of the wire covers, while this value increases to more than 50% when inserting CC. Although normalized current densities for SC and H fluctuate around the same value (~0.6), the fluctuation amplitude for SC is slightly lower than that for H, indicating a slightly more uniform surface finishing performance. Compared with SC and H, inserting CC as the wire cover leads to a lower yet much more uniform current density distribution.

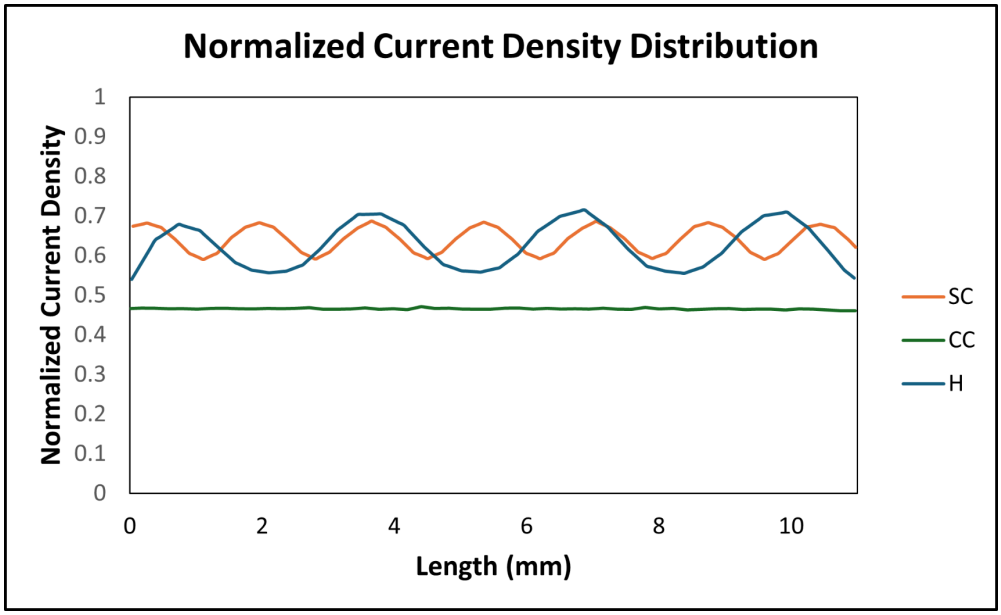


Figure 5.30 Normalized current density distribution along the channel length for SC, CC, and H

Figure 5.31 demonstrates the flow distribution of the cross section of the channels when inserting wire covers SC, CC and H. The figure clearly shows that for wire covers SC and H, there is a flow in the areas inside the wire covers close to the wire surface. However, for wire cover CC, there is almost zero flow in the corresponding region. The information provided by the figure indicates that the design of wire covers SC and H might help with removing the conductive particles, while there might be a higher chance for the short circuit event to happen when using the design of CC.

Similar to characterization of current density distribution, a flow distribution curve was also plotted to quantitating the flow velocity when using the three designed wire covers to make better comparisons. The data were achieved at the locations which have a 0.25 mm distance from the wire surface and were plotted as a function of the cylinder length, as shown in Figure 5.31. The wire cover H has the highest velocity inside the cover area, reaching 0.1 m/s, indicating the best performance for removing solid particles, followed by wire cover SC, which has a velocity value of 0.04 m/s. The velocity for inserting CC is less than 0.01 m/s, showing the worst flow behavior among the three designs.

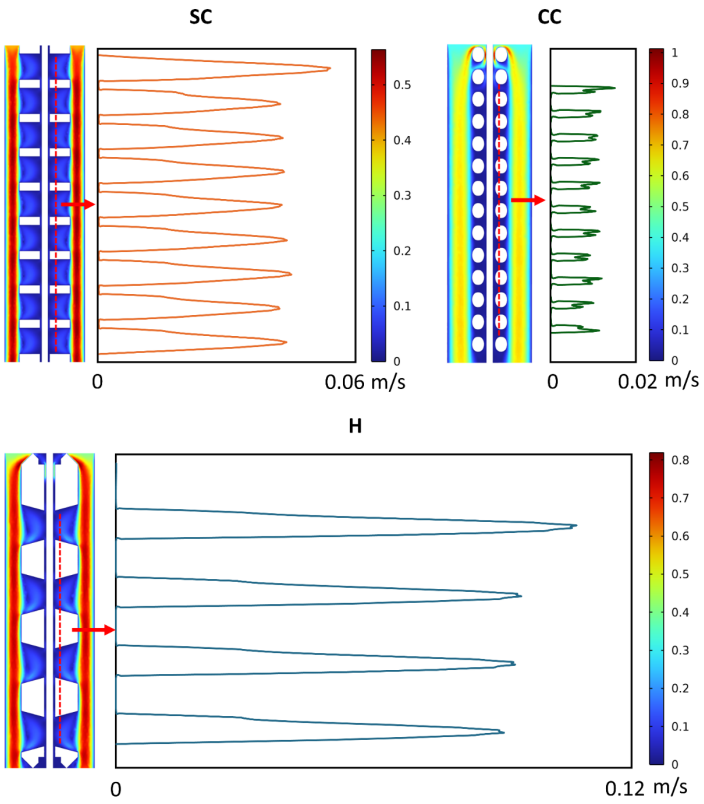


Figure 5.31 Flow velocity distributions for wire cover SC, CC and H (unit: m/s)

To summarize the discussions above, the three wire covers have their own advantages and disadvantages. In terms of general electropolishing efficiency, these wire covers can be ranked as SC≈H>CC. With reference to the uniformity of the electropolishing performance, the ranking would be changed to CC>SC>H. Furthermore, as for the flow behavior for particle removal, they can be ranked as H>SC>CC.

Besides the wire cover SC used in the reported experiments, attempts for fabricating the other two covers including H and CC have also been conducted, which raises a significant printing challenge for the proposed electropolishing methods with the current polymer printer – the lack of capability for printing small features, especially when printing flexible materials, and the deficiency in removing support materials from tiny pores. Therefore, in order for the proposed method to reach the maximized performance, polymer printers with higher resolution and printing capability for small features should be used.

5.5. Summary

In this work, a novel tool for electropolishing internal channels of additively manufactured metal parts was developed and fabricated with the assistance of polymer 3D printing. The specially designed and printed polymeric wire cover was assembled with flexible SS316 wire. The whole assembly functioned as the cathodic electrode for electropolishing both straight channels and curved channels with different curvatures. Preliminary experimental results demonstrate promising performance of the novel method, achieving a maximum surface roughness *Sa* reduction from 10.86 ± 0.50 μm to 1.44 ± 0.46 μm. This technique introduces a non-destructive polishing method for finishing the surfaces of conformal channels. Future work to enhance surface finishing includes continuing optimizing the wire cover design and using higher-resolution polymer printers to apply the process to smaller channels.

6. Methods on Improving Sustainability for Surface Finishing of Additively Manufactured Metal Parts

6.1. Chapter Overview

In this chapter, two methods for improving the sustainability of surface finishing are proposed: 1) the development of green electrolytes for electropolishing; and, 2) the use of shear thickening polishing. The electropolishing performance is evaluated in deep eutectic solvents and alcohol-salt systems, demonstrating effective surface roughness reduction in both types of electrolytes. On the contrary, while shear thickening polishing is capable of removing materials from surfaces with low initial roughness, it proves challenging to use this method to reduce the surface roughness for AM surfaces with meso-/macro- initial surface roughness. Figure 6.1 provides the graphical overview for Chapter 6.

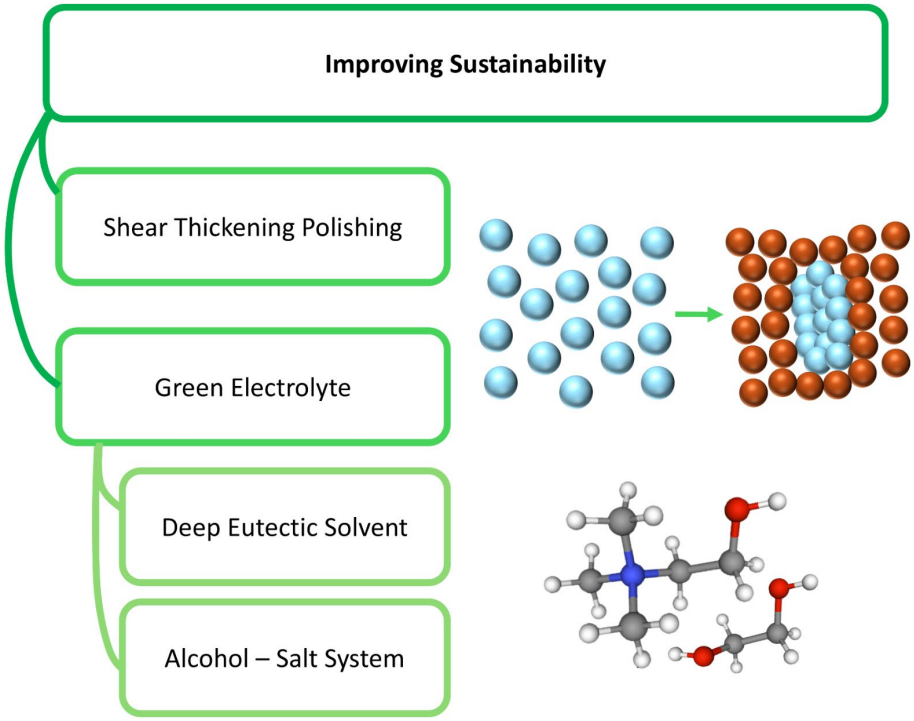


Figure 6.1 Graphical overview for Chapter 6

6.2. Electropolishing Using Green Electrolytes

6.2.1. Introduction and Working Principle

Although electropolishing is an effective approach for reducing surface roughness for additively manufactured metal parts, the acidic electrolytes commonly used in the process pose significant safety risks to operators as well as environmental hazards if not disposed of properly. Therefore, to improve the sustainability of the process, it is necessary to develop green electrolyte with a neutral pH. So far, two different routes have been developed for designing green electrolytes, including deep eutectic solvents (DESs) and alcohol-based electrolytes.

Deep eutectic solvents (DESs) are considered a new class of ionic liquids (ILs) representing salts in the liquid state. DESs are material systems containing a eutectic mixture of Lewis or Brønsted acids and bases, in which various anionic and/or cationic species contribute to their high ionic conductivity. The complex hydrogen bonding network in DESs leads to significant depression of the freezing point (typically lower than room temperature) compared with the parent compounds. The applications of DESs were focused on metal processing and material synthesis. Some electropolishing work has been done in DESs and promising results have been achieved [97]. Compared with traditional aqueous electrolyte, which is highly toxic and corrosive, DESs are benign and non-corrosive. Besides, during the electropolishing process, there will be negligible gas evolution on the anodic workpiece, which improves the current efficiency of the process.

Alcohol-based electrolytes refer to the mixture of alcohol and inorganic salts. The hydroxyl group (-OH) in alcohols can form hydrogen bonds with ions from the dissolved salt, which helps stabilize ionic species in the electrolyte and enhance the ionic mobility. Several alcohol-salt systems have been proposed till now, including ethanol-isopropanol-zinc chloride-aluminum chloride [98], ethylene glycol-lithium chloride [99], ethylene glycol-sodium chloride [99].

Since metal surface produced via AM possesses unique features compared with conventional manufacturing, it is necessary to test the electropolishing performance of these green electrolytes on the AM-made surfaces.

6.2.2. Experiments

The Ti6Al4V coupons fabricated via LPBF were used for electropolishing process. The samples' fabrication and preparation procedure were stated in Section 4.2.1. The initial surface roughness (*Sa*) for the as-built surface was 11.50 ± 0.81 μm. To investigate the electropolishing performance of the aforementioned green electrolytes, two electrolyte solutions were prepared. The first electrolyte is a type of DESs, containing choline chloride and ethylene glycol in a molar ratio of 1:2. The second electrolyte is the mixture of ethylene glycol and sodium chloride, with the salt concentration of 1 mol/L. Heat was applied while mixing two solutions.

Before electropolishing test, current-voltage curves of both electrolytes were obtained by recording the current while sweeping the voltage to determine the best working voltage for electropolishing in the selected material system. Electropolishing tests were conducted with a constant inter-electrode gap of 5 mm for both electrolytes. Electropolishing voltages were selected based on the polarization curves.

6.2.3. Results and Discussions

When mixing choline chloride and ethylene glycol for making the DES, the process absorbs a large amount of heat, causing a significant reduction of the temperature of the solution, which makes the solution to freeze at room temperature. Figure 6.2 shows the camera pictures of the solution at room temperature (20 ºC) and at 30 ºC.

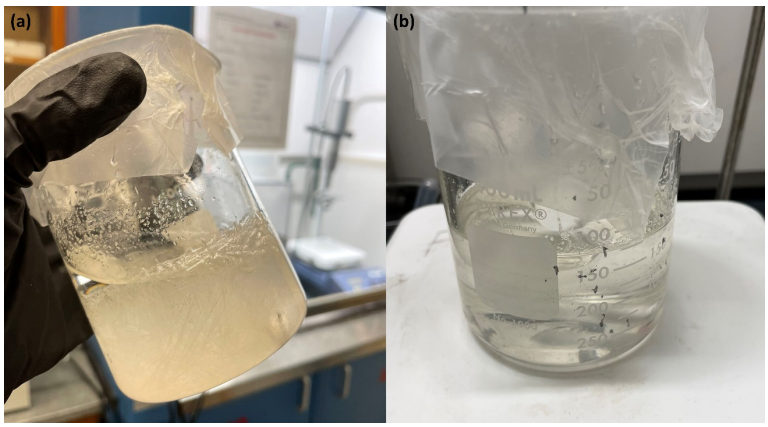


Figure 6.2 Camera picture of the DES at (a) 20 ºC and (b) 30 ºC

The voltage-current curve obtained for the choline chloride – ethylene glycol electrolyte mixture is shown in Figure 6.3. It can be clearly seen that the optimal working voltage for electropolishing Ti6Al4V in the DES electrolyte is in the range of 20 - 25V. Therefore, 22 V was selected as the working voltage. Electropolishing of the Ti6Al4V coupon was conducted at 30 ºC for 40 min, with an applied voltage of 22 V and inter-electrode distance of 5 mm. Figure 6.4 displays the surface profile after the electropolishing test. Surface roughness *Sa* reduces from 11.50 ± 0.81 µm to 2.86 ± 0.36 µm after the electropolishing test.

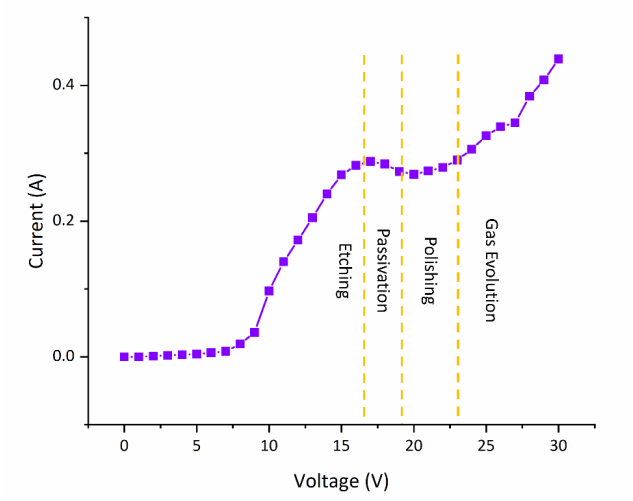


Figure 6.3 Voltage - current curve for DES electrolyte

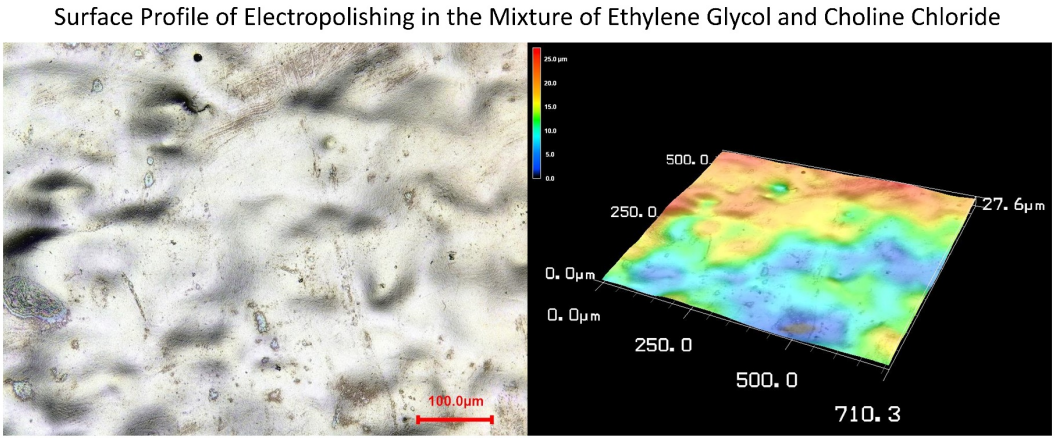


Figure 6.4 Optical image and surface profile after electropolishing in DES electrolyte

Another electropolishing attempt was conducted in the mixture of ethylene glycol and sodium chloride. Figure 6.5 shows the voltage - current curve tested in the electrolyte. Although the plateau region is not as obvious as the one in Figure 6.3, the slope of the curve slows down at around 20 V. Therefore, 20 V was selected as the electropolishing voltage for this test. Electropolishing of the printed coupon for this material system was conducted at room temperature, for 40 min, with an applied voltage of 20 V and inter-electrode distance of 5 mm. Figure 6.6 demonstrates the surface profile after the electropolishing test. Surface roughness *Sa* reduces from 11.50 ± 0.81 μm to 1.88 ± 0.63 μm after the electropolishing test.

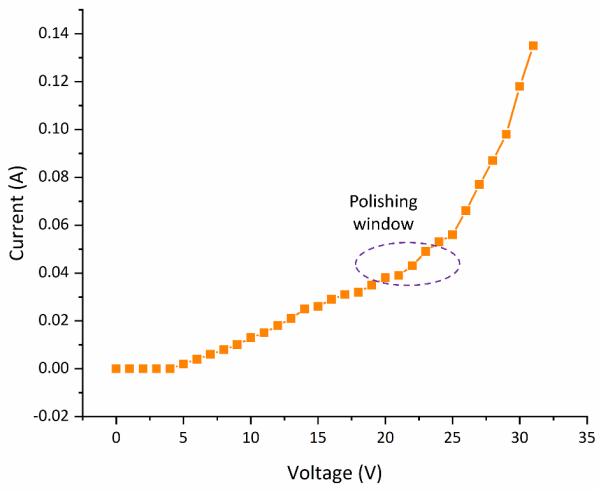


Figure 6.5 Voltage - current curve for alcohol - salt electrolyte

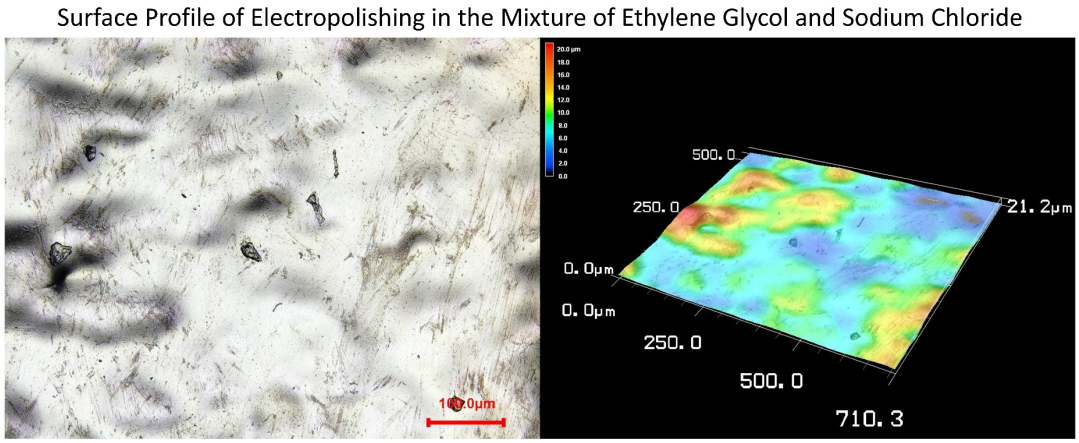


Figure 6.6 Optical image and surface profile after electropolishing in alcohol - salt electrolyte

According to the results above, both electrolytes show promising performance on reducing surface roughness of the metal parts manufactured via AM. However, although partially sintered powders and surface irregularities due to balling effect have been effectively removed, remaining surface waviness after 40 min is still significant compared to electropolishing results presented in Chapter 4. Therefore, for improving surface quality after electropolishing in the proposed green electrolytes, process optimization needs to be done, and proper additives need to be found to modify the electrolytes for improving the uniformity of the electrochemical reaction.

6.3. Shear Thickening Polishing

6.3.1. Introduction and Working Principle

Shear thickening fluid is a type of non-Newtonian fluid, in which viscosity increases when shear stress is applied. Based on the shear thickening mechanism, a shear thickening polishing (STP) method was proposed in [100]. Figure 6.7 (a) [100] is the schematic demonstration of shear thickening mechanism. At low shear stress, shear thickening fluid behaves like a Newtonian fluid which has a low viscosity and good flowability. However, at high shear stress, the viscosity of the fluid increases rapidly, which may even lead to the solid-like behavior of the fluid.

A typical shear thickening fluid contains abrasive particles, multi-hydroxyl polymer

and dispersant, and it is the main influencing factor that influences polishing performance. Figure 6.7 (b) [100] shows the mechanism of the shear thickening polishing process. Without any shear thickening effect, abrasive particles, dispersed evenly in the slurry, will not generate any cutting effect to the chips on the surface due to the lack of enough kinetic energy of the abrasive particles. Shear thickening effect occurs in the contact area when the shear stress exceeds the critical value. Under the circumstances, the shear thickening fluid in the contact area starts to show solid-like behavior and enough force could be provided for cutting by forming an aggregation of particle clusters, where abrasive particles are surrounded by multi-hydroxyl polymeric colloidal particles.

Shear thickening polishing is a fairly new surface polishing concept, and no trials have ever been reported on metal AM parts. Since shear thickening effect has the potential to increase the efficiency of abrasive cutting performance in the fluid, while not needing any tools with special shapes to generate the effect. The STP might be a promising candidate to improve the surface quality for parts with complex geometries.

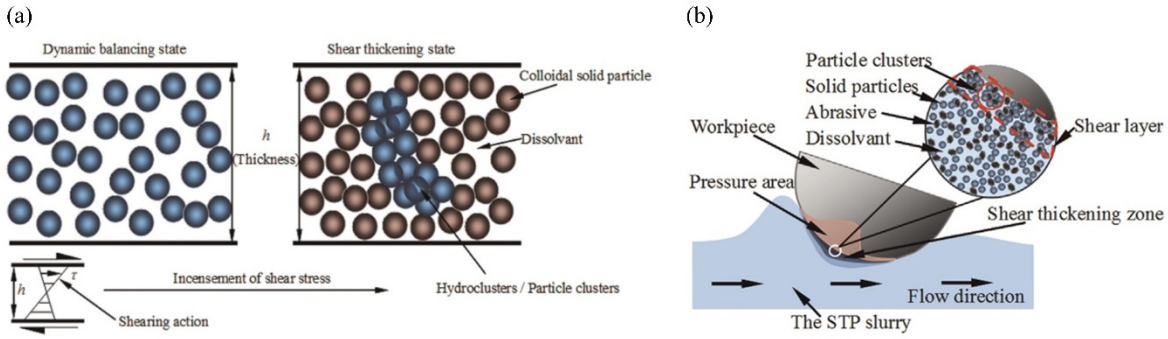


Figure 6.7 (a) Physical mechanism; (b) process mechanism for STP (reused with permission of Elsevier from [100])

6.3.2. Experiments

Corn starch - water mixture is the most commonly known shear thickening fluid. Due to its non-toxic nature and its excellent shear thickening property, it was selected as the polishing fluid in the polishing test. Figure 6.8 [101] demonstrates the rheological

properties of corn starch - water slurry at different concentrations. For all the concentrations under 56%, both shear stress and effective viscosity increase significantly with increasing shear rate. Thus, for the shear thickening polishing process, a slurry mixture containing 52.5wt% of cornstarch (~40% in volume), 5wt% of SiC with the average particle size of 10 μm and 42.5wt% of water was prepared.

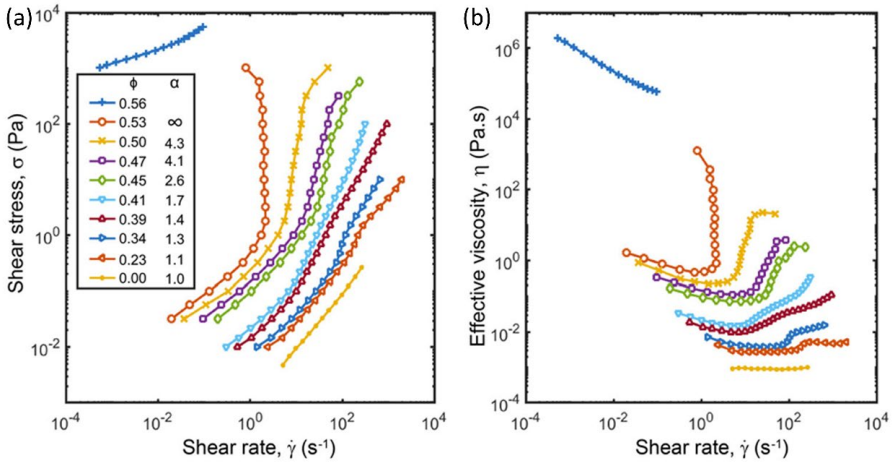


Figure 6.8 (a) Shear stress and (b) effective viscosity at different shear rate for corn starch at different volumetric concentrations (reused under the Creative Commons CC-BY license from [101])

Ti6Al4V cylinders and half-rods was fabricated via LPBF for the shear thickening polishing treatment. The initial surface roughness was measured before the treatment so that the surface roughness reduction due to the treatment could be studied. For creating the shearing motion, the rotation of an electrical drill was used. The sample was fixed to the drill at the hole for holding the drill bit. Lab clamps was used for fixing the drill button for keeping the rotation speed constant at 1500 rpm. The distance between the sample bottom and the beaker was kept constant at 3 mm. Figure 6.9 shows the picture of the experimental setup. Shear thickening polishing test was conducted for different time, and surface profile after polishing was taken and compared.

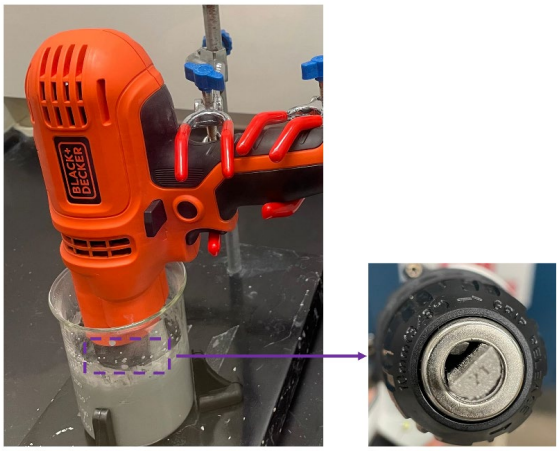


Figure 6.9 Experimental setup for shear thickening polishing

6.3.3. Results and Discussions

Shear thickening polishing was tried on surfaces with low roughness values at first. The surface was the top surface after laser remelting with an initial *Sa* value of 4 μm. After conducting shear thickening polishing on the surface for 30 min, a completely smooth surface was achieved with an average *Sa* value of 1 μm, as shown in Figure 6.10.

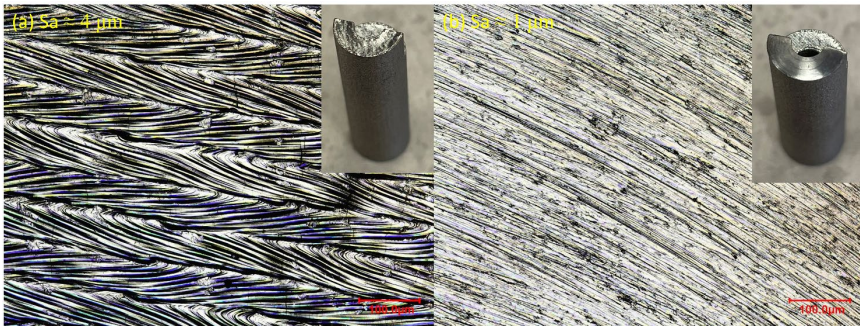


Figure 6.10 (a) Surface after laser melting, and (b) surface after STP

Then the process was conducted on surfaces with a relatively high initial surface roughness, with a Sa value of 17 μm. Figure 6.11 shows the 3D profile of the as-built surface. Compared to the side surface, the bottom surface was more polished due to the closer distance between the sample and the container wall. The polishing starts from the corner of the sample surface, as shown from the surface images after polishing for 30 min in Figure 6.12 (a). The surface profile in Figure 6.12 (b) was achieved after polishing for 60 min, indicating that the polishing behavior propagates to the center

gradually. The average Sa value for the polished surface after 30 min is around 3 μm, while the same value for polishing after 60 min is around 1 μm. Evidence shows that the polishing behavior also happened at the side surface, as shown in Figure 6.12 (c).

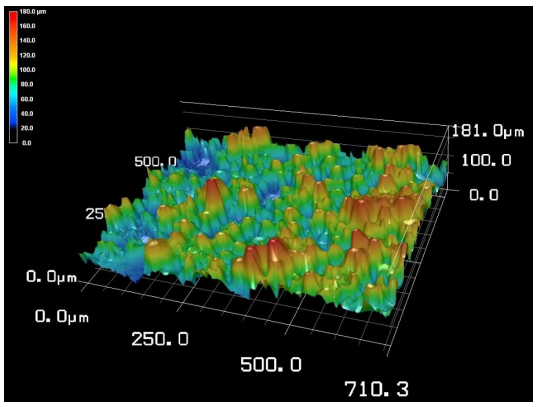


Figure 6.11 3D profile of the as-built surface for shear thickening polishing

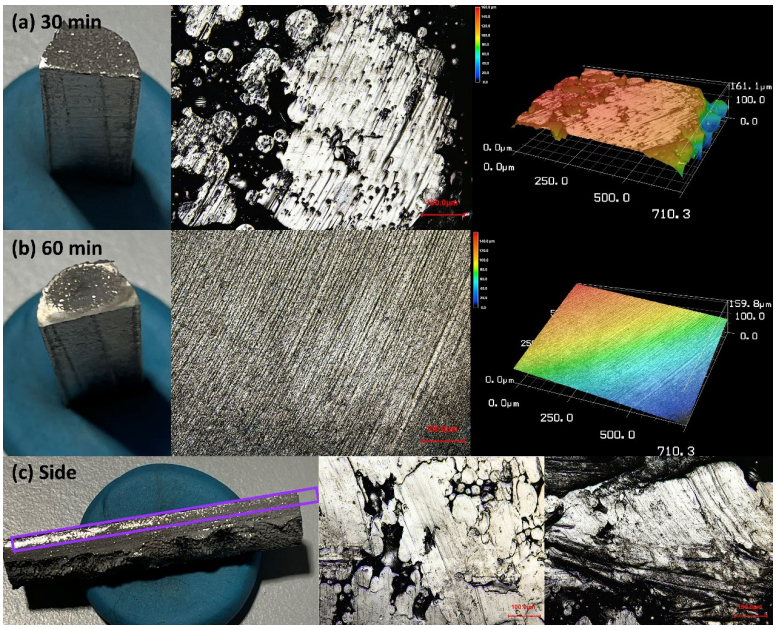


Figure 6.12 Surface profile after STP for (a) 30 min, (b) 60 min and (c) side surface

Although the approach shows promise for reducing surface roughness, the results lack repeatability due to the highly sensitive nature of the experimental conditions. Even minor variations in the experimental setup may lead to significant differences in polishing performance. Several factors influence the polishing outcomes, including the distance between the sample and the container wall, rotation speed, concentration of the shear thickening slurry, abrasive size and concentration, length of the sample in the

slurry, angle between the sample and the container wall, amount of the slurry, etc. Any changes to these parameters alter the flow conditions within the container, which subsequently impacts polishing performance.

6.4. Summary

A surface roughness reduction from ~11 μm to ~2 μm has been achieved via electropolishing in deep eutectic solvents and alcohol-salt systems. Replacing the commonly used acidic electrolyte with the tested electrolyte in the project might improve the sustainability of the electropolishing process significantly. Shear thickening polishing is also tested on additively manufactured cylinders. Although surface roughness has been reduced to some extent, the process lacks repeatability and is not suitable for parts with high surface roughness.

7. Conclusions and Future Work

7.1. Conclusions

In this thesis, surface finishing techniques for reducing surface roughness of additively manufactured metal parts were developed. First, both analytical and numerical models were developed for surface finishing techniques to account for the process mechanisms. Then, a hybrid technique including electropolishing and ultrasonic abrasive finishing were developed. Experimental results show that the hybrid process effectively reduces surface waviness compared to standalone electropolishing. Following that, an innovative electropolishing technique incorporating polymer 3D printing is developed for internal channels with varying curvatures. Finally, methods for improving sustainability of surface finishing processes were tested, including developing green electrolytes for electropolishing and shear thickening polishing techniques.

From the modeling and experimental work presented in the thesis, some conclusions can be drawn, which could serve as the basis for conducting future work in this field.

(1) Electropolishing has the capability for reducing surface roughness of metal parts but is best suited for simple geometries and external surfaces without modifications and improvements of the process. Surface roughness can be reduced from 11.50 ± 0.81 μm to 1.36 ± 0.21 μm after proper process optimization.

(2) The combination of ultrasonic cavitation abrasive finishing and electropolishing has the capability to reduce the surface waviness compared with pure electropolishing. The surface waviness after hybrid finishing is 40% less than that after sole electropolishing.

(3) The introduction of polymer 3D printing provides a promising solution for electropolishing internal channels of additively manufactured metal parts. The proposed method has the capability of adapting to different curvatures while reducing the surface roughness from 10.86 ± 0.50 μm to 1.44 ± 0.46 μm.

(4) A completely green and sustainable electropolishing process is possible owing to the development of deep eutectic solvents and alcohol-salt electrolytes. Surface

roughness can be reduced to 2 μm after electropolishing in these electrolytes.

(5) Shear thickening polishing can reduce the surface roughness to some extent (from 4 μm to 1 μm); however, it does not work well with surfaces with high initial roughness and the process repeatability is low.

7.2. Recommendations and Future Work

In order to improve the surface finishing process efficiency and the surface quality of the polished surface, a few recommendations are proposed here.

(1) For the hybrid process, process optimization needs to be done via optimizing abrasive particle type and size, modifying ultrasound power and frequency, as well as controlling the bath temperature to compensate for the large amount of heat generation during ultrasonic cavitation.

(2) For electropolishing internal channels, the design of the printed polymeric cover needs to be optimized to solve the short-circuited problem. Meanwhile, the polymeric cover needs to be printed with printers with higher resolution for adopting the technique to internal channels with less channel sizes.

(3) Non-corrosive non-toxic green electrolytes need to be developed for extensive material to improve the sustainability of the electropolishing process.

(4) Surface finishing mechanisms need to be further explored for inventing and designing more suitable techniques for reducing surface roughness and surface waviness at the same time.

Letter of Copyright Permission

Figure 2.1



Laser powder bed fusion for metal additive manufacturing: perspectives on recent developments

Author: S. L. Sing, W. Y. Yeong, Yeong W. Y., et al
Publication: Virtual & Physical Prototyping
Publisher: Taylor & Francis
Date: Jun 25, 2020

Rights managed by Taylor & Francis

Taylor & Francis
Taylor & Francis Group

Thesis/Dissertation Reuse Request

Taylor & Francis is pleased to offer reuses of its content for a thesis or dissertation free of charge contingent on resubmission of permission request if work is published.

BACK CLOSE

Figure 2.3 (e-g)



License Number	5925530439517
License date	Dec 10, 2024

Printable Details

Licensed Content

Licensed Content Publisher	Elsevier
Licensed Content Publication	Materials & Design (1980-2015)
Licensed Content Title	Balling phenomena in direct laser sintering of stainless steel powder: Metallurgical mechanisms and control methods
Licensed Content Author	Dongdong Gu,Yifu Shen
Licensed Content Date	Sep 1, 2009
Licensed Content Volume	30
Licensed Content Issue	8
Licensed Content Pages	8

Order Details

Type of Use	reuse in a thesis/dissertation
Portion	figures/tables/illustrations
Number of figures/tables/illustrations	3
Format	electronic
Are you the author of this Elsevier article?	No
Will you be translating?	No

About Your Work

Title of new work	Novel Surface Finishing Techniques for Additively Manufactured Metal Parts
Institution name	University of Waterloo
Expected presentation date	Mar 2025

Additional Data

Portions	Figure 6a, Figure 7a, Figure 8
The Requesting Person / Organization to Appear on the License	Manyou Sun

Figure 2.4 (a)



License Number	5925530940131
License date	Dec 10, 2024

Printable Details

Licensed Content

Licensed Content Publisher	Elsevier
Licensed Content Publication	Measurement
Licensed Content Title	3-Dimensional profile distortion measured by stylus type surface profilometer
Licensed Content Author	Dong-Hyeok Lee
Licensed Content Date	Jan 1, 2013
Licensed Content Volume	46
Licensed Content Issue	1
Licensed Content Pages	12

Order Details

Type of Use	reuse in a thesis/dissertation
Portion	figures/tables/illustrations
Number of figures/tables/illustrations	1
Format	electronic
Are you the author of this Elsevier article?	No
Will you be translating?	No

About Your Work

Title of new work	Novel Surface Finishing Techniques for Additively Manufactured Metal Parts
Institution name	University of Waterloo
Expected presentation date	Mar 2025

Additional Data

Portions	Figure 1
The Requesting Person / Organization to Appear on the License	Manyou Sun

Figure 2.5 (a)

License Number	5925531303266
License date	Dec 10, 2024

Printable Details

Licensed Content

Licensed Content Publisher	Elsevier
Licensed Content Publication	Journal of Materials Processing Technology
Licensed Content Title	Prediction and compensation of material removal for abrasive flow machining of additively manufactured metal components
Licensed Content Author	C.W. Kum,C.H. Wu,S. Wan,C.W. Kang
Licensed Content Date	Aug 1, 2020
Licensed Content Volume	282
Licensed Content Issue	n/a
Licensed Content Pages	1

Order Details

Type of Use	reuse in a thesis/dissertation
Portion	figures/tables/illustrations
Number of figures/tables/illustrations	1
Format	electronic
Are you the author of this Elsevier article?	No
Will you be translating?	No

About Your Work

Title of new work	Novel Surface Finishing Techniques for Additively Manufactured Metal Parts
Institution name	University of Waterloo
Expected presentation date	Mar 2025

Additional Data

Portions	Figure 1
The Requesting Person / Organization to Appear on the License	Manyou Sun

Figure 2.5(f,g)

Taylor & Francis
Taylor & Francis Group

Electromagnetic performance of Ti6Al4V and AlSi7Mg0.6 waveguides with laser beam melting (LBM) produced and abrasive flow machining (AFM) finished internal surfaces

Author: Mathieu François, Sangil Han, Frédéric Segonds, et al
Publication: Journal of Electromagnetic Waves and Applications
Publisher: Taylor & Francis
Date: Jul 21, 2021

Rights managed by Taylor & Francis

Thesis/Dissertation Reuse Request

Taylor & Francis is pleased to offer reuses of its content for a thesis or dissertation free of charge contingent on resubmission of permission request if work is published.

BACK CLOSE

Figure 2.6 (b-c)

License Number	5925551219331
License date	Dec 10, 2024

Printable Details

Licensed Content

Licensed Content Publisher	Springer Nature
Licensed Content Publication	The International Journal of Advanced Manufacturing Technology
Licensed Content Title	Investigation and process optimization for magnetic abrasive finishing additive manufacturing samples with different forming angles
Licensed Content Author	Peixin Zhu et al
Licensed Content Date	Sep 28, 2021

Order Details

Type of Use	Thesis/Dissertation
Requestor Type	academic/university or research institute
Format	electronic
Portion	figures/tables/illustrations
Number of figures/tables/illustrations	2
Will you be translating?	no
Circulation/distribution	500 - 999
Author of this Springer Nature content	no

About Your Work

Title of new work	Novel Surface Finishing Techniques for Additively Manufactured Metal Parts
Institution name	University of Waterloo
Expected presentation date	Mar 2025

Additional Data

Portions	Figure 12, Figure 14
The Requesting Person / Organization to Appear on the License	Manyou Sun

Figure 2.7 (a)

License Number	5925551403204
License date	Dec 10, 2024

Printable Details

Licensed Content

Licensed Content Publisher	Elsevier
Licensed Content Publication	Additive Manufacturing
Licensed Content Title	Surface finishing on IN625 additively manufactured surfaces by combined ultrasonic cavitation and abrasion
Licensed Content Author	K.L. Tan,S.H. Yeo
Licensed Content Date	Jan 1, 2020
Licensed Content Volume	31
Licensed Content Issue	n/a
Licensed Content Pages	1

Order Details

Type of Use	reuse in a thesis/dissertation
Portion	figures/tables/illustrations
Number of figures/tables/illustrations	1
Format	electronic
Are you the author of this Elsevier article?	No
Will you be translating?	No

About Your Work

Title of new work	Novel Surface Finishing Techniques for Additively Manufactured Metal Parts
Institution name	University of Waterloo
Expected presentation date	Mar 2025

Additional Data

Portions	Figure 3
The Requesting Person / Organization to Appear on the License	Manyou Sun

Figure 2.7 (b)

License Number	5925560048218
License date	Dec 10, 2024

Printable Details

Licensed Content

Licensed Content Publisher	Elsevier
Licensed Content Publication	Journal of Materials Processing Technology
Licensed Content Title	Multiphase hydrodynamic flow finishing for surface integrity enhancement of additive manufactured internal channels
Licensed Content Author	Arun Prasanth Nagalingam,Hemanth Kumar Yuvaraj,Vijay Santhanam,S.H. Yeo
Licensed Content Date	Sep 1, 2020
Licensed Content Volume	283
Licensed Content Issue	n/a
Licensed Content Pages	1

Order Details

Type of Use	reuse in a thesis/dissertation
Portion	figures/tables/illustrations
Number of figures/tables/illustrations	1
Format	electronic
Are you the author of this Elsevier article?	No
Will you be translating?	No

About Your Work

Title of new work	Novel Surface Finishing Techniques for Additively Manufactured Metal Parts
Institution name	University of Waterloo
Expected presentation date	Mar 2025

Additional Data

Portions	Figure 4
The Requesting Person / Organization to Appear on the License	Manyou Sun

Figure 2.8 (a)

License Number	5925560378502
License date	Dec 10, 2024

Printable Details

Licensed Content

Licensed Content Publisher	Springer Nature
Licensed Content Publication	Archives of Civil & Mechanical Engineering
Licensed Content Title	Chemical polishing of scaffolds made of Ti-6Al-7Nb alloy by additive manufacturing
Licensed Content Author	E. Łyczkowska et al
Licensed Content Date	Apr 5, 2014

Order Details

Type of Use	Thesis/Dissertation
Requestor Type	academic/university or research institute
Format	electronic
Portion	figures/tables/illustrations
Number of figures/tables/illustrations	2
Will you be translating?	no
Circulation/distribution	500 - 999
Author of this Springer Nature content	no

About Your Work

Title of new work	Novel Surface Finishing Techniques for Additively Manufactured Metal Parts
Institution name	University of Waterloo
Expected presentation date	Mar 2025

Additional Data

Portions	Figure 8, Figure 9
The Requesting Person / Organization to Appear on the License	Manyou Sun

Figure 2.8 (b)

License Number	5925560605464
License date	Dec 10, 2024

Printable Details

Licensed Content

Licensed Content Publisher	Elsevier
Licensed Content Publication	Materials Today Communications
Licensed Content Title	The effect of HF-HNO3 chemical polishing on the surface roughness and fatigue life of laser powder bed fusion produced Ti6Al4V
Licensed Content Author	Martin Bezuidenhout,Gerrit Ter Haar,Thorsten Becker,Sabrina Rudolph,Oliver Damm,Natasha Sacks
Licensed Content Date	Dec 1, 2020
Licensed Content Volume	25
Licensed Content Issue	n/a
Licensed Content Pages	1

Order Details

Type of Use	reuse in a thesis/dissertation
Portion	figures/tables/illustrations
Number of figures/tables/illustrations	1
Format	electronic
Are you the author of this Elsevier article?	No
Will you be translating?	No

About Your Work

Title of new work	Novel Surface Finishing Techniques for Additively Manufactured Metal Parts
Institution name	University of Waterloo
Expected presentation date	Mar 2025

Additional Data

Portions	Figure 6
The Requesting Person / Organization to Appear on the License	Manyou Sun

Figure 2.8 (c)

License Number	5925560749378
License date	Dec 10, 2024

Printable Details

Licensed Content

Licensed Content Publisher	Springer Nature
Licensed Content Publication	The International Journal of Advanced Manufacturing Technology
Licensed Content Title	Reducing surface roughness by chemical polishing of additively manufactured 3D printed 316 stainless steel components
Licensed Content Author	Pawan Tyagi et al
Licensed Content Date	Oct 22, 2018

Order Details

Type of Use	Thesis/Dissertation
Requestor Type	academic/university or research institute
Format	electronic
Portion	figures/tables/illustrations
Number of figures/tables/illustrations	1
Will you be translating?	no
Circulation/distribution	500 - 999
Author of this Springer Nature content	no

About Your Work

Title of new work	Novel Surface Finishing Techniques for Additively Manufactured Metal Parts
Institution name	University of Waterloo
Expected presentation date	Mar 2025

Additional Data

Portions	Figure 2
The Requesting Person / Organization to Appear on the License	Manyou Sun

Figure 2.9 (a)

License Number	5925560990818
License date	Dec 10, 2024

Printable Details

Licensed Content

Licensed Content Publisher	Elsevier
Licensed Content Publication	Journal of Materials Processing Technology
Licensed Content Title	Surface finish control of additively-manufactured Inconel 625 components using combined chemical-abrasive flow polishing
Licensed Content Author	Neda Mohammadian,Sylvain Turenne,Vladimir Brailovski
Licensed Content Date	Feb 1, 2018
Licensed Content Volume	252
Licensed Content Issue	n/a
Licensed Content Pages	11

Order Details

Type of Use	reuse in a thesis/dissertation
Portion	figures/tables/illustrations
Number of figures/tables/illustrations	1
Format	electronic
Are you the author of this Elsevier article?	No
Will you be translating?	No

About Your Work

Title of new work	Novel Surface Finishing Techniques for Additively Manufactured Metal Parts
Institution name	University of Waterloo
Expected presentation date	Mar 2025

Additional Data

Portions	Figure 13
The Requesting Person / Organization to Appear on the License	Manyou Sun

Figure 2.9 (b)

License Number	5926020712649
License date	Dec 11, 2024

Printable Details

Licensed Content

Licensed Content Publisher	Elsevier
Licensed Content Publication	Journal of Manufacturing Processes
Licensed Content Title	Electrochemical mechanical polishing of internal holes created by selective laser melting
Licensed Content Author	Chenhao Zhao,Ningsong Qu,Xiaochuan Tang
Licensed Content Date	Apr 1, 2021
Licensed Content Volume	64
Licensed Content Issue	n/a
Licensed Content Pages	19

Order Details

Type of Use	reuse in a thesis/dissertation
Portion	figures/tables/illustrations
Number of figures/tables/illustrations	1
Format	electronic
Are you the author of this Elsevier article?	No
Will you be translating?	No

About Your Work

Title of new work	Novel Surface Finishing Techniques for Additively Manufactured Metal Parts
Institution name	University of Waterloo
Expected presentation date	Mar 2025

Additional Data

Portions	Figure 1
The Requesting Person / Organization to Appear on the License	Manyou Sun

Figure 2.9 (c)

License Number	5926021074027
License date	Dec 11, 2024

Printable Details

Licensed Content

Licensed Content Publisher	Elsevier
Licensed Content Publication	CIRP Annals - Manufacturing Technology
Licensed Content Title	A new hybrid electrochemical-mechanical process (PEMEC) for polishing complex and rough parts
Licensed Content Author	J. Rech,D. Krzak,F. Roy,F. Salvatore,A. Gidon,S. Guérin
Licensed Content Date	Jan 1, 2022
Licensed Content Volume	71
Licensed Content Issue	1
Licensed Content Pages	4

Order Details

Type of Use	reuse in a thesis/dissertation
Portion	figures/tables/illustrations
Number of figures/tables/illustrations	1
Format	electronic
Are you the author of this Elsevier article?	No
Will you be translating?	No

About Your Work

Title of new work	Novel Surface Finishing Techniques for Additively Manufactured Metal Parts
Institution name	University of Waterloo
Expected presentation date	Mar 2025

Additional Data

Portions	Figure 7
The Requesting Person / Organization to Appear on the License	Manyou Sun

Figure 2.10

License Number	5926021371189
License date	Dec 11, 2024

Printable Details

Licensed Content

Licensed Content Publisher	John Wiley and Sons
Licensed Content Publication	Materialwissenschaft und Werkstofftechnik
Licensed Content Title	Process parameter dependencies of continuous and pulsed laser modes on surface polishing of additive manufactured aluminium AlSi10Mg parts
Licensed Content Author	H. Riegel, A.K.M. De Silva, D.K. Harrison, et al
Licensed Content Date	Apr 14, 2021
Licensed Content Volume	52
Licensed Content Issue	4
Licensed Content Pages	24

Order Details

Type of use	Dissertation/Thesis
Requestor type	University/Academic
Format	Electronic
Portion	Figure/table
Number of figures/tables	1
Will you be translating?	No

About Your Work

Title of new work	Novel Surface Finishing Techniques for Additively Manufactured Metal Parts
Institution name	University of Waterloo
Expected presentation date	Mar 2025

Additional Data

Portions	Figure 1
The Requesting Person / Organization to Appear on the License	Manyou Sun

Figure 6.7

License Number	5926030070222
License date	Dec 11, 2024

Printable Details

Licensed Content

Licensed Content Publisher	Elsevier
Licensed Content Publication	International Journal of Machine Tools and Manufacture
Licensed Content Title	Shear-thickening polishing method
Licensed Content Author	Min Li,Binghai Lyu,Julong Yuan,Chenchen Dong,Weitao Dai
Licensed Content Date	Jul 1, 2015
Licensed Content Volume	94
Licensed Content Issue	n/a
Licensed Content Pages	12

Order Details

Type of Use	reuse in a thesis/dissertation
Portion	figures/tables/illustrations
Number of figures/tables/illustrations	1
Format	electronic
Are you the author of this Elsevier article?	No
Will you be translating?	No

About Your Work

Title of new work	Novel Surface Finishing Techniques for Additively Manufactured Metal Parts
Institution name	University of Waterloo
Expected presentation date	Mar 2025

Additional Data

Portions	Figure 2
The Requesting Person / Organization to Appear on the License	Manyou Sun

References

[1] ISO/ASTM 52900 - Standard Terminology for Additive manufacturing - General Principles - Terminology., 2015.

[2] A.T. Beaucamp, Y. Namba, P. Charlton, S. Jain, A.A. Graziano, Finishing of Additively Manufactured Titanium Alloy by Shape Adaptive Grinding (SAG), *Surf Topogr* 3 (2015). https://doi.org/10.1088/2051-672X/3/2/024001.

[3] S. Bagehorn, J. Wehr, H.J. Maier, Application of Mechanical Surface Finishing Processes for Roughness Reduction and Fatigue Improvement of Additively Manufactured Ti-6Al-4V parts, *Int J Fatigue* 102 (2017) 135–142. https://doi.org/10.1016/j.ijfatigue.2017.05.008.

[4] B. AlMangour, J.M. Yang, Integration of Heat Treatment with Shot Peening of 17-4 Stainless Steel Fabricated by Direct Metal Laser Sintering, *JOM* 69 (2017) 2309–2313. https://doi.org/10.1007/s11837-017-2538-9.

[5] N. Sanaei, A. Fatemi, Analysis of the Effect of Surface Roughness on Fatigue Performance of Powder Bed Fusion Additive Manufactured Metals, *Theor Appl Fract Mech* 108 (2020). https://doi.org/10.1016/j.tafmec.2020.102638.

[6] A. Toloei, V. Stoilov, D. Northwood, The Relationship between Surface Roughness and Corrosion, in *ASME International Mechanical Engineering Congress and Exposition, Proceedings (IMECE)*, 2 (2013).

[7] S.L. Sing, W.Y. Yeong, Laser Powder Bed Fusion for Metal Additive Manufacturing: Perspectives on Recent Developments, *Virtual Phys Prototyp* 15 (2020) 359–370. https://doi.org/10.1080/17452759.2020.1779999.

[8] H. Hassanin, A. Elshaer, R. Benhadj-Djilali, F. Modica, I. Fassi, Surface Finish Improvement of Additive Manufactured Metal Parts, in: *Engineering Materials*, 2018. https://doi.org/10.1007/978-3-319-68801-5_7.

[9] L.N. Carter, V.M. Villapún, L. Grover, S.C. Cox, Exploring the Duality of Powder

Adhesion and Underlying Surface Roughness in Laser Powder Bed Fusion Processed Ti-6Al-4V, *J Manuf Process* 81 (2022) 14–26. https://doi.org/10.1016/j.jmapro.2022.06.057.

[10] A. Charles, A. Elkaseer, L. Thijs, V. Hagenmeyer, S. Scholz, Effect of Process Parameters on the Generated Surface Roughness of Down-facing Surfaces in Selective Laser Melting, *Appl Sci* 9 (2019). https://doi.org/10.3390/app9061256.

[11] I. Yadroitsev, I. Smurov, Surface Morphology in Selective Laser Melting of Metal Powders, in: *Phys Procedia*, 2011. https://doi.org/10.1016/j.phpro.2011.03.034.

[12] E. Toyserkani, D. Sarker, O.O. Ibhadode, F. Liravi, P. Russo, K. Taherkhani, Metal Additive Manufacturing, Wiley: Hoboken, NJ, USA, 2022. https://doi.org/10.1002/9781119210801.

[13] D. Gu, Y. Shen, Balling Phenomena in Direct Laser Sintering of Stainless Steel Powder: Metallurgical Mechanisms and Control Methods, *Mater Des* 30 (2009) 2903–2910. https://doi.org/10.1016/j.matdes.2009.01.013.

[14] A.R. Balachandramurthi, J. Moverare, N. Dixit, R. Pederson, Influence of Defects and As-built Surface Roughness on Fatigue Properties of Additively Manufactured Alloy 718, *Mater Sci Eng A* 735 (2018) 463–474. https://doi.org/10.1016/j.msea.2018.08.072.

[15] M. Nakatani, H. Masuo, Y. Tanaka, Y. Murakami, Effect of Surface Roughness on Fatigue Strength of Ti-6Al-4V Alloy Manufactured by Additive Manufacturing, *Procedia Struct Integr* 19 (2019) 294–301. https://doi.org/10.1016/j.prostr.2019.12.032.

[16] R.F. Schaller, A. Mishra, J.M. Rodelas, J.M. Taylor, E.J. Schindelholz, The Role of Microstructure and Surface Finish on the Corrosion of Selective Laser Melted 304L, *J Electrochem Soc* 165 (2018) C234–C242. https://doi.org/10.1149/2.0431805jes.

[17] J.T. Miller, H.J. Martin, E. Cudjoe, Comparison of the Effects of a Sulfuric Acid

Environment on Traditionally Manufactured and Additive Manufactured Stainless Steel 316L Alloy, *Addit Manuf* 23 (2018) 272–286. https://doi.org/10.1016/j.addma.2018.08.023.

[18] D.H. Lee, 3-Dimensional Profile Distortion Measured by Stylus Type Surface Profilometer, *Measurement* 46 (2013) 803–814. https://doi.org/10.1016/j.measurement.2012.09.022.

[19] D. Walczak, J.B. Krolczyk, R. Chudy, M.K. Gupta, C. Pruncu, G.M. Krolczyk, Role of Optical Measurement Systems in Analysing the Surface Topography of an Industry Standard Component, *Optik (Stuttg.)* 283 (2023). https://doi.org/10.1016/j.ijleo.2023.170919.

[20] F. Marinello, A. Pezzuolo, Application of ISO 25178 Standard for Multiscale 3D Parametric Assessment of Surface Topographies, in: *IOP Conf Ser Earth Environ Sci*, Institute of Physics Publishing, 2019. https://doi.org/10.1088/1755-1315/275/1/012011.

[21] J.Y. Lee, A.P. Nagalingam, S.H. Yeo, A Review on the State-of-the-art of Surface Finishing Processes and Related ISO/ASTM Standards for Metal Additive Manufactured Components, *Virtual Phys Prototyp* 16 (2021). https://doi.org/10.1080/17452759.2020.1830346.

[22] C.W. Kum, C.H. Wu, S. Wan, C.W. Kang, Prediction and Compensation of Material Removal for Abrasive Flow Machining of Additively Manufactured Metal Components, *J Mater Process Technol* 282 (2020). https://doi.org/10.1016/j.jmatprotec.2020.116704.

[23] C. Peng, Y. Fu, H. Wei, S. Li, X. Wang, H. Gao, Study on Improvement of Surface Roughness and Induced Residual Stress for Additively Manufactured Metal Parts by Abrasive Flow Machining, *Procedia CIRP*, 71 (2018). https://doi.org/10.1016/j.procir.2018.05.046.

[24] A. Adiaconitei, I.S. Vintila, R. Mihalache, A. Paraschiv, T. Frigioescu, M. Vladut,

L. Pambaguian, A Study on Using the Additive Manufacturing Process for the Development of a Closed Pump Impeller for Mechanically Pumped Fluid Loop Systems, *Materials* 14 (2021). https://doi.org/10.3390/ma14040967.

[25] M. François, S. Han, F. Segonds, C. Dupuy, M. Rivette, S. Turpault, M. Mimouna, F. Salvatore, J. Rech, P. Peyre, Electromagnetic Performance of Ti6Al4V and AlSi7Mg0.6 Waveguides with Laser Meam Melting (LBM) Produced and Abrasive Flow Machining (AFM) Finished Internal Surfaces, *J Electromagn Waves Appl* 35 (2021). https://doi.org/10.1080/09205071.2021.1954554.

[26] Y. Zhao, J. Ratay, K. Li, H. Yamaguchi, W. Xiong, Effects of Magnetic Abrasive Finishing on Microstructure and Mechanical Properties of Inconel 718 Processed by Laser Powder Bed Fusion, *J Manuf Mater Process* 6 (2022). https://doi.org/10.3390/jmmp6020043.

[27] P. Zhu, G. Zhang, X. Teng, J. Du, L. Jiang, H. Chen, N. Liu, Investigation and Process Optimization for Magnetic Abrasive Finishing Additive Manufacturing Samples with Different Forming Angles, *Int J Adv Manuf Tech* 118 (2022) 2355–2371. https://doi.org/10.1007/s00170-021-08083-2.

[28] I. Karakurt, K.Y. Ho, C. Ledford, D. Gamzina, T. Horn, N.C. Luhmann, L. Lin, Development of a Magnetically Driven Abrasive Polishing Process for Additively Manufactured Copper Structures, *Procedia Manuf* 26 (2018) 798–805. https://doi.org/10.1016/j.promfg.2018.07.097.

[29] K.L. Tan, S.H. Yeo, Surface Modification of Additive Manufactured Components by Ultrasonic Cavitation Abrasive Finishing, *Wear* 378–379 (2017) 90–95. https://doi.org/10.1016/j.wear.2017.02.030.

[30] K.L. Tan, S.H. Yeo, Surface Finishing on IN625 Additively Manufactured Surfaces by Combined Ultrasonic Cavitation and Abrasion, *Addit Manuf* 31 (2020). https://doi.org/10.1016/j.addma.2019.100938.

[31] A.P. Nagalingam, H.K. Yuvaraj, V. Santhanam, S.H. Yeo, Multiphase

Hydrodynamic Flow Finishing for Surface Integrity Enhancement of Additive Manufactured Internal Channels, *J Mater Process Technol* 283 (2020). https://doi.org/10.1016/j.jmatprotec.2020.116692.

[32] E. Lyczkowska, P. Szymczyk, B. Dybała, E. Chlebus, Chemical Polishing of Scaffolds Made of Ti-6Al-7Nb Alloy by Additive Manufacturing, *Arch Civ Mech Eng* 14 (2014) 586–594. https://doi.org/10.1016/j.acme.2014.03.001.

[33] M. Bezuidenhout, G. Ter Haar, T. Becker, S. Rudolph, O. Damm, N. Sacks, The Effect of HF-HNO_3 Chemical Polishing on the Surface Roughness and Fatigue Life of Laser Powder Bed Fusion Produced Ti6Al4V, *Mater Today Commun* 25 (2020). https://doi.org/10.1016/j.mtcomm.2020.101396.

[34] P. Tyagi, T. Goulet, C. Riso, F. Garcia-Moreno, Reducing Surface Roughness by Chemical Polishing of Additively Manufactured 3D Printed 316 Stainless Steel Components, *Int J Adv Manuf Technol* 100 (2019) 2895–2900. https://doi.org/10.1007/s00170-018-2890-0.

[35] K. Alrbaey, D.I. Wimpenny, A.A. Al-Barzinjy, A. Moroz, Electropolishing of Re-melted SLM Stainless Steel 316L Parts Using Deep Eutectic Solvents: 3 × 3 Full Factorial Design, *J Mater Eng Perform* 25 (2016) 2836–2846. https://doi.org/10.1007/s11665-016-2140-2.

[36] P. Tyagi, T. Goulet, C. Riso, R. Stephenson, N. Chuenprateep, J. Schlitzer, C. Benton, F. Garcia-Moreno, Reducing the Roughness of Internal Surface of an Additive Manufacturing Produced 316 Steel Component by Chempolishing and Electropolishing, *Addit Manuf* 25 (2019) 32–38. https://doi.org/10.1016/j.addma.2018.11.001.

[37] E. Langi, L.G. Zhao, P. Jamshidi, M. Attallah, V. V. Silberschmidt, H. Willcock, F. Vogt, A Comparative Study of Microstructures and Nanomechanical Properties of Additively Manufactured and Commercial Metallic Stents, *Mater Today Commun* 31 (2022). https://doi.org/10.1016/j.mtcomm.2022.103372.

[38] J. Dillard, A. Grizzle, W. Demisse, L. Rice, K. Klein, P. Tyagi, Alternating Chempolishing and Electropolishing for Interior and Exterior Surface Finishing of Additively Manufactured (AM) Metal Components, *Int J Adv Manuf Technol* 121 (2022) 8159–8170. https://doi.org/10.1007/s00170-022-09857-y.

[39] H. Zhu, A. Rennie, R. Li, Y. Tian, Two-Steps Electrochemical Polishing of Laser Powder Bed Fusion 316L Stainless Steel, *Surf Interfaces* 35 (2022) 102442. https://doi.org/10.1016/j.surfin.2022.102442.

[40] V. Urlea, V. Brailovski, Electropolishing and Electropolishing-related Allowances for Powder Bed Selectively Laser-melted Ti-6Al-4V Alloy Components, *J Mater Process Technol* 242 (2017) 1–11. https://doi.org/10.1016/j.jmatprotec.2016.11.014.

[41] Y.C. Wu, C.N. Kuo, Y.C. Chung, C.H. Ng, J.C. Huang, Effects of Electropolishing on Mechanical Properties and Bio-corrosion of Ti6Al4V Fabricated by Electron Beam Melting Additive Manufacturing, *Materials* 12 (2019). https://doi.org/10.3390/ma12091466.

[42] Y. Zhang, J. Li, S. Che, Y. Tian, Electrochemical Polishing of Additively Manufactured Ti–6Al–4V Alloy, *Met Mater Int* 26 (2020) 783–792. https://doi.org/10.1007/s12540-019-00556-0.

[43] H. Fayazfar, I. Rishmawi, M. Vlasea, Electrochemical-Based Surface Enhancement of Additively Manufactured Ti-6Al-4V Complex Structures, *J Mater Eng Perform* 30 (2021) 2245–2255. https://doi.org/10.1007/s11665-021-05512-x.

[44] S. Jiang, D. Guo, L. Zhang, K. Li, B. Song, Y.A. Huang, Electropolishing-Enhanced, High-Precision 3D Printing of Metallic Pentamode Metamaterials, *Mater Des* 223 (2022). https://doi.org/10.1016/j.matdes.2022.111211.

[45] C.H. Chen, C.Y. Lee, M. Der Ger, S.Y. Jian, J.C. Hung, P.J. Yang, C.H. Kao, Y.C. Ferng, Y.S. Huang, K.K. Jen, The Effect of Oxalic Acid as the Pre-Activator for

the Electropolishing of Additive Manufactured Titanium-Based Materials and Its Characterization, *Polymers* 14 (2022). https://doi.org/10.3390/polym14194198.

[46] V. Urlea, V. Brailovski, Electropolishing and Electropolishing-Related Allowances for IN625 Alloy Components Fabricated by Laser Powder-bed Fusion, *Int J Adv Manuf Technol* 92 (2017) 4487–4499. https://doi.org/10.1007/s00170-017-0546-0.

[47] Z. Min, Y. Wu, K. Yang, J. Xu, S.N. Parbat, M.K. Chyu, Dimensional Characterizations Using Scanning Electron Microscope and Surface Improvement with Electrochemical Polishing of Additively Manufactured Microchannels, *J Eng Gas Turbine Power* 143 (2020) 041020. https://doi.org/10.1115/1.4049908.

[48] A. Shrivastava, S. Anand Kumar, B.K. Nagesha, T.N. Suresh, Electropolishing of Inconel 718 Manufactured by Laser Powder Bed Fusion: Effect of Heat Treatment on Hardness, 3D Surface Topography and Material Ratio Curve, *Opt Laser Technol* 144 (2021). https://doi.org/10.1016/j.optlastec.2021.107448.

[49] U. Ali, H. Fayazfar, F. Ahmed, E. Toyserkani, Internal Surface Roughness Enhancement of Parts Made by Laser Powder-bed Fusion Additive Manufacturing, *Vacuum* 177 (2020). https://doi.org/10.1016/j.vacuum.2020.109314.

[50] N. Mohammadian, S. Turenne, V. Brailovski, Surface Finish Control of Additively-Manufactured Inconel 625 Components Using Combined Chemical-abrasive Flow Polishing, *J Mater Process Technol* 252 (2018) 728–738. https://doi.org/10.1016/j.jmatprotec.2017.10.020.

[51] C. Zhao, N. Qu, X. Tang, Electrochemical Mechanical Polishing of Internal Holes Created by Selective Laser Melting, *J Manuf Process* 64 (2021) 1544–1562. https://doi.org/10.1016/j.jmapro.2021.03.003.

[52] J. Rech, D. Krzak, F. Roy, F. Salvatore, A. Gidon, S. Guérin, A New Hybrid Electrochemical-Mechanical Process (PEMEC) for Polishing Complex and Rough Parts, *CIRP Ann* 71 (2022) 173–176. https://doi.org/10.1016/j.cirp.2022.03.011.

[53] J. Boban, A. Ahmed, E.K. Jithinraj, M.A. Rahman, M. Rahman, Polishing of Additive Manufactured Metallic Components: Retrospect on Existing Methods and Future Prospects, *Int J Adv Manuf Technol* 121 (2022) 83–125. https://doi.org/10.1007/s00170-022-09382-y.

[54] M. Hofele, J. Schanz, A. Roth, D.K. Harrison, A.K.M. De Silva, H. Riegel, Process Parameter Dependencies of Continuous and Pulsed Laser Modes on Surface Polishing of Additive Manufactured Aluminium AlSi10Mg Parts, *Materwiss Werksttech* 52 (2021) 409–432. https://doi.org/10.1002/mawe.202000335.

[55] S. Lee, Z. Ahmadi, J.W. Pegues, M. Mahjouri-Samani, N. Shamsaei, Laser Polishing for Improving Fatigue Performance of Additive Manufactured Ti-6Al-4V Parts, *Opt Laser Technol* 134 (2021). https://doi.org/10.1016/j.optlastec.2020.106639.

[56] K.C. Yung, W.J. Wang, T.Y. Xiao, H.S. Choy, X.Y. Mo, S.S. Zhang, Z.X. Cai, Laser Polishing of Additive Manufactured CoCr Components for Controlling Their Wettability Characteristics, *Surf Coat Technol* 351 (2018) 89–98. https://doi.org/10.1016/j.surfcoat.2018.07.030.

[57] F. Davoodi, M. Taghian, G. Carbone, A. Saboori, L. Iuliano, An Overview of the Latest Progress in Internal Surface Finishing of the Additively Manufactured Metallic Components, *Materials* 16 (2023). https://doi.org/10.3390/ma16103867.

[58] N. Dixit, V. Sharma, P. Kumar, Research Trends in Abrasive Flow Machining: A Systematic Review, *J Manuf Process* 64 (2021) 1434–1461. https://doi.org/10.1016/J.JMAPRO.2021.03.009.

[59] S. Han, F. Salvatore, J. Rech, J. Bajolet, Abrasive Flow Machining (AFM) Finishing of Conformal Cooling Channels Created by Selective Laser Melting (SLM), *Precis Eng* 64 (2020) 20–33. https://doi.org/10.1016/j.precisioneng.2020.03.006.

[60] J. Guo, C. Song, Y. Fu, K.H. Au, C.W. Kum, M.H. Goh, T. Ren, R. Huang, C.N.

Sun, Internal Surface Quality Enhancement of Selective Laser Melted Inconel 718 by Abrasive Flow Machining, *J Manuf Sci Eng* 142 (2020). https://doi.org/10.1115/1.4047141.

[61] J. Zhang, H. Wang, Magnetically Driven Internal Finishing of AISI 316L Stainless Steel Tubes Generated by Laser Powder Bed Fusion, *J Manuf Process* 76 (2022) 155–166. https://doi.org/10.1016/j.jmapro.2022.02.009.

[62] A.P. Nagalingam, H.K. Yuvaraj, V. Santhanam, S.H. Yeo, Multiphase Hydrodynamic Flow Finishing for Surface Integrity Enhancement of Additive Manufactured Internal Channels, *J Mater Process Technol* 283 (2020). https://doi.org/10.1016/j.jmatprotec.2020.116692.

[63] M. Shen, F. Fang, Two-Step Electropolishing of Internal Surfaces of 316L Stainless Steel Made by Laser-Based Powder Bed Fusion, *J Manuf Process* 89 (2023) 298–313. https://doi.org/10.1016/j.jmapro.2023.01.052.

[64] L. An, D. Wang, D. Zhu, Electrochemical Polishing with Glycol-Based Electrolyte of the Curved Internal Channels Fabricated via Laser Powder Bed Fusion, *J Manuf Process* 117 (2024) 375–386. https://doi.org/10.1016/j.jmapro.2024.03.009.

[65] B. Parvandar Asadollahi, M. Pour Panah, A. Javdani, Experimental Investigation and Molecular Dynamics Simulation of Contributing Variables on Abrasive Water Jet on Aluminum Alloy 7075 Reinforced with Al_2O_3, Graphite and Silicon Carbide, *Arab J Sci Eng* 47 (2022) 15303–15321. https://doi.org/10.1007/s13369-022-06585-z.

[66] J. Xu, J. Li, P. Zhu, B. Li, C. Zhao, Coarse-Grained Molecular Dynamics Simulations of Particle Behaviors in Magnetorheological Polishing Fluid, *Comput Mater Sci* 163 (2019) 68–81. https://doi.org/10.1016/j.commatsci.2019.03.023.

[67] Y. Makiuchi, F. Hashimoto, A. Beaucamp, Model of Material Removal in Vibratory Finishing, Based on Preston's Law and Discrete Element Method, *CIRP Ann* 68 (2019) 365–368. https://doi.org/10.1016/j.cirp.2019.04.082.

[68] M. Kopp, E. Uhlmann, Prediction of the Roughness Reduction in Centrifugal Disc Finishing of Additive Manufactured Parts Based on Discrete Element Method, *Machines* 10 (2022). https://doi.org/10.3390/machines10121151.

[69] V.K. Jain, R. Kumar, P.M. Dixit, A. Sidpara, Investigations into Abrasive Flow Finishing of Complex Workpieces Using FEM, *Wear* 267 (2009) 71–80. https://doi.org/10.1016/j.wear.2008.11.005.

[70] I. Chaieb, & Naoufel, B. Moussa, & Nabil, B. Fredj, & Nizar, B. Salah, An Innovative Contactless Finite Element Simulation of the Shot Peening Process, *Int J Adv Manuf Technol* 113 (2021) 2121-2136. https://doi.org/10.1007/s00170-021-06809-w/Published.

[71] M. Chai, Z. Li, H. Yan, X. Sun, Experimental Investigations on Aircraft Blade Cooling Holes and CFD Fluid Analysis in Electrochemical Machining, *Adv Mater Sci Eng* 2019 (2019). https://doi.org/10.1155/2019/4219323.

[72] C. Bouland, V. Urlea, K. Beaubier, M. Samoilenko, V. Brailovski, Abrasive Flow Machining of Laser Powder Bed-fused Parts: Numerical Modeling and Experimental Validation, *J Mater Process Technol* 273 (2019). https://doi.org/10.1016/j.jmatprotec.2019.116262.

[73] W. Han, F. Fang, Fundamental Aspects and Recent Developments in Electropolishing, *Int J Mach Tools Manuf* 139 (2019) 1–23. https://doi.org/10.1016/j.ijmachtools.2019.01.001.

[74] A. Córdova, P. Henríquez, H. Nuñez, F. Rico-Rodriguez, C. Guerrero, C. Astudillo-Castro, A. Illanes, Recent Advances in the Application of Enzyme Processing Assisted by Ultrasound in Agri-Foods: A Review, *Catalysts* 12 (2022). https://doi.org/10.3390/catal12010107.

[75] H. Every, A.G. Bishop, M. Forsyth, D.R. Macfarlane, Ion Diffusion in Molten Salt Mixtures, *Electrochim Acta* 45 (2000) 1279-1284. https://doi.org/10.1016/S0013-4686(99)00332-1

[76] C. Wagner, Contribution to the Theory of Electropolishing, *J Electrochem Soc* 101 (1954). https://doi.org/10.1149/1.2781235.

[77] COMSOL Multiphysics®, version 6.2, COMSOL AB, Stockholm, Sweden.

[78] Y. Fu, X. Zhu, J. Wang, T. Gong, Numerical Study of the Synergistic Effect of Cavitation and Micro-abrasive Particles, *Ultrason Sonochem* 89 (2022). https://doi.org/10.1016/j.ultsonch.2022.106119.

[79] S. Behnia, A.J. Sojahrood, W. Soltanpoor, L. Sarkhosh, Towards Classification of the Bifurcation Structure of a Spherical Cavitation Bubble, *Ultrasonics* 49 (2009) 605–610. https://doi.org/10.1016/j.ultras.2009.05.005.

[80] L. Kinsler, A. Frey, A. Coppens, J. Sanders, Fundamentals of Acoustics, Wiley: Hoboken, NJ, USA, 2000.

[81] A. Vogel, S. Busch, U. Parlitz, Shock Wave Emission and Cavitation Bubble Generation by Picosecond and Nanosecond Optical Breakdown in Water, *J Acoust Soc Am* 100 (1996). https://doi.org/10.1121/1.415878.

[82] M.H. Rice, J.M. Walsh, Equation of State of Water to 250 Kilobars, *J Chem Phys* 26 (1957). https://doi.org/10.1063/1.1743415.

[83] M.S. Plesset, R.B. Chapman, Collapse of an Initially Spherical Vapour Cavity in the Neighbourhood of a Solid Boundary, *J Fluid Mech* 47 (1971). https://doi.org/10.1017/S0022112071001058.

[84] M.S. ElTobgy, E. Ng, M.A. Elbestawi, Finite Element Modeling of Erosive Wear, *Int J Mach Tools Manuf* 45 (2005) 1337–1346. https://doi.org/10.1016/j.ijmachtools.2005.01.007.

[85] S. Liu, Y.C. Shin, Additive Manufacturing of Ti6Al4V Alloy: A Review, *Mater Des* 164 (2019). https://doi.org/10.1016/j.matdes.2018.107552.

[86] H. Fayazfar, I. Rishmawi, M. Vlasea, Electrochemical-Based Surface Enhancement of Additively Manufactured Ti-6Al-4V Complex Structures, *J*

Mater Eng Perform 30 (2021) 2245–2255. https://doi.org/10.1007/s11665-021-05512-x.

[87] I.O. Aver'yanova, D.Y. Bogomolov, V. V. Poroshin, ISO 25178 Standard for Three-Dimensional Parametric Assessment of Surface Texture, *Russ Eng Res* 37 (2017). https://doi.org/10.3103/S1068798X17060053.

[88] J.C. Snyder, K.A. Thole, Understanding Laser Powder Bed Fusion Surface Roughness, *J Manuf Sci Eng* 142 (2020) 071003. https://doi.org/10.1115/1.4046504.

[89] P.A. Jacquet, Electrolytic Polishing of Metallic Surfaces, *Met Finish* 47 (1949).

[90] G. Wang, Z. Liu, J. Niu, W. Huang, B. Wang, Effect of Electrochemical Polishing on Surface Quality of Nickel-Titanium Shape Memory Alloy after Milling, *J Mater Res Technol* 9 (2020) 253–262. https://doi.org/10.1016/j.jmrt.2019.10.053.

[91] K. Su, J. Wu, D. Xia, Dual Role of Microparticles in Synergistic Cavitation–Particle Erosion: Modeling and Experiment, *Wear* 470–471 (2021) 203633. https://doi.org/10.1016/j.wear.2021.203633.

[92] E. Szwajczakaf, A. Szymański, On the Relation Between Mobility of lons and Viscosity. The Walden's Rule, *Mol Cryst Liq Cryst* 139 (1986) 253–261. https://doi.org/10.1080/00268948608080131.

[93] L. Liu, S. Q. Wu, H. F. Gu, Y. Yang, H. Wang and A. J. Huang, Effect of The Number of Hydroxyls and Carbons on the Solubility of Sodium Chloride in Alcohol and The Electropolishing Behavior of Ti-6Al-4V Alloy in Alcohol-Salt System, *J. Electrochem. Soc.* 168 (2021) 093503. https://doi.org/10.1149/1945-7111/ac24b3.

[94] M. Sun, E. Toyserkani, A Novel Hybrid Ultrasound Abrasive-Driven Electrochemical Surface Finishing Technique for Additively Manufactured Ti6Al4V Parts, *Inventions* 9 (2024). https://doi.org/10.3390/inventions9020045.

[95] A. Mirabal, I. Loza-Hernandez, C. Clark, D.E. Hooks, M. McBride, J.A. Stull, Roughness measurements across topographically varied additively manufactured metal surfaces, *Addit. Manuf.* 69 (2023). https://doi.org/10.1016/j.addma.2023.103540.

[96] S.J. Lee, Y.H. Chen, J.C. Hung, The Investigation of Surface Morphology Forming Mechanisms in Electropolishing Process, *Int J Electrochem Sci* 7 (2012) 12495-12506. https://doi.org/10.1016/s1452-3981(23)16561-8.

[97] E.L. Smith, A.P. Abbott, K.S. Ryder, Deep Eutectic Solvents (DESs) and Their Applications, *Chem Rev* 114 (2014) 11060–11082. https://doi.org/10.1021/cr300162p.

[98] N. Morita, Study of Pure Titanium Electrolytic Polishing, *Dent Mater J* 9 (1990).

[99] K. Fushimi, H. Kondo, H. Konno, Anodic Dissolution of Titanium in Chloride-Containing Ethylene Glycol Solution, *Electrochim Acta* 55 (2009). https://doi.org/10.1016/j.electacta.2009.08.047.

[100] M. Li, B. Lyu, J. Yuan, C. Dong, W. Dai, Shear-Thickening Polishing Method, *Int J Mach Tools Manuf* 94 (2015) 88–99. https://doi.org/10.1016/j.ijmachtools.2015.04.010.

[101] D. Ozturk, M.L. Morgan, B. Sandnes, Flow-to-Fracture Transition and Pattern Formation in a Discontinuous Shear Thickening Fluid, *Commun Phys* 3 (2020). https://doi.org/10.1038/s42005-020-0382-7.